Investigating the effect of liposomal membrane fluidity and antibody lateral mobility on endothelial cell targeting

Investigating the effect of liposomal membrane fluidity and antibody lateral mobility on endothelial cell targeting

A dissertation presented

by

Dariela Almeda

to

The School of Engineering and Applied Sciences

in partial fulfillment of the requirements

for the degree of

Doctor of Philosophy

in the subject of

Engineering Sciences

Harvard University

Cambridge, Massachusetts

February 2014

Prof. Debra T. Auguste and Prof. David J. Mooney **Dariela Almeda**

Investigating the effect of liposomal membrane fluidity and antibody mobility on endothelial cell targeting

Abstract

Atherosclerosis is initiated by the adhesion of leukocytes to the endothelial surface of arteries followed by migration beneath the intima. Current therapies to combat atherosclerotic plaque, such as statins or antihypertensive drugs, treat atherosclerosis indirectly; they do not specifically target inflamed vasculature or improve the vascular condition. Few studies have focused on antibody mobility or membrane fluidity as an approach to improve drug delivery vehicle binding and uptake.

Here, we present a biomimetic liposomal design targeting vascular adhesion molecule (VCAM1) and E-selectin, which are upregulated on inflamed endothelial cells (ECs). We hypothesized that increased lateral antibody diffusivity may be used as a strategy to enhance liposome targeting to ECs expressing high levels of VCAM1 and E-selectin. We first characterized the physical properties of our liposomal system, including membrane fluidity and quantification of antibody surface density, and evaluated the temporal EC expression of VCAM1 and E-selectin. We then examined the effects of membrane fluidity, antibody surface density, and incubation time on activated EC binding and uptake. Finally, we also conducted a preliminary *in vivo* study where we assessed the biodistribution of our liposomes.

The results of this dissertation may be utilized to design liposomes with enhanced targeting efficiency to inflamed endothelium, present not only in atherosclerosis but also in a wide range of vascular inflammatory conditions. These liposomes can be further developed to have diagnostic, imaging and/or therapeutic capabilities.

Table of Contents

List of Figures and Tables

Figures

Tables

Acknowledgements

I would like to thank my former adviser Prof. Debra T. Auguste for giving the opportunity to work with her and allowing me to become an independent scientist. I would especially like to thank Prof. Guido Guidotti, for helping me so much in the last stage of my Ph.D. by providing invaluable guidance and by helping stir my project in a successful direction. He was always available to hold long discussions about my project and without his help, the culmination of my project would have been much more difficult. I am also grateful to Prof. David J. Mooney. He was always available to discuss my progress and provided me with useful advice. I would also like to thank Prof. Kevin K. Parker for always being so welcoming and allowing me to finish up my last year of experiments in his lab. He also provided me with helpful advice during challenging times. I would especially like to thank Dean Cherry Murray for her support and time.

I would like to thank members of the former Auguste Lab whom I worked with side by side: Dr. Marjan Rafat, Dr. George Ye, Dr. Renita Horton, Kyle Satterstrom, Dr. Jin-Oh You, Dr. Rico Gunawan, Dr. Peng Guo, Joanna Deveau, Lisa Rotenstein, Jennifer Hu, Yongtian Tan, Justine Cheng, Aikaterini Mantzavinou, Ted Ho, and Bib Yang. You guys were always so supportive and helpful; graduate school would have definitely not been the same without you. I will always be grateful for not only having had the chance to learn from you, but also for having the chance to create such strong friendships. A special thanks to all of the members of the Parker Lab for being so kind

and supportive during the last stage of my Ph.D. They always provided me with the space my equipment and I needed, and I will always be grateful to them for making my lab transition a smoother one. To Erin Anderson, thank you so much for all your help with the *in vivo* mice studies. To Anand B. Subramaniam, thank you for your advice on the preparation of supported lipid bilayers. To Mindy Tam, Patricia Rogers, and Brian Tilton from the FAS Center for Systems Biology, thank you so much for providing useful flow cytometry advice and always greeting me with a warm hello. To Jessa Piaia, thank you so much for your help in processing all of my purchase orders and reimbursements so efficiently and for caring so much about my progress. I am also grateful to Arlene Stevens who was there when I needed advice.

Thank you to all of my other dear friends that supported me throughout the years: Nefeli Georgoulia, Sofia Bahena, Amy Sutton, Helen Park, Lynn Trever, Sarah Lockwood, Katharyn Hurd, among others. And to my mentors Tania Betancourt and Amber Doiron who have supported me since I was an undergraduate student.

Finally, I would like to thank my parents above all, for your love, for always believing in me, and for encouraging me to always do my best at even the most unimportant of tasks. This dissertation is dedicated to you. To my sister and brother, thank you for your unconditional support and understanding. To Ruben, thanks for all your support during the last stages of my Ph.D.

This work was supported by the Ford Foundation Predoctoral Fellowship administered by the National Research Council of the National Academies.

To my parents.

Chapter 1.

Introduction

1.1 Cardiovascular Disease: Current Treatments and Diagnostic Tools

Cardiovascular disease is, according to statistics, considered to be a pandemic affecting millions of people in developed countries. According the World Health Organization, 18 million people die annually from cardiovascular disease (CVD) and by the year 2030, this number is projected to increase to 24 million deaths per year [1]. Cardiovascular disease includes complications such as heart attack and ischemic stroke, but also encompasses heart failure, arrhythmia, and heart valve problems. Atherosclerosis is known to be the major contributor of coronary heart disease, carotid artery disease, peripheral arterial disease, and chronic kidney disease. It is a condition that develops when narrowing of the arteries occurs due to the presence of plaque.

Current life-long treatments of atherosclerosis include the administration of medications such as: β blockers, angiotensin-converting-enzyme (ACE) inhibitors and calcium blockers to treat hypertension, aspirin to inhibit production of thromboxane, statins to decrease cholesterol levels, and anti-ischemic nitrates [2,3]. Preventive life style changes such as maintaining a healthy diet, abstaining from smoking, maintaining a healthy weight, exercising, and being physically active are also recommended [4]. When patients are in the late stages of the disease, invasive surgical procedures are required and include angioplasty and coronary artery bypass grafting [5].

There are several limitations in how we currently diagnose coronary heart and carotid artery disease caused by atherosclerosis. Narrowing of the arteries is

diagnosed by detecting any artery blood flow insufficiencies via an electrocardiogram that may be accompanied with a treadmill exercise test and/or with a coronary angiography [5]. Efforts have been placed on developing non-invasive cardiac imaging techniques that include functional imaging, focused on detecting hemodynamic changes, and anatomical imaging, focused on visualizing the coronary artery tree [6]. These techniques although powerful in certain aspects, tend to lack in others [7–9]. For example, techniques like positron emission tomography (PET) and single-photon emission computed tomography (SPECT) have high sensitivity, but lack good spatial resolution. Similarly, magnetic resonance imaging (MRI) and computed tomography (CT) have great spatial resolution, but less sensitivity. Recent focus has gone into investigating cardiac molecular imaging involving the targeting of pathophysiologic molecules of interest, such as vascular cell adhesion molecule1 (VCAM1), to achieve imaging with greater specificity and resolution [7,9,10].

There are also limitations to the current treatment modality of atherosclerosis. Current medications do not address changes in vessel wall mechanics or directly treat plaque formation. Targeted therapeutics that promote vasodilation, inhibit proteases (to prevent thrombosis), and reestablish vessel compliance may revolutionize clinical treatment by improving the physical condition of the vessel wall. The inability to accurately target inflamed areas of the endothelium has hindered the design of local cardiovascular therapies. Improved targeting techniques are necessary to develop radically new treatments for cardiovascular disease.

1.2 The Role of Inflammation in Atherosclerosis

The role of inflammation in atherosclerosis has been elucidated during the last two decades. There are three main stages of atherosclerosis; inflammation is present at every single stage. A variety of conditions such as low-density lipoprotein (LDL) oxidation, hypertension, diabetes, obesity, and infection are thought to trigger the initial stages of atherosclerosis [11]. During the early stages of atherosclerosis, patches of endothelium begin to express molecules termed cell adhesion molecules (CAMs) that bind specifically to circulating leukocytes [12]. These CAMs include, VCAM1, intercellular cell adhesion molecule1 (ICAM1), and selectins (P-, E-, and L-), which all have different functions in the inflammatory cascade. Selectins are type-I transmembrane glycoproteins that bind to sialylated carbohydrate moieties present on target proteins. E-selectin or CD62A has a molecular weight ranging between 107 kDa – 115 kDa and is responsible for mediating the rolling of leukocytes on the surface of endothelial cells (ECs) [12]. Both VCAM1 and ICAM1 are members of the immunoglobulin superfamily and mediate the firm adhesion of leukocytes on ECs after the initial rolling stage mediated by the selectins [13]. VCAM1-expressing ECs bind to the leukocytes via very late antigen4 (VLA4), an $\alpha_4\beta_1$ integrin [13,14]. The third stage of atherosclerosis involves the chemotactic migration of leukocytes into the intima. Once inside the vascular wall, leukocytes secrete cytokines that promote the migration and proliferation of smooth muscle cells (SMCs). These SMCs express matrix metalloproteinases (MMPs), which in turn degrade collagen and elastin allowing SMCs to penetrate into the elastic laminae. Ultimately, foam cells express collagenases that weaken the fibrous cap and consequently, make it vulnerable to rupture. T lymphocytes

and macrophages increase the expression of pro-coagulant tissue factor, which is responsible for triggering a thrombus when plaque rupture occurs, leading to acute complications such as stroke.

1.3 Liposomes as Drug Delivery Vehicles

Liposomes are defined as phospholipids that self-assemble into vesicles when exposed to an aqueous phase [15]. Since their discovery in the 1960s by A. D. Bangham, liposomes have become one of the most comprehensively studied drug delivery vehicles. Additionally, liposomes have been utilized for other related applications including vaccines, gene therapy and imaging [16–18]. There exists great versatility to the design of liposomes because of the availability of lipids with different physical characteristics such as pH-sensitivity, light-sensitivity, charge, fluorescence and polymerizability. Liposomes are also able to encapsulate both hydrophilic and hydrophobic substances within the aqueous compartment and within the lipid bilayer, respectively.

When lipids self-assemble in water they tend to form lamellar bilayers. Liposomes can be classified into two categories: multilamellar vesicles (MLVs) containing more than one concentric lamellar bilayer and unilamellar vesicles containing only one bilayer. MLVs can range between 0.1 to 10 μm while the range of sizes of unilamellar vesicles varies. Small unilamellar vesicles (SUVs) are less than 100 nm, large unilamellar vesicles (LUVs) are between 100 to 500 nm and giant unilamellar vesicles (GUVs) are greater than 1 μm in size [17]. SUVs are most commonly used for

drug delivery applications due to their size and homogeneity. The lamellarity and size distribution of MLVs is usually too heterogeneous, which renders them inadequate as drug carriers. Below are some detailed examples of different clinical applications targeting various diseases in which liposomes have been used as drug delivery vehicles.

1.3.1 Liposomes and the Blood Brain Barrier

Transporting therapeutic molecules across the blood brain barrier (BBB) for central nervous system (CNS) access has long been a challenge since more than 98% of neuronal drug molecules cannot cross the BBB [19]. Passive crossing of drugs through the BBB is possible with the correct lipophilicity and a molecular weight below 500 Da [20]. Because of these limitations, pathways involving liposomes have been explored for efficient delivery of therapeutics to the brain. Three mechanisms of BBB transport include carrier-mediated transport (CMT), active-efflux transport (AET), and receptor-mediated transcytosis (RMT) [19]. CMT involves the transport of small-molecule hydrophilic nutrients through transporter proteins into and out of the brain, and AET allows transport of low molecular weight lipophilic metabolic products from the brain to the blood. RMT uses peptide-specific receptors to mediate the transport of essential circulating proteins and peptides, such as insulin, leptin, and transferrin, into the brain. Understanding these mechanisms allows for the design of drug delivery vehicles that can target the brain while bypassing the rejection from the BBB.

Liposomes between 80-100 nm have been used to target the CNS due to their lipophilic character [21]. To avoid immediate clearance when introduced systemically,

polyethylene glycol (PEG) can be inserted into the lipid bilayer for avoidance of protein adsorption and recognition by macrophages. Many RMT pathways have been used to deliver liposomes across the BBB. The transferrin receptor (TR) provides iron to cells. Although designing vehicles that bind to transferrin itself cannot be used for specific BBB targeting due to high plasma levels, conjugation of specific monoclonal antibodies (mAb) against TR has been explored for the fabrication of drug delivery vehicles. Using another RMT approach, specific mAbs targeting the human insulin receptor (HIR) have also been used. The conjugation of mAbs to liposomes creates what is termed immunoliposomes.

Researchers have designed “Trojan Horse Liposomes” (THL) for BBB delivery of therapeutics with *in vivo* stability, which allow for the stealth passage of the liposomes through the BBB and then the release of its therapeutic contents [22]. For example, 100 nm 1-palmitoyl-2-oleoyl-*sn*-glycerol-3-phosphocholine (POPC):didodecyldimethylammonium bromide (DDAB):Distearoylphosphatidylethanolamine (DSPE)-PEG 2000 liposomes have been made to encapsulate single DNA strands encoding for luciferase or β-galactosidase [23]. This liposome formulation is neutral in charge, which allows for *in vivo* stability in blood. DSPE-PEG 2000 allows the evasion of clearance by the immune system. Additionally, 1-2% of the PEG strands were conjugated with the OX26 mAb rat TR. After intravenous injection of these immunoliposomes in rats, it was found that specific gene expression in the brain was achieved. Targeting the HIR has also been explored using the same liposome composition at 85 nm [24]. The immunoliposome was selectively targeted to the murine 83-14 mAb against the HIR in the rhesus monkey brain *in vivo*. Global expression of β-galactosidase was shown in the rhesus monkey

brain, which shows the feasibility of using immunoliposomes for gene therapy in the brain. Although these mAbs cannot be used in humans, genetically engineered humanized mAbs to HIR have been developed and may be used in humans in the future [25].

Liposomes have also been used to combat specific neurodegenerative diseases. Research has shown that immunoliposomes encapsulating tyrosine hydroxylase with TR targeting functionality using OX26 mAbs against experimental Parkinson's disease models can improve rat motor function [26]. RNAi therapies have also been investigated for anti-angiogenic brain tumor therapies targeting human epidermal growth factor receptor (EGFR) [27]. Immunoliposomes encapsulated short hairpin RNA (shRNA) against EGFR, and passage across the BBB was achieved using both the murine 83-15 mAb to HIR and the rat 8D3 mAb to the mouse TR. Intravenous administration of immunoliposomes successfully suppressed EGFR expression and increased survival of mice with advanced intracranial brain tumors.

Although using liposomes to bypass the BBB has not proceeded to human clinical trials, there is much promise in using these materials for treating neurodegenerative diseases and brain tumors in the future.

1.3.2 Liposomes and Cancer

The delivery of low molecular weight chemotherapeutics to tumors is limited by high and rapid uptake by macrophages in the reticuloendothelial system (RES) of the kidneys and liver and inactivation of active drugs due to protein binding [28]. However, tumors exhibit high microvessel permeability to higher molecular weight compounds due

to a discontinuous basement membrane, fenestrated endothelium, and increased transendothelial transport compared to normal tissues [29]. Tumors possess these pathophysiological characteristics to sustain adequate levels of oxygen and nutrients for growth, and this phenomenon has been termed the “enhanced permeability and retention effect” (EPR). Similarly, long-circulating liposomes that are modified with PEG have been shown to increase deposition within extravascular and extracellular tumor areas due to “leaky” vasculature and an irregular lymphatic system [30,31]. Although using macromolecules or liposomes has increased tumor targeting, many limitations exist, including small avascular tumors that cannot be targeted, high interstitial fluid pressure preventing diffusion into the tumor parenchyma, and increased toxicity due to high drug retention [28].

Cationic 100-200 nm liposomes have been designed to target the tumor vasculature specifically with the aim of depleting oxygen and nutrient supply from the tumors [32]. PEGylated, cationic 1,2-dioleoyl-sn-glycero-3-phosphatidylcholine (DOPC): 1,2-diacyl-3-trimethylammonium propane (DOTAP):cholesterol:PEG-distearoylphosphatidylethanolamine (PEG-PE) liposomes were shown to preferentially accumulate in the tumor vasculature compared to normal vessels 24 hr after tail vein injection in tumor bearing mice [31]. It was found that cationic character in the liposomes improved specific targeting to tumor vessels and including PEG allowed for long-circulation of liposomes in the bloodstream without interfering with tumor vasculature uptake. Many preclinical trials in murine models of human cancer have been performed using cationic liposomes to show that delivering chemotherapeutics to tumor vasculature can suppress tumor growth [32]. For example, a cationic formulation

of doxorubicin encapsulating egg phosphatidylcholine (EPC):Chol:dimethyl dioctadecyl ammonium bromide (DDAB) (40:40:20) and PEG- PE was shown to increase mouse survival after tail vein injection at 5 mg/kg [33]. In addition, cationic cisplatin loaded hydrogenated soybean phosphatidylcholine (HSPC):Chol:3,5-dipentadecycloxybenzamidine hydrochloride (TRX-20) (50:42:8) and PEG-PE liposomes were administered through intracardiac injection at 3.5 mg/k [34]. It was found that these liposomes accumulated in the tumor and suppressed tumor growth and liver metastasis while significantly increasing the survival of the mice.

The success of preclinical trials using cationic liposomes for cancer treatment has led to clinical trials in humans. The cationic composition of DOTAP:DOPC:paclitaxel or fluorouracil (5-FU) (50:47:3), named EndoTAG-1, has been used in phase I, phase Ib, and phase II clinical trials [32,35]. In phase I trials, EndoTAG-1 using 5-FU was tolerated and safe in patients with advanced, metastatic gastrointestinal cancer. Patients with metastatic breast cancer were treated in phase II trials with EndoTAG-1 using paclitaxel, and it was found that after a dose of 0.55 mg/kg, 6% of patients had a partial response while 28% presented with stable disease. Nausea and vomiting related to the infusion were the main side effects. Ongoing phase II trials in patients with advanced pancreatic cancer are being conducted with EndoTAG-1 using paclitaxel in combination with gemcitabine. It has been shown that 75% of patients survived after 1 year, demonstrating the effectiveness of using this liposome formation for treatment of advanced pancreatic cancer [35].

Other methods of targeting tumors include conjugation of tumor-specific mAbs and peptides. Immunoliposomes made from soy phosphatidyl choline (PC):Chol:cyanur-

PEG_{2000}-PE:3,3′-dioctadecyloxacarbocyanine perchlorate (DiO) in a ratio of 64.5:30:5:0.5 mol% were conjugated with anti- vascular cell adhesion molecule (a-VCAM) monoclonal antibody since VCAM1 is overexpressed on tumor vessels [36]. After intravenous injection of the liposomes in mice with human Colo677 non-small cell lung tumor xenografts, it was found that the immunoliposomes selectively targeted the tumor vascular endothelial cells. Some concerns still remain regarding the specificity of these immunoliposomes due to the presence of VCAM1 expression by healthy endothelial cells. For increased specificity, the commercially available Doxil (PEGylated liposomal doxorubicin) was modified with PEG_{3400}-DSPE conjugated to the 2C5 mAb to bind to cancer cells but not normal cells [37]. This liposome formulation was able to increase the efficacy of doxorubicin by suppressing the growth of breast, colon, and prostate cancer tumors in mice.

Another study used *in vivo* phage display to probe specific antibodies that target tumor vessels for anti-angiogenic purposes [38]. Doxorubicin-loaded PEGylated DSPE liposomes conjugated with specific tumor endothelial cell targeting peptides PIVO-8 and PIVO-24 were shown to enhance the efficacy of the chemotherapeutic in lung, breast, liver, pancreatic, and colon cancer xenografts by significantly decreasing vessel density in solid tumors, increasing cancer cell death, and inhibiting tumor growth. Targeting tumor angiogenesis is not sufficient to remove a tumor completely. Tumors are able to receive nutrients and oxygen from surrounding tissue. To combat this, multifunctional liposomes have been fabricated that target not only the tumor vasculature but also the surrounding tumor cells [39]. Doxorubicin loaded immunoliposomes were made from HSPC:CHOL:DSPE-PEG_{2000}:DSPE-PEG_{2000}-maleimide and conjugated to the NGR

peptide that targets an angiogenic endothelial cell marker to bind and kill angiogenic blood vessels. The immunoliposomes were also modified with anti-GD_2 mAbs, an antibody to a disialoganglioside receptor expressed in neuronal cancer cells, for targeting the tumor periphery independent of the vasculature. The two liposomal formulations were administered sequentially, and a synergistic effect was observed where tumor proliferation was inhibited and endothelial cell density decreased significantly in neuroblastoma animal models.

Liposomes have been shown selectively target tumor vasculature using the EPR and also specific targeting ligands. Although many limitations still exist, including the inability to remove the entire tumor, liposome formulations have been shown to reduce tumor size and increase survival in animal models. Cationic lipids are currently being tested in human clinical trials for multiple advanced cancers. Using liposomes for targeting tumors is promising and a number of targeted treatments may successfully translate into the clinic in the near future.

1.3.3 Liposomes and the Immune System

Immunosuppression and immunostimulation via nanoparticle systems, particularly liposomes, has been widely investigated. Liposomes have been engineered to target and interact with immune cells but have also been designed to avoid immune detection. Activation of the immune system is highly desirable when developing vaccines or enhancing immune responses to diseases such as cancer. Immunosuppression, on the other hand, is necessary to a certain degree when introducing a drug delivery vehicle in the body. Systemically-administered drug carriers

tend to be rapidly cleared from the bloodstream by the immune system. Drug carriers must therefore elude detection in order to prolong their circulation time and increase their binding efficiency. Autoimmune disorders, characterized by a marked increase in an immune response against healthy cells, can also evidently benefit from a modulated immune inhibitory effect induced by drug carriers.

Liposomes are ideal immunoadjuvants because of their safety, ability to encapsulate a wide variety of molecules and most importantly because of their high accumulation in the RES organs [40]. They may have covalently attached antigens on their surface or may encapsulate antigens in order to elicit an immune response. Liposome-based vaccines against HIV, hepatitis, tuberculosis, influenza and malaria have been investigated [41–45]. For example, Schwendener et al. reported methods of liposomal vaccine preparations based on encapsulation of antigenic peptides derived from the hepatitis C virus and plasmid DNAs encoding glycoproteins of the lymphocytic choriomeningitis virus [46]. Vaxfectin, a cationic lipid-based adjuvant for influenza vaccines was shown to elicit the strongest antibody response *in vivo* when compared to the commercially available seasonal trivalent influenza vaccine [42]. Steers et al. formulated a liposome-based HIV vaccine composed of lipid A and encapsulating the antigen Gag p24, which is often used in HIV-1 vaccine candidates. Results demonstrated that liposomal carrier induced activation of CD4+ and CD8+ T-cells in the spleen and lymph nodes of mice [47]. Liposomes have also been proposed as a means to enhance cell-mediated immunity in general, i.e. without targeting a specific disease. For example, Inoue et al. reported an induced natural killer T (NKT) cell response *in vivo* by liposomes composed of DOTAP:DOPE, cholesterol and a glycosphingolipid

[48]. Liposomal vaccine administration routes other than systemic delivery have also been pursued. Nasal and transcutaneous vaccinations have been reported [47,49]. Liposomes for nasal immunization formulated with mannotriose (Man3), dipalmitoylphosphatidylethanolamine (DPPE), and coated with a neoglycolipid showed an increase in uptake by antigen presenting cells (APCs) when compared to non-coated control liposomes [50].

Inflammation is a natural immune response and represents one of the key characteristics of autoimmune diseases, organ transplant rejections, and inflammatory disorders such as asthma. Most liposome studies have therefore focused on combating inflammation by encapsulating anti-inflammatory drugs or immune inhibitors. Recently, a study done by Capini et al. showed that egg phosphatidylcholine liposomes, which encapsulated a lipophilic innate immune inhibitor (NF-κB) and ovalbumin, induced antigen-specific tolerance in a rheumatoid arthritis mouse model [51].

Immunosuppression is crucial for successful organ transplantations. Liposomal nanocarriers have been used to target immune cells as a way to decrease the incidence of graft-versus-host disease. In 2009, a clinical trial involving patients receiving a liposome-based immunosuppressant after a lung transplant was reported. Typical immunosuppressant drug therapy is systemically administered and has not proved to be effective; the leading cause of death after lung transplantation is immune rejection. Aerosolized SUVs 40 to 50 nm in diameter encapsulating cyclosporine A (CsA), an interleukin-2 inhibitor blocking T-lymphocyte proliferation, were administrated to patients via electronic nebulizers. Results showed that intrapulmonary deposition of the liposomal drug carrier was therapeutically relevant and well tolerated by the patients

[52]. However, further long-term clinical trials must assess the efficacy of the liposomal drug solution in terms of reducing the mortality rate caused by immune rejection in patients with lung transplants. Cationic liposome-DNA complexes have also been investigated as a possible vaccine against asthma [53]. A vaccine composed of Ag proteins and liposome-DNA complexes was administered to allergen-sensitized mice and results showed the vaccine could induce production of allergen-specific T cells and diminish the development of airway hyper-responsiveness, a hallmark of asthma.

1.4 The Endothelium as a Drug Delivery Target

Endothelial cells were once thought of as a quiescent cell population having no specific function other than being a nonreactive barrier to protect tissues [54]. However, the endothelium is at the interface between the bloodstream and tissues, thus giving it the important function of regulating the transport of molecules and cells into tissues. In the late 1980s and early 1990s it was established that the endothelium responded to various cytokines including interleukin-1α and β (IL-1α and β), tumor necrosis factor (TNF), lymphotoxin (LT), interferon-γ (IFN-γ) and transforming growth factor-β (TGF- β), during processes such as immune responses, angiogenesis and activation [42,55,56]. It was shown that exposure of endothelial cells to these cytokines (IL-1 and TNF) increased the expression of cell adhesion molecules, such as ICAM1, ICAM2, and VCAM1 and members of the selectin family including E-selectin, L-selectin, and P-selectin [42,54,56,57]. Studies also showed that the levels of these cellular adhesion molecules and selectins were elevated 2-, 3-, and up to 23-fold in numerous

diseased conditions such as inflammation, atherosclerosis, hypertension, diabetes, septic shock, tumor metastasis, arthritis, gastrointestinal inflammation, asthma, adult respiratory distress syndrome, ischemia and reperfusion injury, vasculitis, hepatic diseases, renal diseases, central nervous system diseases and transplant rejections [58–61].

Drug delivery systems targeting the endothelium have taken advantage of the increased surface expression of CAMs and selectins on diseased endothelial cells. Liposomes, in particular, represent one of the most studied drug delivery systems targeting the endothelium due to their stability under physiological conditions, biocompatibility, ease of fabrication, homogeneity, narrow size distribution, and ability to encapsulate both hydrophilic and hydrophobic drugs [62]. Liposomes decorated on the surface with antibodies aE-selectin, aICAM1, aVCAM1 or a combination of these has been studied [31,36,63–66]. For example, Gosk et al. reported successful selective *in vitro* and *in vivo* targeting of tumor blood vessels by aVCAM1-conjugated liposomes [36].

One of the major challenges to deliver drugs to the endothelium is the rapid clearance of the drug carrier from the bloodstream by the reticuloendothelial system (RES) in addition to rapid renal clearance and hepatic uptake. This problem has been addressed by sterically stabilizing the liposomes through the use of PEG, as previously mentioned, which provides a barrier against antibody opsonization. Spragg et al. prepared pH-sensitive, cationic and classical liposomes in addition to sterically stabilized liposomes conjugated with aE-selectin. After activation with IL-1β, human vein endothelial cells (HUVECs) showed increased binding of classical and sterically

stabilized liposomes [63]. Although PEG has been extensively studied and has been shown to greatly extend circulation time of drug delivery vehicles, some disadvantages such as immunological reactions, changes in pharmacokinetic behavior, non-biodegradability, and toxicity of side-products still exist [67]. Recently, Parodi et al. reported a clever way to circumvent the problem of immediate detection and clearance by the immune system without the use of PEG. They cloaked silica nanoparticles with freshly harvested leukocyte membranes, which were able to retain critical transmembrane proteins that allowed them to selectively bind inflamed ECs [68].

1.5 Thesis Hypothesis and Experimental Strategy

Motivated by the current need to address limitations in the treatment and diagnosis of atherosclerosis, we decided to design a leukocyte-inspired liposomal based drug delivery system that directly targeted inflamed endothelium. We hypothesized that increased diffusivity of targeting antibodies to VCAM1 and E-selectin, facilitated by increased liposomal membrane fluidity, may improve the targeting efficiency of liposomes. Our experimental strategy to test this dissertation's hypothesis developed into three separate aims; a brief description of each aim is provided below.

In aim 1, we characterized both our liposomal and endothelial cell systems to set a foundation for experiments in aim 2. We hypothesized that the lateral diffusivity of antibodies aVCAM1 and aE-selectin increased with increasing liposomal membrane fluidity. Based on these results, we were able to lay the groundwork that allowed us to examine the interaction between liposome and ECs as specified subsequently aim 2.

Aim 2 focused on evaluating liposomal targeting efficiency *in vitro*. We explored the question of how lateral diffusion of antibodies affected liposome targeting. As a result, we also investigated how low antibody surface densities and membrane fluidity played a role in EC binding and uptake.

The driving hypothesis of aim 3 was to evaluate the liposome targeting efficiency, with low and high antibody diffusivities, in a small rodent model of atherosclerosis. However, we were only able to complete a preliminary *in vivo* study where we examined the biodistribution of antibody coupled-PEGylated liposomes in healthy mice.

Chapter 2.

Endothelial Cell and Liposomal System Characterization

2.1 Introduction

The endothelium represents an ideal target for intravenous drug delivery because it plays an important role in numerous diseases such as atherosclerosis, inflammation, ischemia, cancer, and it is the first barrier between the bloodstream and tissue [62]. Leukocyte recruitment is a fundamental part of the inflammation process. Leukocytes are able to localize and extravasate thanks to the redistribution of various cell adhesion molecules, namely E-selectin, VCAM1, and ICAM1, from storage granules to the surface of vascular endothelial cells [56].

It is widely known in the field of endothelial cell biology, there are a number of molecules, which include interleukin-1, TNF-α, TNF-β, interferons, interleukin-2, interleukin-4, interleukin-6, and transforming growth factor-β (TGF-β) that stimulate the production of surface EC adhesion molecules [54,69]. Due to the myriad of studies present which have reported the use of different cytokine types, concentrations, and treatment times, we sought to characterize specific EC response to IL-1α and TNF-α in order to establish a good *in vitro* model to test the role liposome membrane fluidity plays in a targeted, drug delivery liposomal system.

Membrane fluidity is an important aspect in both cells and artificial membranes i.e. vesicles. It is now well known that components, such as flavonoids [70] and cholesterol [71], as well as the oxidation of unsaturated lipids [72] increase lipid membrane rigidity. Although the physical properties of DOPC and DSPC have been

previously characterized [73], the physical properties of our formulations, which include 5 mol % of 1,2-dioleoyl-sn-glycero-3-phosphoethanolamine-N-dodecanoyl (N-dod-PE) have not been fully examined.

In this aim, we determined how protein expression profiles of EC adhesion molecules changed as a function of cytokine type, dose, and treatment time. We focused on characterizing the antibody-lipid conjugation efficiency and on quantifying the antibody surface densities. Finally, we characterized two liposome formulations by measuring their lipid anisotropy and lateral diffusivity to quantify membrane characteristics important in targeting liposomes. This body of work provided a strong platform for succeeding *in vitro* experiments and enabled us to distinguish the differences between the physical properties of the two lipid formulations being tested.

2.2 Materials and Methods

2.2.1 Endothelial Cell Culture

Human umbilical vein endothelial cells (HUVECs) were grown in endothelial growth medium-2 (EGM-2) with supplements as described by the distributor (Lonza, Allendale, NJ). Cells were maintained at 37 °C in a humidified incubator with 5% CO_2 and used for experiments at passages 2 - 3. Growth medium was changed the day after cell seeding and every other day thereafter.

2.2.2 Endothelial Cell Gene Expression

HUVECs were seeded in 12 well plates and grown to confluence in EGM-2 media with 2% FBS. Cells were treated with 1, 10, or 25 ng/ml of TNF-α (Sigma Aldrich) or IL-1α (R&D Systems, Minneapolis, MN, USA) at 1, 5, or 10 ng/ml for 2, 4, 6, 12, or 24 h. Experiments were done in triplicate, and controls were performed with no cytokine treatment. Total RNA was isolated from cells using a Qiagen RNeasy Mini Kit following the manufacturer's procedures (Qiagen, Valencia, CA, USA). The cells were lysed immediately after each incubation time point. Quantitative reverse transcriptase polymerase chain reaction (qRT-PCR) was performed on a 7300 real-time PCR system using the Taqman method (Applied Biosystems, Carlsbad, CA, USA). An endogenous control of glyceraldehyde 3-phosphate dehydrogenase (GAPDH) was used, and evaluations were done in triplicate. All primers were obtained from Applied Biosystems. Relative expression levels of VCAM1, E-selectin, and ICAM1 were assessed.

2.2.3 VCAM1 and E-selectin Immunostaining

ECs (2 x 10^5 cells) were seeded on 18 x 18 mm^2 coverslips in 6-well plates with 2 ml media (VWR, West Chester, PA) and cultured overnight at 37 °C. Cells were incubated with IL-1α at 5 ng/ml or TNF-α at 20 ng/ml in fresh EGM-2 media the next day for 6 h or 24 h. After medium was removed, cells were rinsed with PBS three times and fixed with 4% formaldehyde in PBS at RT for 15 min followed by washing with PBS. Samples were blocked with 1% BSA in PBS (1% BSA) at 4 °C for 1 h. Samples were then stained with aVCAM1 and aE-selectin mAbs (10 ng/ml in 1% BSA) at 4 °C for 2 h and rinsed with PBS. Samples were incubated with FITC-conjugated goat anti-mouse

(1:300), TRITC-conjugated rabbit anti-sheep secondary mAbs (1:300) and Hoescht 33258 (1:1000) at 4 °C for 1 h followed by washing with PBS. Samples were then mounted on microscope slides (3" x 1", VWR, Radnor, PA) with VECTASHIELD® mounting medium (Vector Laboratories, Burlingame, CA), and sealed. Samples were examined under an Axiovert 200 inverted fluorescent microscope (Carl Zeiss, Thornwood, NY) equipped with a Hammamatsu CCD camera (Bridgewater, NJ). Digital images were captured with AxioVision digital image processing software (Zeiss).

2.2.4 VCAM1 and E-selectin Expression

VCAM1 and E-selectin expression by ECs was evaluated by flow cytometry after 1, 6, 12, and 24 h incubations with either IL-1α (5 ng/ml) or TNF-α (25 ng/ml). Quantification of the density of molecules on the surface was determined using Quantum™ Simply Cellular® microbeads. After ECs were activated with IL-1α or TNF-α, 10^6 cells were collected from a 6-well plate, spun down, and resuspended with ice cold 1% BSA. ECs were rinsed 3 times through suspension-spin cycles and blocked with 1% BSA for 30 min in an ice bath. ECs were incubated with mouse anti-human VCAM1 and sheep anti-human E-selectin mAbs (1 ml, 10 ng/ml) for 30 min in an ice bath. After rinsing with 1% BSA 3 times to remove free mAbs, ECs were stained with FITC-conjugated goat anti-mouse and TRITC-conjugated rabbit anti-sheep secondary antibodies for 30 min in an ice bath. ECs were finally rinsed with 1% BSA three times, resuspended in PBS, and analyzed by flow cytometry.

2.2.5 Measurement of Lipid Concentration

The concentration of lipid in solution was determined by a phosphate assay as previously described [74]. Briefly, a diluted liposome sample was ashed with 0.2 ml sulfuric acid (10% v/v) at 200°C for 1 h, followed by addition of 50 µl hydrogen peroxide (30% v/v) and further heating at 200°C for 40 min. After the sample was cooled down to room temperature, 480 ml deionized water and 0.5 ml of color reagent (0.5% w/v ammonium molybdate, 2% w/v ascorbic acid) were added to each sample followed by heating at 45°C for 20 min. The samples were read at 820 nm using a SpectraMax Plus 384 spectrophotometer (Molecular Devices, Sunnyvale, CA). A calibration curve was prepared with known phosphate quantities.

2.2.6 Antibody Surface Characterization

To determine the antibody density of aVCAM1 and aE-selectin, 2 µm borosilicate glass beads (Duke Scientific, Palo Alto, CA) were thoroughly washed three times in ethanol and water each through centrifugation-suspension cycles. Microbeads were suspended in a solution of 4% hydrogen peroxide and 4% ammonium hydroxide and incubated at 80 °C for 10 min, followed by a 10 min incubation at 80 °C in 4% hydrogen peroxide and 0.4 M HCl. Microbeads were washed 3 times after each incubation and immersed in PC:N-dod-PE (95:5) liposomes at the end. Liposomes and microbeads were agitated for 6 h and washed through centrifugation–suspension cycles to separate excess free liposomes. Conjugation of different ratios of FITC-conjugated aE-selectin, PE-conjugated aVCAM1, and FITC-conjugated IgG_1 (nonspecific binding control) to microbeads was performed using EDC/NHS chemistry. Fluorophore labeled primary antibodies were separated using suspension–spin cycles. The density of aE-selectin

and aVCAM1 conjugated to the microbeads was determined with reference to Quantum Simply Cellular microbeads (Bangs Laboratory, Inc., Fishers, IN), which have defined numbers of antibody binding site per bead. In addition, confocal microscopy of microbeads conjugated with FITC-conjugated aE-selectin, PE-conjugated aVCAM1, and FITC-conjugated IgG_1 was performed in order to verify conjugation prior to evaluation with flow cytometry. Samples were examined under a Zeiss LSM710 upright confocal microscope (Carl Zeiss, Thornwood, NY).

2.2.7 Fluorescence Polarization

A 1:200 mol Bodipy® FL (Life Technologies/Thermo Fisher Scientific, Grand Island, NY):lipid was added to the different lipid mixtures of 1,2-di-(9Z-octadecenoyl)-*sn*-glycero-3-phosphocholine:1,2-dioleoyl-sn-glycero-3-phosphoethanolamine-N-dodecanoyl (DOPC):(N-dod-PE), 1,2-distearoyl-*sn*-glycero-3-phosphocholine (DSPC):N-dod-PE as well as pure DOPC and DSPC. Lipid mixtures were dried under a nitrogen stream and liposomes were prepared as mentioned in the previous section. The final lipid concentration was kept at 1 mM. Fluorescence polarization was measured at 22 ºC and 37 ºC at excitation wavelength of 500 nm using a SpectraMax Gemini XS plate reader (Molecular Devices, Sunnyvale, CA). Fluorescence anisotropy (A) values were calculated using the equation below:

$$r = \frac{I_{\parallel} - I_{\perp}}{I_{\parallel} + 2I_{\perp}} \qquad (2.1)$$

where $I_{\parallel}$ and $I_{\perp}$ correspond to the fluorescence intensities in the parallel and perpendicular directions, respectively, with respect to the polarized excitation wave.

2.2.8 Preparation of Supported Lipid Bilayers

Supported lipid bilayers (SLBs) were prepared as described previously [75]. Briefly, small unilamellar vesicles were prepared via extrusion as mentioned previously. Lipid films were dried under nitrogen gas and rehydrated with Tris-HCl buffer (10 mM Tris, 150 mM NaCl, 2 mM $CaCl_2$, adjusted with HCl to pH 7.5). The final lipid concentration was kept at 1 mg/ml. To induce fusion, glass bottom dishes were cleaned by sonicating for 10 min subsequently in 3 M NaOH, 100% ethanol, and ultra pure distilled water. The glass bottom dishes were then dried and exposed to air plasma (Plasma System Femto PCCE, Diener Electronic) at maximum power for 1.5 min to produce a hydrophilic surface. A 1:20 liposome:Tris-HCl buffer volume ratio were deposited onto the clean glass surface and incubated for 1 h. After 1 h, excess unfused liposomes were removed by carefully washing with ultrapure water. Bilayers were kept hydrated at all times.

2.2.9 Fluorescence Recovery After Photobleaching (FRAP)

FRAP studies were conducted with a Zeiss LSM710 upright confocal microscope utilizing the 561 nm laser (Carl Zeiss, Thornwood, NY) and a 63X water immersion objective. Digital 2D images were captured and analyzed with Zen 2012 digital image processing software (Zeiss). Further FRAP analysis was done with ImageJ and Matlab. SLBs were labeled with 0.5 mol% rhodamine conjugated DOPE. A circular region of 20 nm in diameter was photobleached for 0.04 s after initially monitoring bilayers for 0.15 s and recovery was monitored for a total of 4.5 s. A total of 20 regions were photobleached (5 per sample). Frame size was set to 4.32 μm by 4.32 μm or 48 x 48 pixels (0.09 μm/pixel). Frames were acquired every 0.04 s. Laser was utilized at 50%

power to acquire images and further increased to 100% when photobleaching the lipid bilayers. All photobleaching settings remained the same for all samples. Images were normalized by dividing the post-bleach fluorescence intensities by the first pre-bleach intensity.

2.3 Results

2.3.1 Gene Expression Profiles of Cell Adhesion Molecules

As a way to optimally reproduce inflammatory conditions *in vitro*, endothelial cells were exposed to different cytokines at various concentrations and incubation times. VCAM1, E-selectin, and ICAM1 are cell adhesion molecules known to be upregulated on the surface of endothelial cells when immersed in an inflammatory environment. The HUVEC gene expression profiles of VCAM1, E-selectin, and ICAM1 were determined as shown below in **Figures 2.1 and 2.2** [76]. ECs were exposed to 1, 10, and 25 ng/ml of TNF-α for 2, 6, and 24 h and then harvested and lysed. As can be seen on **Figure 2.1 (A)**, VCAM1 gene expression increased with increasing exposure time at all cytokine concentrations, but peaked after 24 h exposure to 25 ng/ml of TNF-α. Both E-selectin and ICAM1 gene expression, as shown in **Figure 2.1 (B)** and **(C)**, respectively, followed this exact same trend having their maximum expression levels after 24 h exposure to TNF-α. HUVECs were also exposed to 1, 5, and 10 ng/ml of IL-1α. VCAM1 gene expression was highest after 6 h of exposure to the cytokine at all three concentrations as shown in **Figure 2.2 (A)**. E-selectin gene expression followed the same trend as VCAM1, having highest expression levels after a 6 h exposure to the

cytokine (**Figure 2.2 (B)**). E-selectin gene expression levels also reached a maximum when exposed to 5 ng/ml of IL-1α. ICAM1 gene expression exhibited the lowest levels of all three cell adhesion molecules. Activation of HUVECs with 5 ng/ml IL-1α for 6 h provided the maximum upregulation of all three cell adhesion molecules. Based on these results, we chose to focus only on VCAM1 and E-selectin with the remainder of experiments going forward.

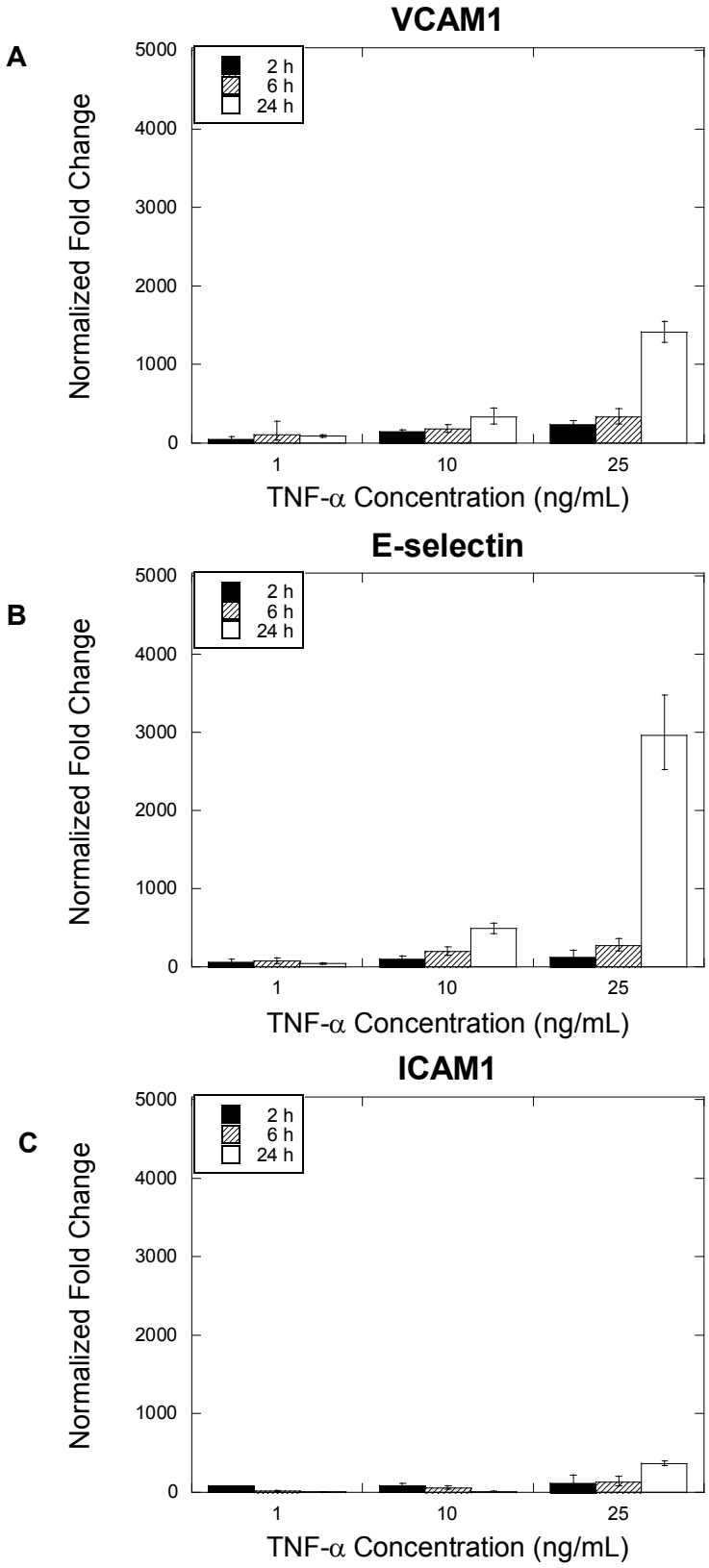

Figure 2.1: HUVEC gene expression profiles after exposure to TNF-α. Profiles of (A) VCAM1, (B), E-selectin, and (C) ICAM1 after treatment with 1-25 ng/ml TNF-α for 2 - 24 h.

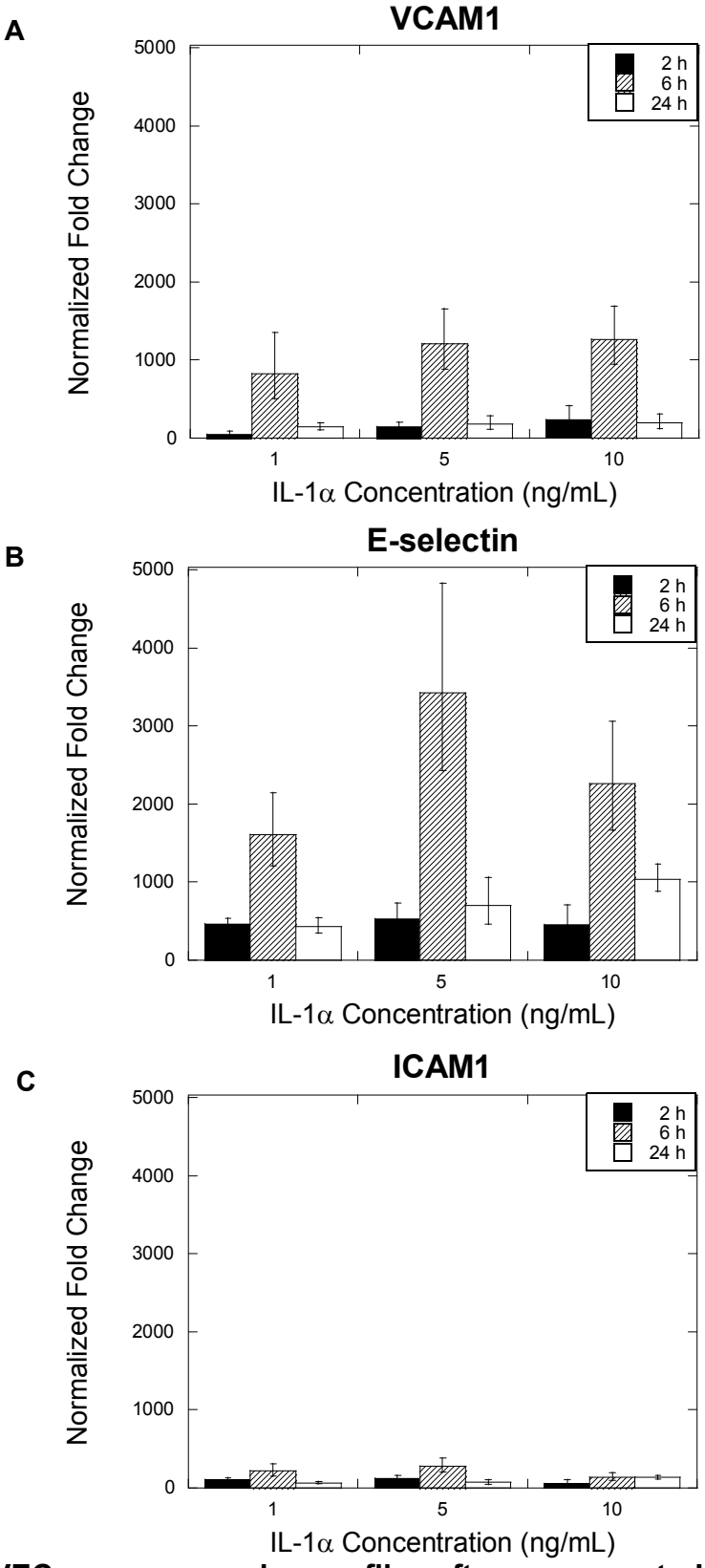

Figure 2.2: HUVEC gene expression profiles after exposure to IL-1α. Profiles of (A) VCAM1, (B), E-selectin, and (C) ICAM1 after treatment with 1-10 ng/ml IL-1α for 2 - 24 h.

2.3.2 Protein Expression of VCAM1 and E-selectin

After the gene expression profiles of the three main cell adhesion molecules present in inflammation were examined, we decided to evaluate the expression of VCAM1 and E-selectin over the course of 24 h. The results are shown below in **Figures 2.3** and **2.4**. HUVECs were activated with 25 ng/ml TNF-α and 5 ng/ml IL-1α. Flow cytometry results showed VCAM1 expression increased consistently with increasing activation times. E-selectin expression peaked after the 6 h activation time with both cytokines and declined thereafter. Upregulation of VCAM1 and E-selectin was also qualitatively evident after immunostaining ECs at the 6h and 24 h incubation points. Given that we confirmed 5 ng/ml of IL-1α for 6 h produced the highest upregulation of both VCAM1 and E-selectin, we decided to perform all subsequent *in vitro* experiments under these conditions.

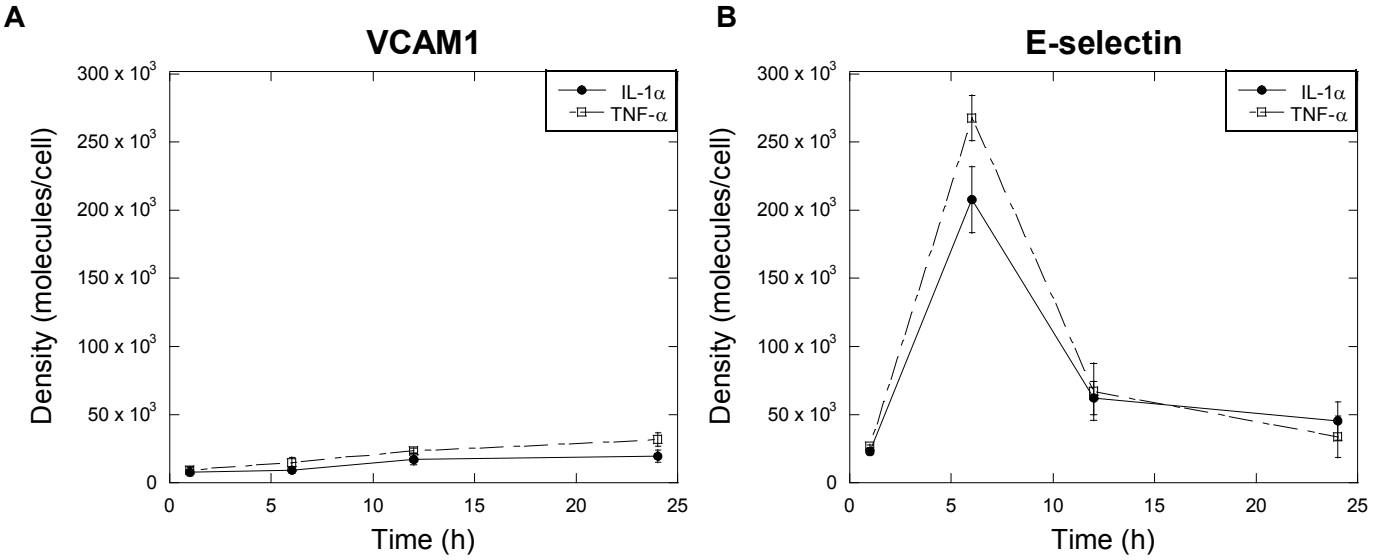

Figure 2.3: Time-course expression of VCAM1 and E-selectin on TNF-α and IL-1α activated ECs. ECs were activated with either TNF-α or IL-1α for various durations. Expression of VCAM1 (A) and E-selectin (B) was determined using flow cytometry as a function of time. Error reported is standard error with n = 3.

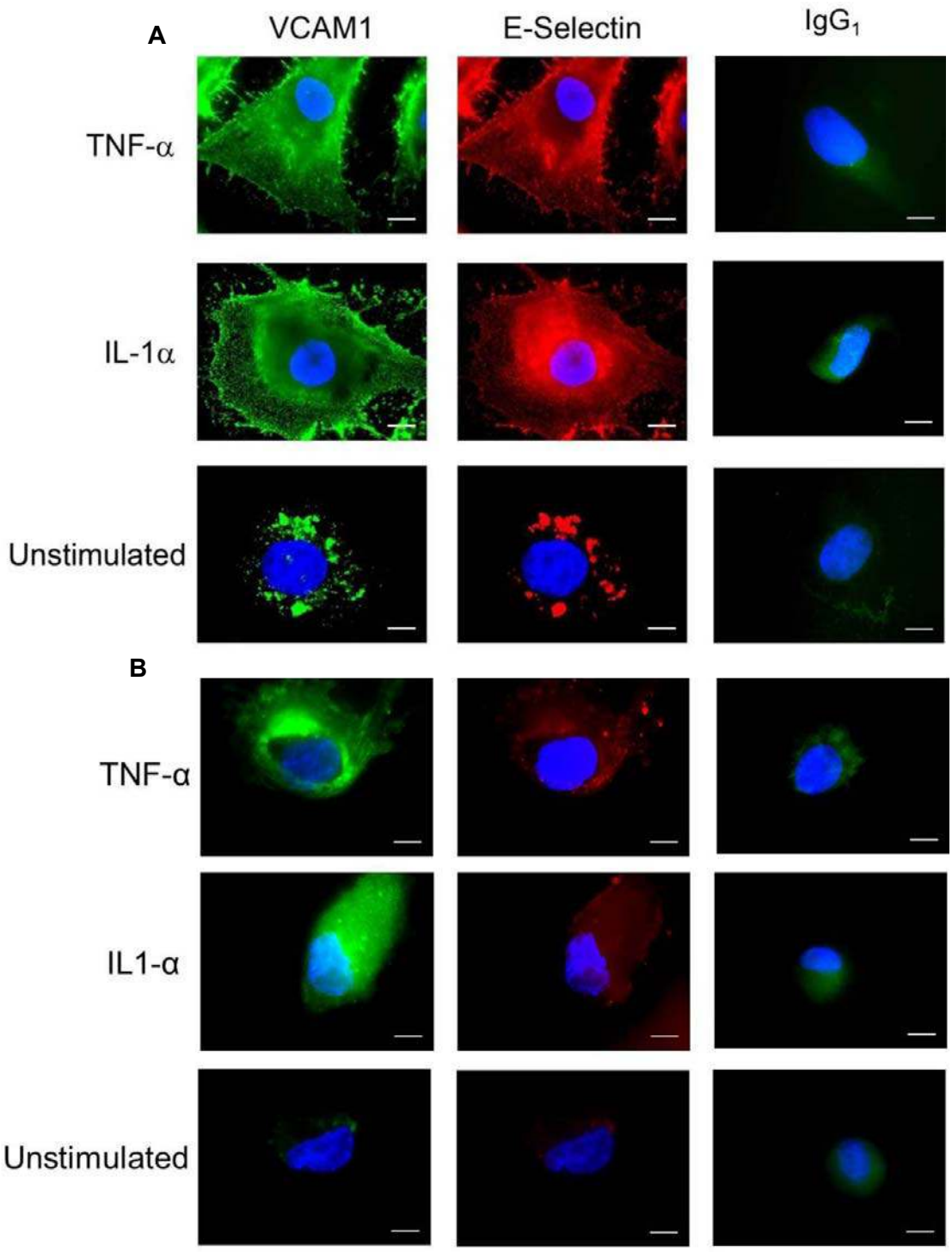

Figure 2.4: VCAM1, E-selectin, and IgG_1 isotype control immunostaining for TNF-α and IL-1α-activated and non-activated ECs. ECs were activated with TNF-α and IL-1α for 6 h (A) and 24 h (B), then fixed, and immunostained with aVCAM1 and aE-selectin. Scale bar, 10 μm.

2.3.3 Characterization of Lipid Coated Glass Microbeads

Lipid coated microbeads were used to quantify the antibody surface density of liposomes. Borosilicate glass microbeads were coated with a lipid bilayer conjugated with fluorescently tagged aVCAM1 and aE-selectin. In this manner, the number of antibody molecules on the surface of the beads was calculated by detecting the mean fluorescence intensity of each bead population via flow cytometry. The lipid concentration of liposomes used to coat the microbeads was determined by a phosphate assay. A standard calibration curve, shown below in **Table 2.1** and **Figure 2.5**, correlating the phospholipid amounts to absorbance units was used to calculate final lipid concentration after the last extrusion step. Once the concentration was known, the correct concentration of liposomes was added to the glass microbeads to begin the coating process. It should be noted that all lipid concentrations were calculated in this manner for each experiment involving liposomes throughout all aims.

Table 2.1: Phosphate Assay Standard Calibration Curve.

Volume of Lipid (µl)	Phosphate Concentration (nmol)	Average Absorbance (A.U.)
0	0	0.03
2	6.4	0.20
4	12.7	0.42
8	25.4	0.79
10	31.8	1.02

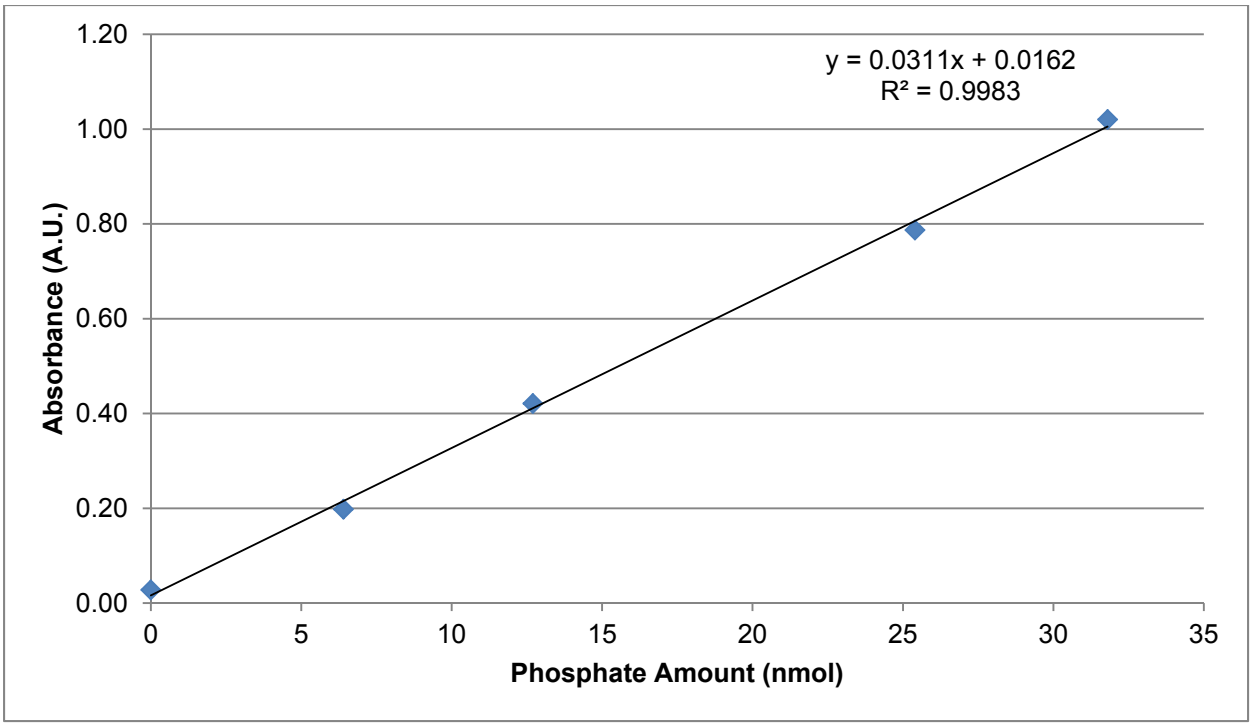

Figure 2.5: Determination of lipid concentration utilizing a phosphate assay. Sample of a standard calibration curve used to correlate absorbance values to known lipid amounts in order to calculate concentrations of liposome samples using a standard linear regression equation.

In order to corroborate vesicle rupture and successful coating, glass microbeads were agitated with liposomes containing 0.5% rhodamine-DOPE and imaged after removing excess liposomes. Complete coverage of microbeads by lipid membranes was evident and can be observed in **Figure 2.6 (A)**. A new batch of microbeads was lipid-coated and conjugated with PE-conjugated aVCAM1 (**Figure 2.6. (B)**) and FITC-conjugated aE-selectin (**Figure 2.6. (C)**). The images confirmed not only successful lipid coating of microbeads, but also successful conjugation of both antibodies.

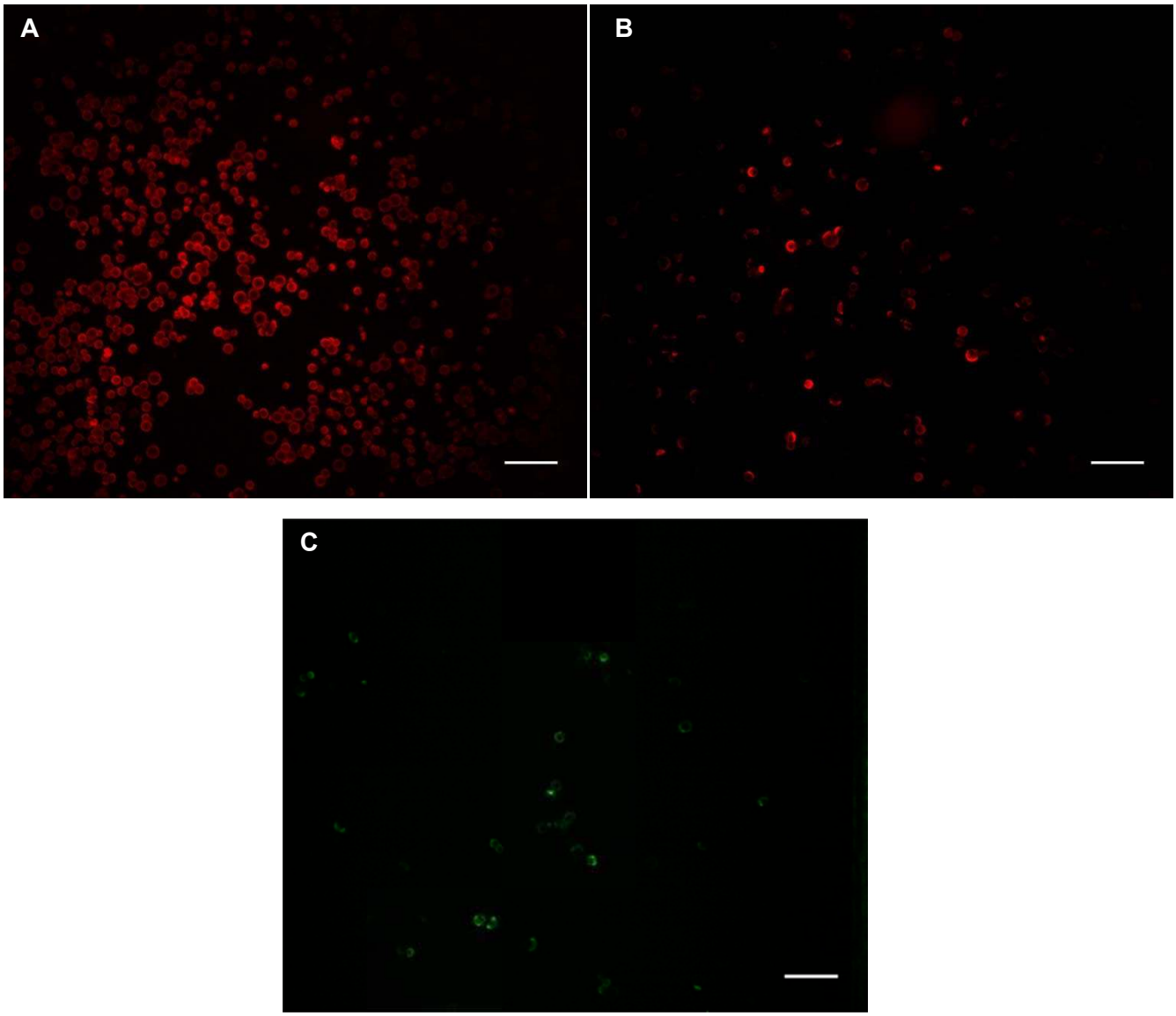

Figure 2.6: Lipid Coated Microbeads. Confocal microscopy of borosilicate glass microbeads coated with 94.5:5:0.5 DOPC:N-dod-DOPE:Rhodamine-DOPE bilayers (A). Lipid coated microbeads were then conjugated with PE-conjugated aVCAM1 (B) and FITC-conjugated aE-selectin (C). Scale bar, 25 μm.

2.3.4 Quantification of Antibody Surface Densities

Antibody density characterization was determined by using standardized microbeads that have calibrated binding sites on their surfaces and allow the user to correlate fluorescence intensity to number of bound antibody molecules. In light of investigating the effect of liposomal membrane fluidity on EC uptake and binding, we characterized our two lipid formulations, 95:5 DOPC:N-dod-PE and 95:5 DSPC:N-dod-PE, composed of unsaturated and saturated lipids, respectively (**Figure 2.7 (A) and (B)**). The average antibody density at the maximum concentration of aE-selectin and aVCAM1 averaged 1108 ± 119 and 940 ± 394 molecules/μm^2 for DOPC coated beads, and 1040 ± 228 and 1449 ± 261 for DSPC coated beads. At the lowest concentration of antibodies, only 148 ± 15 of aE-selectin and 64 ± 10 of aVCAM1 molecules/μm^2 were present on DOPC coated beads while only 108 ± 62 aE-selectin and 142 ± 24 aVCAM1 molecules/μm^2 were present on DSPC coated beads. These values were converted to the number of antibody molecules/liposome and are shown on **Table 2.2**. Our results were consistent with previously reported antibody surface densities on drug delivery vehicles [65,77,78].

DSPC exhibited a stronger PE-VCAM1 signal compared to DOPC conjugated with PE-VCAM1. However, only mean fluorescence intensities conjugated with 0.5% PE-VCAM1 between these two conditions were found to be significantly different ($p < 0.05$). The differences between the remaining concentrations were found to not be statistically significant ($p > 0.05$). DSPC conjugated with PE-VCAM1 also exhibited higher fluorescence values compared to DSPC conjugated with FITC-E-selectin, but none of the mean fluorescence intensities were found to be significantly different ($p >$

0.05). Additionally, one cannot directly compare antibody binding capacities if a different fluorophore is utilized between conditions due to the difference in fluorophore size and brightness [79]. In this case, we were forced to utilize two different fluorophores, FITC and PE, simultaneously because we needed to quantify the 1:1 VCAM1:E-selectin DOPC and DSPC conditions.

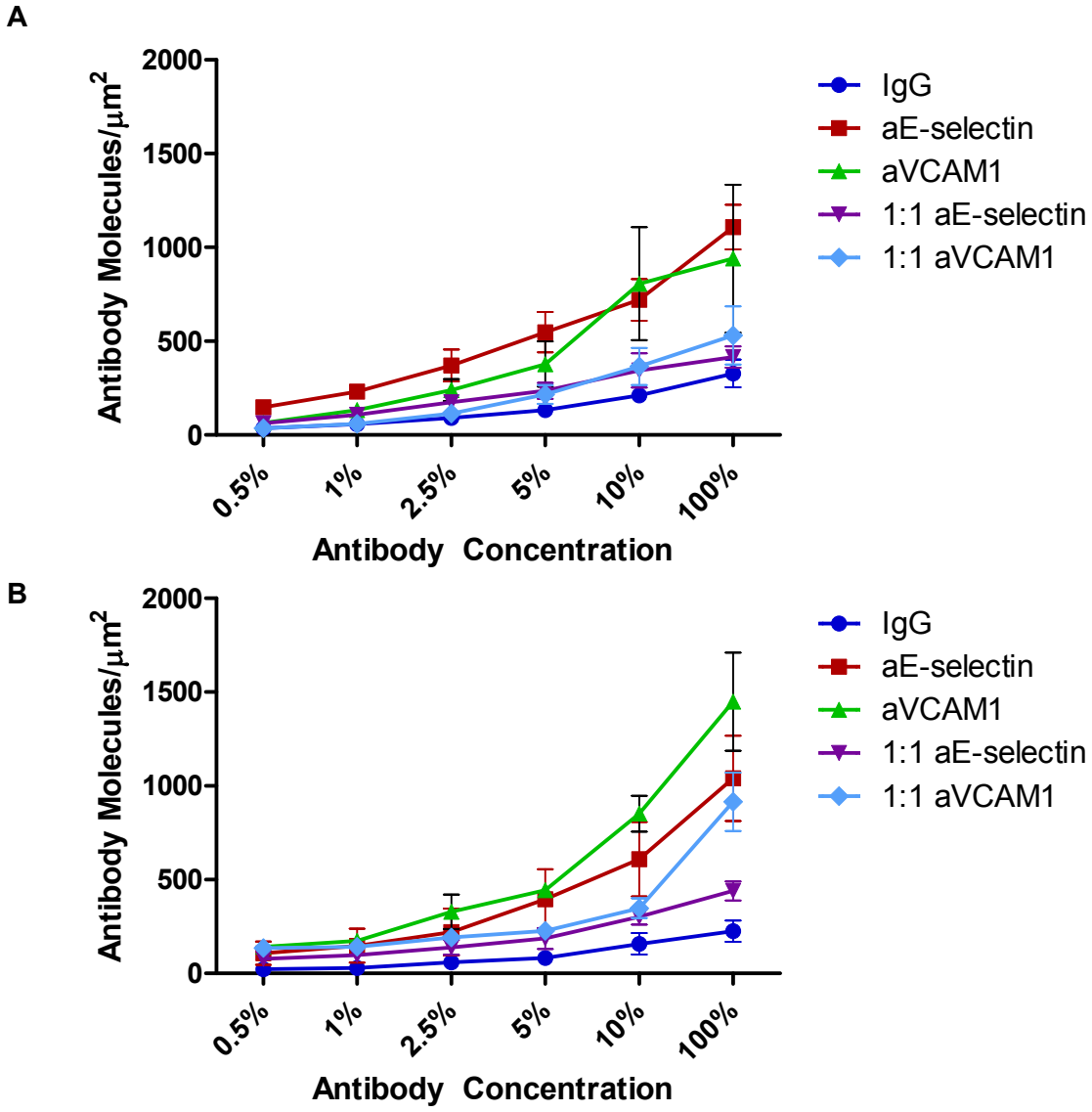

Figure 2.7: Characterization of Antibody Surface Density. DOPC (A) and DSPC (B) coated borosilicate glass beads were conjugated with different antibody concentrations

Figure 2.7 (Continued): and ratios and quantified via flow cytometry. Error bars are reported as standard deviation with n = 3.

Table 2.2: Calculation of Number of Antibody Molecules per Liposome. The average number of antibody molecules per liposome was converted from the values shown in **Figure 2.7**. Lipid coated glass beads were conjugated with 1:1 PE-labeled aVCAM1: FITC-labeled aE-selectin simultaneously and assayed by flow cytometry twice in order to measure both PE and FITC signals. It was assumed liposomes had a diameter of 100 nm.

	Average			Standard Deviation	
	DOPC	DSPC		DOPC	DSPC
0.5% IgG	1	1		1	1
1% IgG	2	1		1	1
2.5% IgG	3	2		1	1
5% IgG	4	3		1	1
10% IgG	7	5		1	2
100% IgG	10	7		2	2
0.5% aE-selectin	5	3		1	2
1% aE-selectin	7	5		1	3
2.5% aE-selectin	12	7		3	4
5% aE-selectin	17	12		3	5
10% aE-selectin	23	19		3	6
100% aE-selectin	35	33		4	7
0.5% aVCAM1	2	4		1	1
1% aVCAM1	4	5		1	1
2.5% aVCAM1	8	10		2	3
5% aVCAM1	12	14		4	1
10% aVCAM1	25	27		9	3
100% aVCAM1	30	46		12	8

Table 2.2 (Continued).

0.5% 1:1 FITC-labeled aE-selectin	2	2		1	1
1% 1:1	3	3		1	1
2.5% 1:1	5	4		1	1
5% 1:1	7	6		1	2
10% 1:1	11	9		3	1
100% 1:1	13	14		2	2
0.5% 1:1 PE-labeled aVCAM1	1	4		1	1
1% 1:1	2	4		1	1
2.5% 1:1	4	6		1	1
5% 1:1	7	7		2	1
10% 1:1	11	11		3	2
100% 1:1	17	29		5	5

2.3.5 Characterization of Membrane Fluidity

Differences in membrane fluidity were assessed by fluorescence polarization as reported previously [80]. To determine membrane fluidity, the fluorescence intensity of a hydrophobic fluorophore that inserts itself within the lipid bilayer was measured. We utilized the hydrophobic dye BODIPY® FL as our membrane probe. Higher anisotropy values corresponded to decreased probe motion within the bilayer and hence increased membrane rigidity. DSPC is a saturated lipid (**Figure 2.8 (A)**) that has a melting transition temperature (T_m) of 55 °C and it is therefore in the solid gel phase (L_β) at 22 °C and 37 °C. On the other hand, DOPC is an unsaturated lipid (**Figure 2.8 (B)**) that has a T_m of -20 °C and it is in the liquid crystalline phase (L_α) at these same temperatures. Our fluorescence anisotropy results reflect the difference in both of these lipids' phases (**Figure 2.9**). The decrease in DOPC's anisotropy values when N-dod-

PE, whose chemical structure is shown in (**Figure 2.8 (C)**), is introduced may indicate a higher fluidity is observed possibly due to imperfections in the lipid packing order of the membrane caused by the presence of phosphoethanolamines in the lipid composition [81]. The differences between 100% and 95:5 DSPC were determined to not be significant.

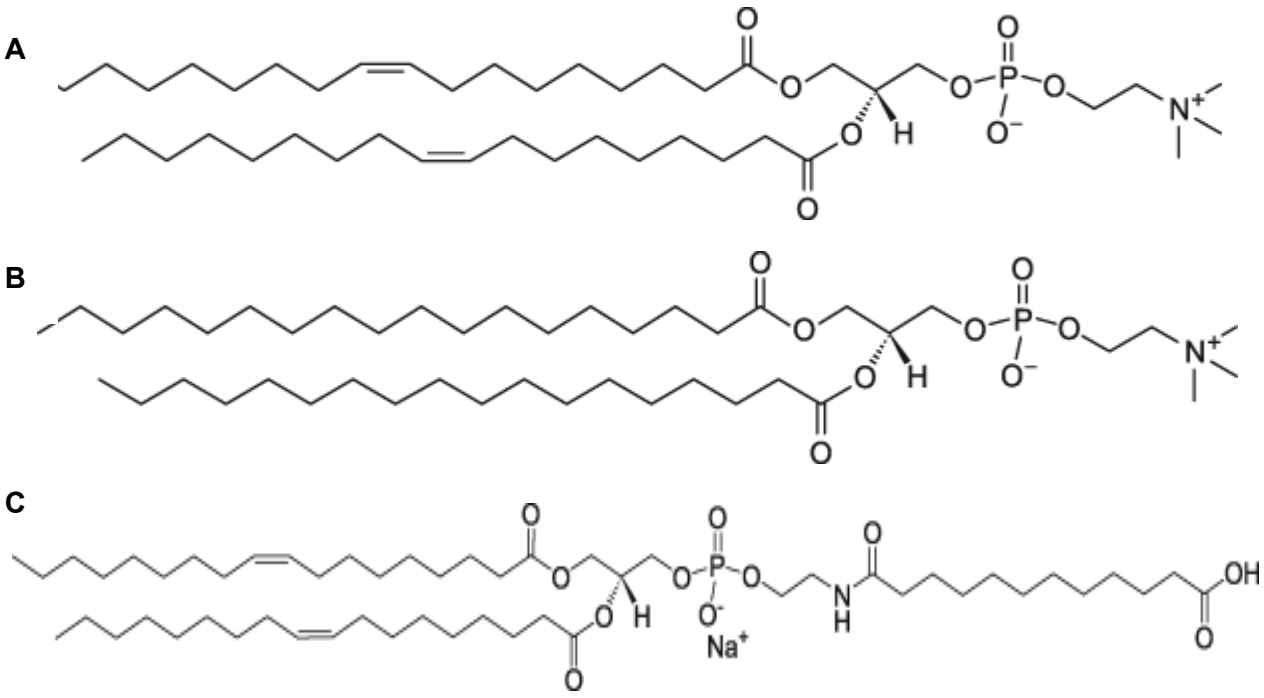

Figure 2.8: Chemical structures of lipids. Chemical structures of unsaturated DOPC (A), saturated DSPC (B), and antibody lipid anchor N-dod-PE (C) are shown.

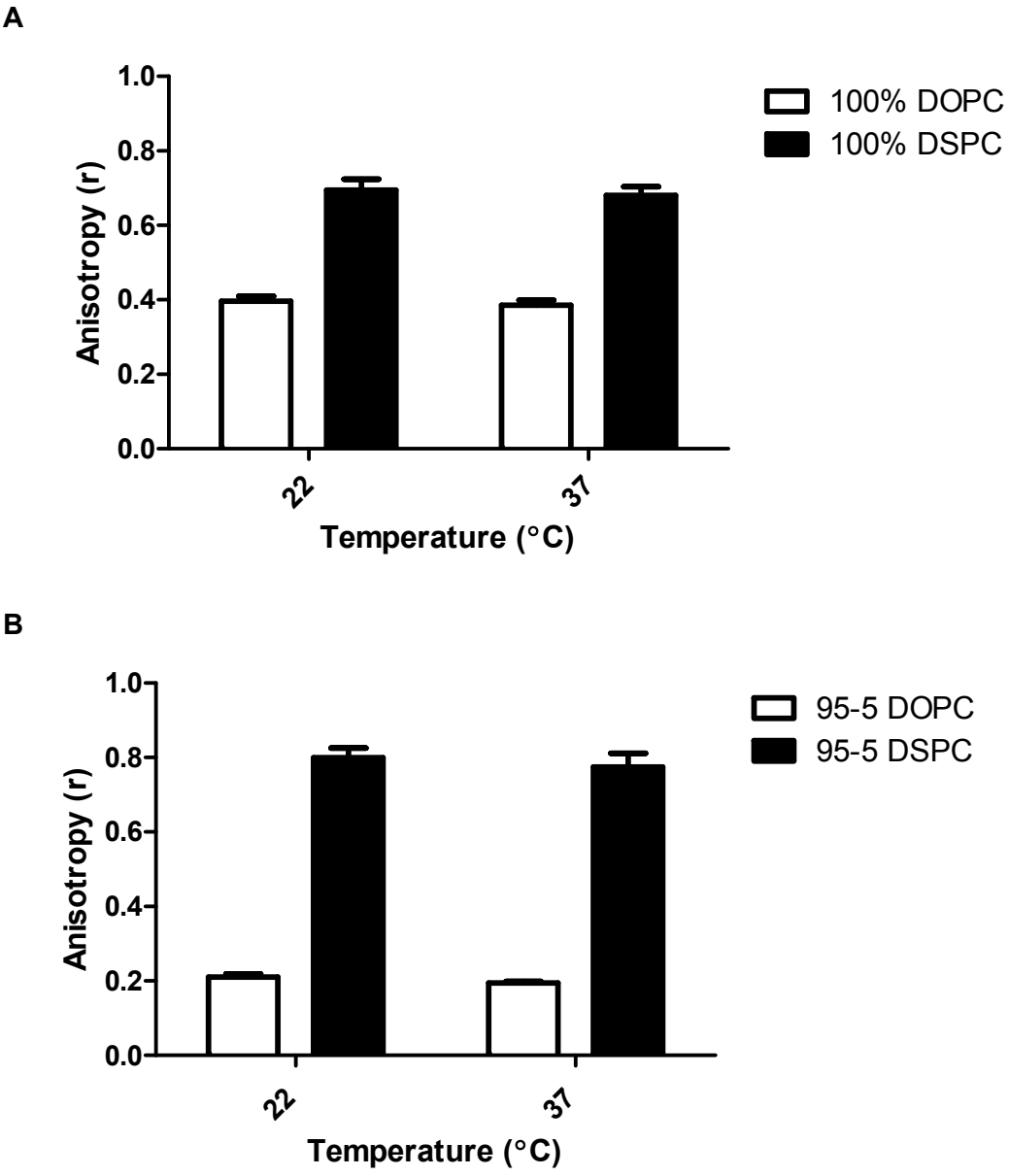

Figure 2.9: Characterization of Membrane Fluidity. Fluorescence anisotropy values of both 100 mol% DOPC and DSPC (A) and DOPC:N-dod-PE and DSPC:N-dod-PE (95:5 mol:mol) (B). Measurements were taken at 22°C and 37°C. Error bars are reported as standard deviation with n = 3.

To further characterize membrane fluidity, a FRAP study was conducted with 94.5:5 DOPC:N-dod-PE and 94.5:5 DSPC:N-dod-PE supported lipid bilayers (SLBs). SLBs were labeled with 0.5 mol% rhodamine conjugated DOPE. Raw data were analyzed in ImageJ and Matlab. Sample images and their intensity bleach depth profiles are shown in **Figure 2.10**. Differences on bleach spots were observed between DOPC and DSPC bilayers. Both sets of bleach depth data followed a Gaussian profile. Rhodamine-PE in DOPC bilayers showed a larger bleach radius and a shallower bleach depth. In contrast, the bleach radius was narrower and deeper in DSPC bilayers, as expected.

The mean intensity values in the bleached region vs. time were obtained via Zen digital image processing software. Furthermore, these data were fitted to the Axelrod series solution for a Gaussian intensity profile, as previously reported [82,83]:

$$F(t) = A \sum_{n=0}^{\infty} \frac{(-K)^n}{n!} \left(1 + n\left(1 + \frac{2t}{\tau}\right)\right)^{-1} \quad (2.2)$$

where A is a free parameter, K is the bleach depth, and τ is the diffusion recovery time. FRAP data were fitted to the Axelrod equation using Matlab with the help of the routine, FRAPé (beta) developed by Sanii B et al. **Figures 2.11 and 2.12** show marked differences between diffusion kinetics of 95:5 DOPC and DSPC bilayers. Fluorescent membrane probe, rhodamine-DOPE, was observed to have a fast recovery in DOPC bilayers, but not in DSPC bilayers. Diffusion coefficients were calculated using $D = \frac{R^2}{4\tau}$ and averaged as shown in **Figure 2.13**. Diffusion coefficients of rhodamine-DOPE in DOPC bilayers were found to be an order of magnitude higher than in DSPC bilayers. The 95:5 DOPC:N-dod-PE's greater fluidity is confirmed by its fast recovery observed

within the 5 s interval; this correlates with previously reported data of unsaturated lipids [84]. 95:5 DSPC:N-dod-PE SLBs on the other hand, were unable to recover within this time frame. The limited diffusivity of the probe molecules in 95:5 DSPC:N-dod-PE bilayers was expected as the experiments were all conducted at room temperature, which is below DSPC's T_m. The differences between membrane fluidities were evident; this correlated with previous reports of FRAP studies involving unsaturated and saturated lipid bilayers [85–87].

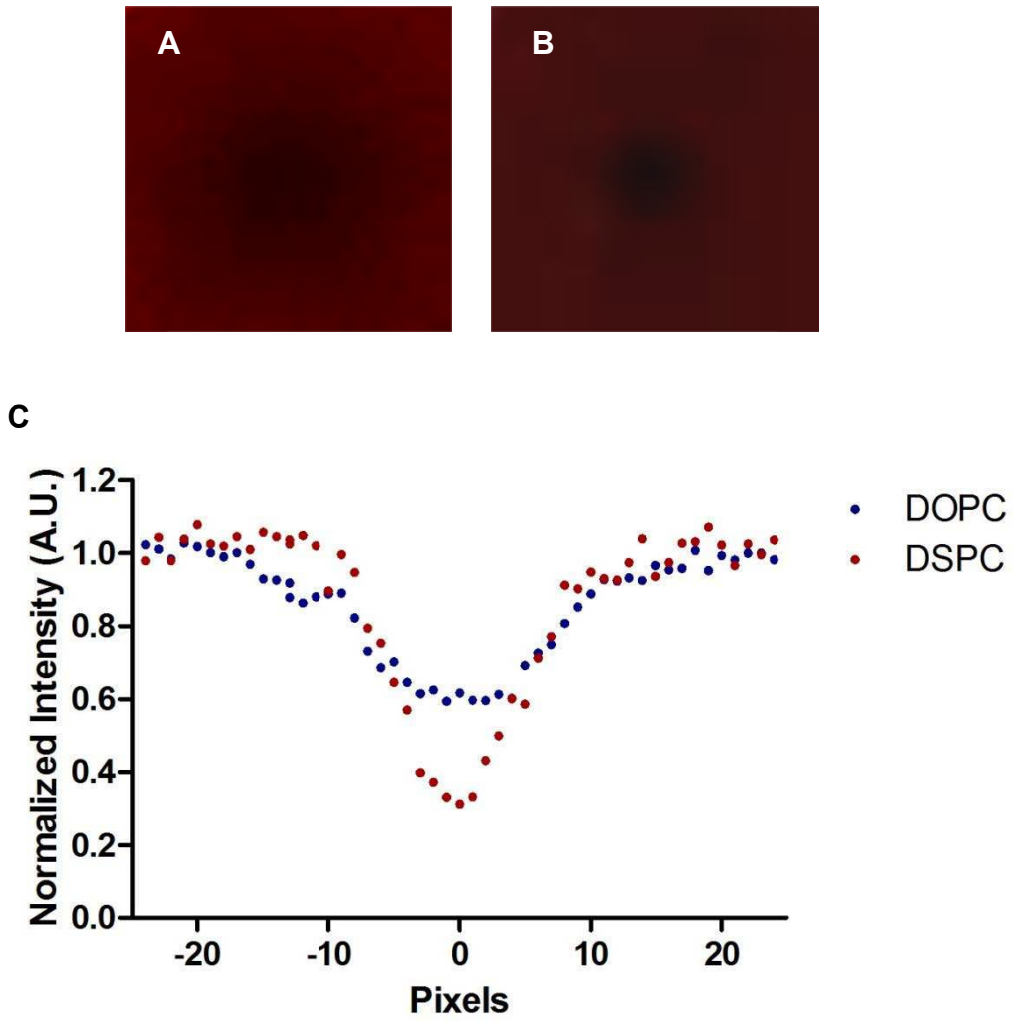

Figure 2.10: Bleach depth profile of supported lipid bilayers. Representative images of the first frame after photobleaching bilayers composed of DOPC:N-dod-PE:rhodamine-DOPE (94.5:5:0.5 mol:mol:mol) (A) and DSPC:N-dod-PE:rhodamine-DOPE (94.5:5:0.5 mol:mol:mol) (B) are shown. Frames are 4.32 x 4.32 μm. The normalized line intensity profiles through the diagonal of sample first post-bleach images are shown (C).

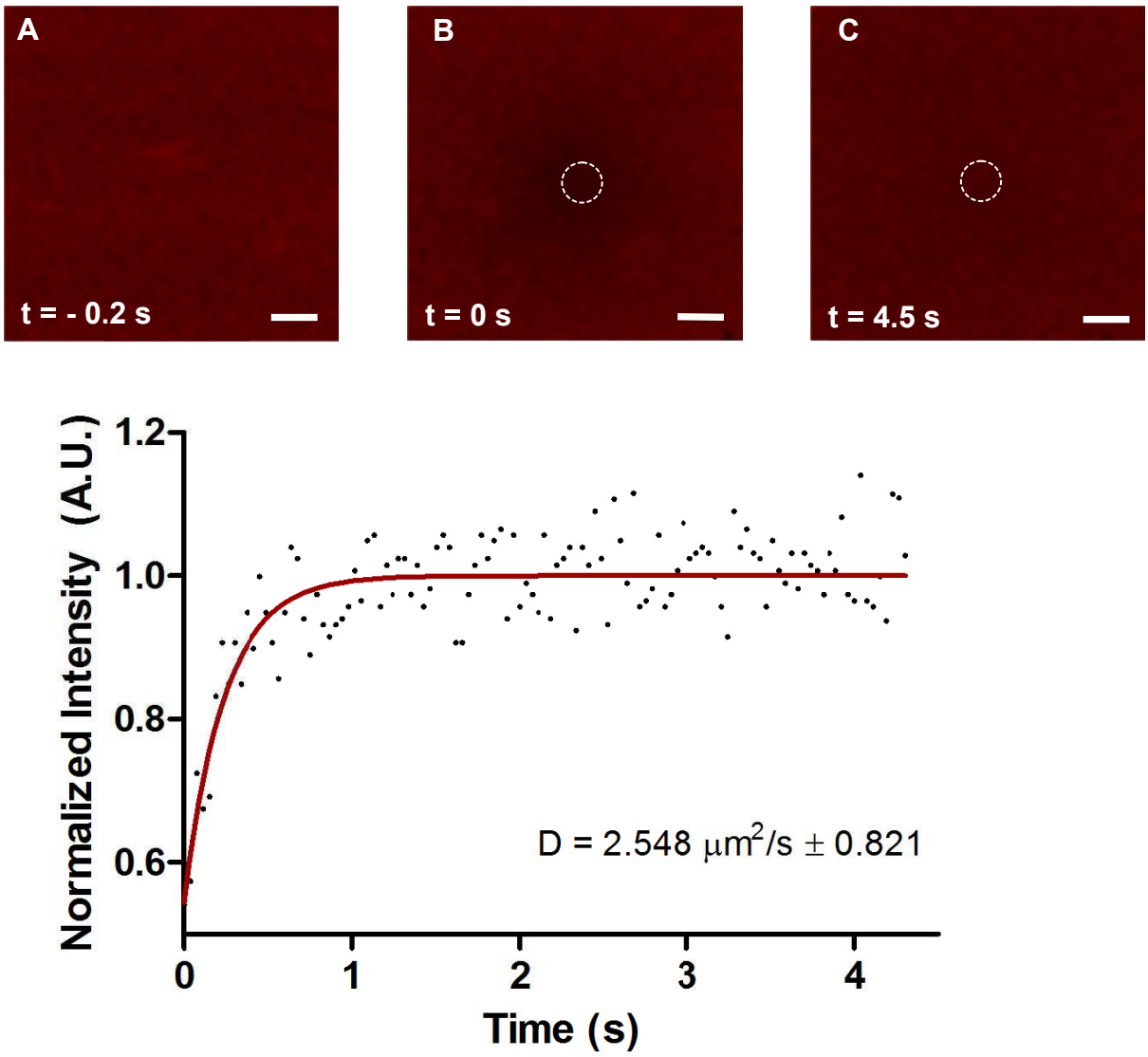

Figure 2.11: Sample FRAP study of DOPC supported lipid bilayers. (A) – (C) show representative frames of a DOPC FRAP experiment. Time was set to 0 at the first post-bleach image and the bleached area was monitored for approximately 4.5 s. Scale bar, 0.5 μm. Normalized intensity data were fitted to the Axelrod equation and diffusion coefficients were calculated using Matlab (C).

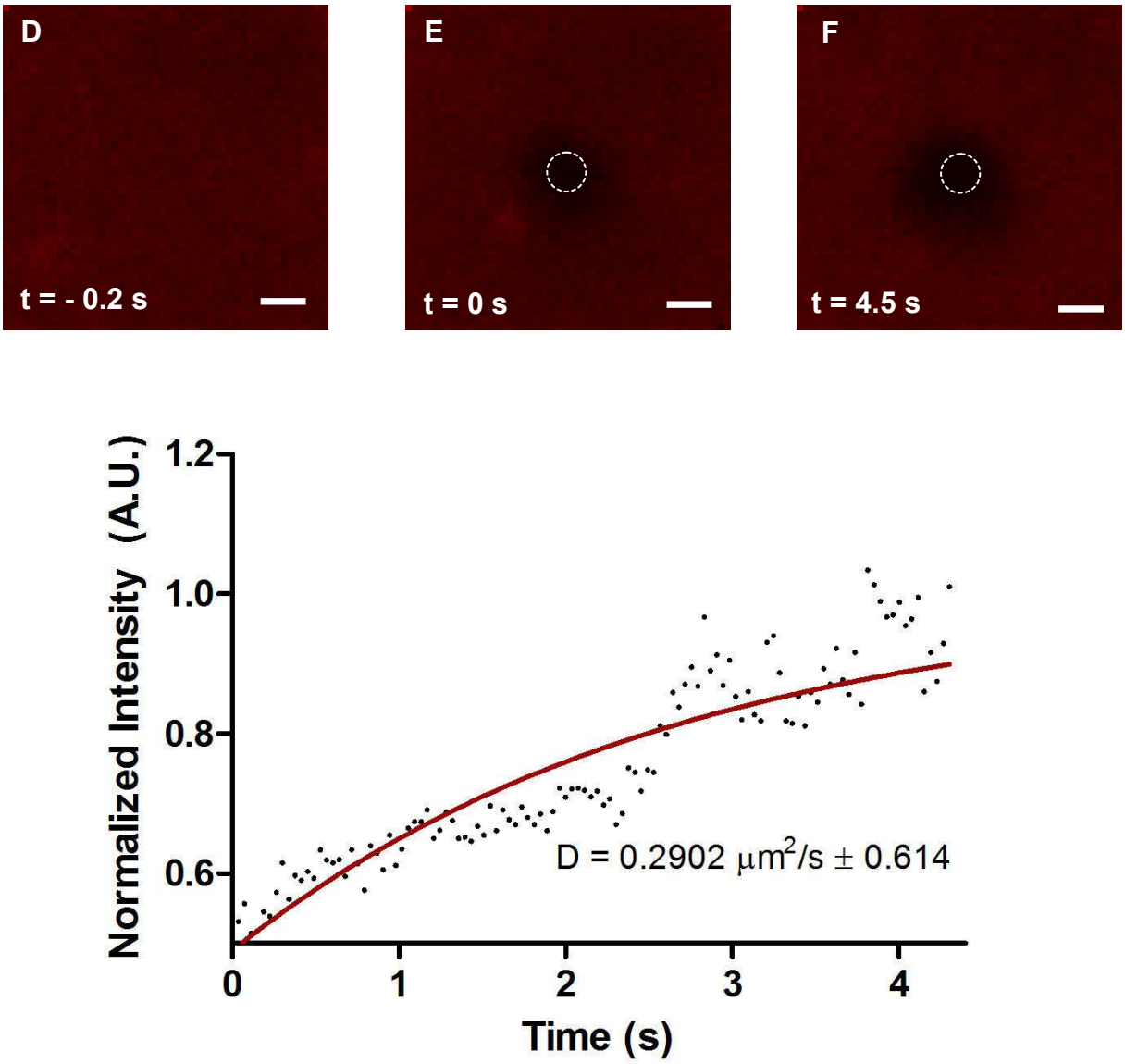

Figure 2.12: Sample FRAP study of DSPC supported lipid bilayers. (A) – (C) show representative frames of a DSPC FRAP experiment. Time was set to 0 at the first post-bleach image and the bleached area was monitored for approximately 4.5 s. Scale bar, 0.5 μm. Normalized intensity data were fitted to the Axelrod equation and diffusion coefficients were calculated using Matlab (C).

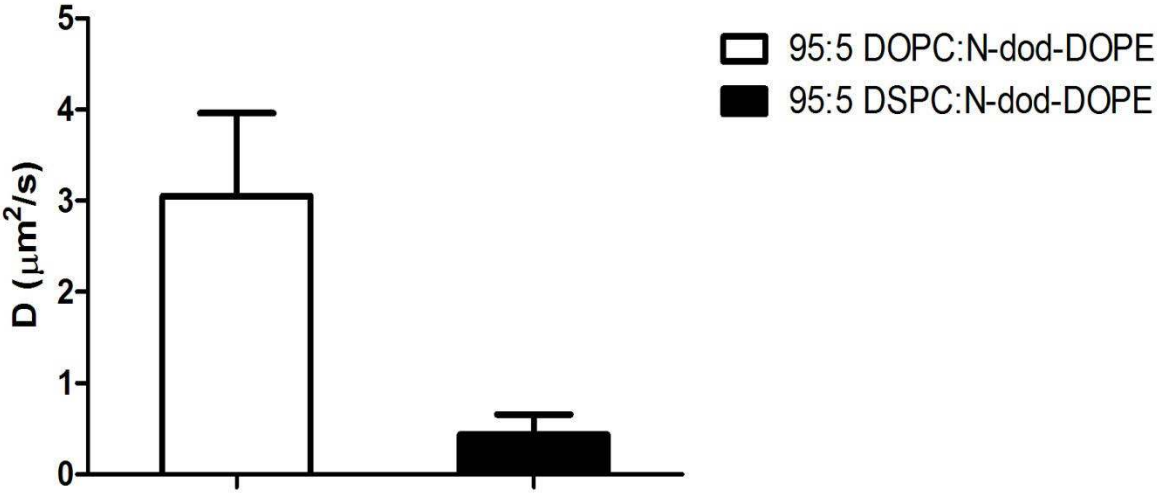

Figure 2.13: Average diffusion coefficients of rhodamine-DOPE in DOPC and DSPC supported lipid bilayers. Diffusion coefficients indicate higher probe mobility in unsaturated DOPC bilayers (average D = 3.1 ± 0.9 $\mu m^2/s$) than in saturated DSPC bilayers (average D = 0.44 ± 0.22 $\mu m^2/s$). Error bars are reported as standard deviation, n = 20.

2.4 Discussion

Cytokine concentrations and exposure times were optimized in order to establish an optimal *in vitro* model of inflammation at the endothelial cell level. Gene expression analysis of VCAM1, E-selectin, and ICAM1, three of the most important cell adhesion molecules upregulated during inflammation were performed [56,88]. Results showed that a 24 h exposure of ECs to 25 ng/ml of TNF-α increased gene expression levels of all three cell adhesion molecules to a maximum. In addition, a 6 h exposure to 5 ng/ml

of IL-1α produced the highest gene expression levels of all three molecules. ICAM1 gene expression was significantly lower than VCAM1 and E-selectin expression upon exposure to all three different concentrations of each cytokine. ICAM1 gene expression levels were the lowest among all three molecules tested. Furthermore, ICAM1 is known to be constitutively expressed at low levels on the surface of ECs [89]. Therefore, we decided to focus only on VCAM1 and E-selectin as we moved forward with experiments.

The surface expression of VCAM1 and E-selectin on TNF-α and IL-1α-activated ECs was quantified as a function of time. The expression of VCAM1 and E-selectin was affected by the duration of exposure, but not cytokine type (no statistical difference, $p > 0.05$). The density of E-selectin peaked at 6 h by ten-fold and nine-fold relative to non-activated ECs for both TNF-α and IL-1α, respectively. VCAM1 expression increased constantly with time; it increased by three- and two-fold relative to expression on non-activated ECs after 24 h of exposure to TNF-α and IL-1α, respectively. Upregulation of VCAM1 and E-selectin by the inflammatory cytokines at 6 h and 24 h was also confirmed by immunostaining.

Antibody surface density of vesicles was characterized by conjugating antibodies onto lipid coated glass microbeads and analyzing with flow cytometry. We established a phosphate assay to measure final liposome concentrations of vesicles utilized to coat the glass microbeads. This assay was also used in all subsequent liposome preparations in order to quantify final concentrations before exposing ECs to liposomes. We verified successful coating of the microbeads and antibody conjugation to the lipid bilayer by confocal microscopy. DOPC and DSPC coated beads conjugated with increasing amounts of PE-conjugated aVCAM1 and FITC-conjugated aE-selectin were

analyzed by flow cytometry. We were able to construct an antibody concentration curve and indirectly quantify the number of antibody molecules per area. At the maximum concentration of each antibody, there were approximately 1000 antibody molecules/μm^2 regardless of the lipid utilized to coat the microbeads. At the lowest concentration, roughly 100 antibody molecules/μm^2 were calculated to be present on the bead surface. No statistically significant differences were found between mean fluorescence intensities across conditions, except for DOPC and DSPC 0.5% PE-conjugated VCAM1.

We calculated the theoretical maximum number of antibody molecules that could potentially be conjugated on the surface of each liposome. To do our calculation we assumed the following: each liposome had a diameter of 100 nm, each phospholipid had a phosphate head group area of 70 $Å^2$, which is the value that has been reported for DOPC [90], each antibody occupied an area of 100 nm^2, which is consistent with previous reports of IgG molecule gyration radii [91], and finally that all 5 mol % of N-dod-PE molecules were localized in the outer bilayer. Based on these parameters, we calculated that a maximum of 300 antibodies would be able to be conjugated on the surface of one liposome. This number correlates with the data obtained, however, it should be noted the areas of the IgG antibody and N-dod-PE molecules were being approximated. It is also very likely that only a fraction of the total number of N-dod-PE molecules incorporated into the outer bilayer and allowed its conjugation site to become available. Neither N-dod-PE's nor the antibody molecule's precise configuration and orientation were controlled during the chemical conjugation reaction. Efficient antibody immobilization is highly desirable in order to increase specificity and strength of

antibody-antigen binding and should be subject of further optimization of our liposomal system.

We characterized membrane fluidity of unsaturated DOPC and saturated DSPC liposomes by utilizing a fluorescence polarization assay. DOPC liposomes with and without N-dod-DOPE had significantly lower anisotropy levels compared to DSPC. This trend was confirmed at both 22 °C and 37 °C. We measured the diffusivity of a fluorescent probe in supported lipid bilayers composed of 94.5 mol % DSPC and DOPC, 5% N-dod-DOPE, and 0.5 mol % rhodamine labeled DOPE. Our results corroborated our fluorescence polarization results and showed the fluorescent probe is able to quickly diffuse back to the photobleached spot in DOPC bilayers. Diffusion of the probe back to the photobleached spot does not occur in DSPC bilayers.

As a result of completing this aim, we were able to establish optimal cytokine concentrations and exposure times to elicit an inflammatory response in endothelial cells that produced high levels of VCAM1 and E-selectin cell surface expression. The results of these experiments set the foundation of an optimal *in vitro* inflamed EC model to use as the basis of our liposome targeting experiments. Our protein cell surface experiment results correlated with our qRT-PCR results, indicating gene expression of VCAM1 and E-selectin was comparable to the amount of protein present on the cell surface. Since exposing ECs with 5 ng/ml of IL-1α for 6 h produced the highest VCAM1 and E-selectin gene expression, we determined to use this protocol for all subsequent liposome targeting experiments. Furthermore, completion of this aim allowed us to characterize important properties of our liposome system such as: lipid concentration, liposome-antibody conjugation efficiency, and liposome membrane fluidity.

Chapter 3.

Effect of Liposomal Membrane Fluidity on Endothelial Cell Binding and Uptake

3.1 Introduction

Chronic inflammation is the underlying mechanism of atherosclerosis, governed by monocyte and T lymphocyte recruitment upon the upregulation of vascular cell adhesion molecule-1 (VCAM1), E-selectin, and intercellular adhesion molecule-1 (ICAM1) on endothelial cell membranes [54,56]. These molecules enable the endothelium to bind and transport leukocytes from the bloodstream to diseased tissue [92,93], making it an attractive drug delivery target. We and others have proposed using molecules to target inflamed endothelium to localize drug and/or block leukocyte recruitment [94–96]. Traditionally, the focus has been to identify a single receptor-ligand pair that will amplify vehicle localization in inflamed tissue relative to normal. However, the targeting paradigm has evolved; it has become more widely accepted that both the chemical and physical properties of drug delivery vehicles drive endothelial cell binding and internalization [97].

Chemical modification of liposomes with antibodies or ligands has shown promise in increasing binding towards cells that overexpress a particular receptor [98,99]. *In vitro* endothelial cell (EC) overexpression of VCAM1, ICAM1, and E-selectin by cytokine activation is analogous to gene expression profiles observed in *in vivo* inflammation [69]. We quantified the surface density of VCAM1, ICAM1, and E-selectin in normal and cytokine-activated ECs. We demonstrated that liposomes that complement the ratio of ICAM1:E-selectin or VCAM1:E-selectin enhanced cytokine-

activated EC uptake [65,100]. Several papers have adopted a dual targeting strategy to improve their targeting results [101,102]. Nonetheless, the challenge in the field is to increase liposome-cell binding prior to clearance by the reticulo-endothelial system (RES).

Methods to improve liposome binding and uptake include increasing the surface concentration and altering the surface chemistry [103,104]. Optimizing the antibody surface density is a balance between cell targeting and immune recognition; high antibody densities lead to a faster rate of liposome clearance from circulation, above 70 - 80 μg antibody/μmol phospholipid [78,105], which would correspond to approximately 30 to 40 antibody molecules per liposome with a 100 nm diameter [78]. Additionally, the use of multiple antibodies [106,107] and multivalent polymers [108] have shown advantages over single antibody or monovalent approaches. These findings, however, may be dependent on whether the targeting ligand is bound to a liquid phase liposome, gel phase liposome, or nanoparticle.

Identification of VCAM1 and E-selectin localization within lipid rafts - saturated lipid-rich microdomains on the cell membrane - spurred our interest to identify the contribution of the lipid membrane in ligand-receptor adhesion. Saturated lipids often exist in the gel phase at physiological temperature, resulting from their ability to closely pack with like molecules, whereas unsaturated molecules that have kinks in their carbon chain exist in the liquid phase. It has also been shown that liposomes composed of neutral, saturated lipids are cleared from the bloodstream more rapidly than unsaturated liposomes due to plasma protein affinity for hydrophobic domains, characteristic of saturated lipid membrane packing defects [109]. Molecules, such as cholesterol and

hydrophobic drugs, that partition into liposomal membranes can affect lipid bilayer elasticity [110]. Theoretical models of the mechanics of receptor-mediated endocytosis and cell adhesion support that membrane rigidity plays an important role in internalization and binding [111,112].

In this report, we investigated the synergy between both chemical and mechanical properties of liposomes to ascertain quantitative metrics with which to engineer EC binding and uptake. Single parameters have been independently tested, such as size, shape, and targeting moiety. However, the impact of each of these components relative to another is unclear. Little has been done on the mechanics of membrane though it is clear that small changes in liposome formulation can result in significant changes in bilayer mechanics. Therefore, we decided to explore the effect liposomal membrane fluidity and antibody diffusivity had on the efficiency of EC targeting. We determined an optimal formulation for binding activated and non-activated endothelial cells. We demonstrated that liposome binding and internalization are significantly enhanced by these metrics.

3.2 Materials and Methods

3.2.1 Liposome Preparation

Unilamellar liposomes were prepared by the extrusion method as previously described [13]. A mixture of DOPC:N-dod-PE or DSPC:N-dod-PE (95:5 mol%) (Avanti Polar Lipids, Alabaster, AL) in chloroform was dried under a nitrogen stream. The lipids were then dissolved in a mixture of DMSO:EtOH (7:3 v/v). Lipid mixtures (1 ml) were

injected in 6 ml 10 mM N-[Tris(hydroxymethyl)methyl]-2-aminoethanesulfonic acid (TES) (Sigma Aldrich, St. Louis, MO) buffer (pH 7.4) with or without rhodamine-conjugated dextran (1 mg/ml) while being agitated at 1000 rpm with a stir bar to yield 8.33 mM lipid. The multilamellar vesicles were subjected to 10 freeze-thaw cycles (utilizing liquid nitrogen) prior to extrusion. Large unilamellar vesicles were prepared by utilizing a LIPEX^{TM} extruder (Northern Lipids, Burnaby, BC, Canada). Vesicles were extruded 10 times through two 100 nm polycarbonate membranes (Whatman Nucleopore 25 mm track-etched membranes, GE Healthcare Biosciences, Piscataway, NJ). Dextran-encapsulated liposomes were dialyzed against 10 mM TES buffer using a Slide-A-Lyzer dialysis cassette (MWCO 20 kDa, Pierce Biotechnology, Inc., Rockford, IL) overnight at room temperature (RT). Liposome size was measured by dynamic light scattering on a ZetaPALS analyzer (Brookhaven Instruments, Corp., Holtsville, NY) in 10 mM TES buffer (pH 7.4). The exact same procedure was repeated for double labeled liposomes with the exception of the addition of 2 mol% NBD-DOPE dissolved in ethanol and added as 1% volume. NBD-DOPE was added to the liposomes after extrusion to ensure only the outer membrane would contain the fluorescent lipid.

The concentration of lipid in solution was determined by a phosphate assay as previously described [74]. Briefly, a diluted liposome sample was ashed with 0.2 ml sulfuric acid (10% v/v) at 200°C for 1 h, followed by addition of 50 µl hydrogen peroxide (30% v/v) and further heating at 200°C for 40 min. After the sample was cooled down to room temperature, 480 ml deionized water and 0.5 ml of color reagent (0.5% w/v ammonium molybdate, 2% w/v ascorbic acid) were added to each sample followed by heating at 45°C for 20 min. The samples were read at 820 nm using a Spectramax Plus

384 spectrophotometer (Molecular Devices, Sunnyvale, CA). A calibration curve was prepared with known phosphate quantities.

3.2.2 Liposome-Antibody Conjugation

Antibodies were conjugated to liposomes via the N-dod-PE anchor. EDC (3 mg) and NHS (4 mg) (Sigma Aldrich, St. Louis, MO) were added to 8.33 mM lipid (liposomes) in 10 mM TES buffer (pH 7.4) and incubated for 6 h at room temperature. Excess EDC and NHS were removed using Slide-a-Lyzer dialysis cassettes (20 kDa MWCO). IgG_1 isotype monoclonal antibody (mAb) (100 mol%, non-specific binding control) or mixtures of aVCAM:aE-selectin mAbs (1:0, 0:1, and 1:1 molar ratios) were added to EDC-modified liposomes at a molar ratio of 1:1000 antibody:phospholipids and incubated overnight at room temperature. All mAbs were purchased from R&D Systems (Minneapolis, MN). Free antibodies were separated using Float-a-Lyzer dialysis tubes (300 kDa, Spectrum Labs, Rancho Dominguez, CA) dialyzed against 10 mM TES buffer at pH 7.4.

3.2.3 Cell Culture

Human umbilical vein endothelial cells (ECs) were grown in endothelial growth medium-2 (EGM-2) with supplements as described by the distributor (Lonza, Allendale, NJ). Cells were maintained at 37°C in a humidified incubator with 5% CO_2 and used for experiments always at passage 4. Growth medium was changed the day after cell seeding and every other day thereafter.

3.2.4 Liposome Uptake by ECs

Liposome binding and uptake was first assessed by incubating ECs with liposomes encapsulating rhodamine-dextran. Incubations took place at 37°C for 1 h and 4 h. Additionally, binding and uptake was further assessed by incubating ECs with double labeled liposomes encapsulating rhodamine-dextran and incorporating NBD-DOPE in the outer lipid monolayer. Incubations took place at 37° C for 5 min, 30 min, and 1 h.

Liposome binding and uptake by ECs was analyzed using flow cytometry as previously described [113,114]. ECs were seeded in 6-well plates (3 x 10^5 cells/well) and allowed to adhere overnight. After activation with IL-1α (5 ng/ml) for 6 h, ECs were incubated for the various time points previously mentioned at 37°C with either dextran-loaded only or dextran-loaded and NBD-DOPE-labeled: (1) nonspecific (IgG_1) liposomes; (2) bare liposomes (no antibodies conjugated on liposome surface); and (3) liposomes conjugated with different ratios of aVCAM1:aE-selectin mAbs. The dose concentration used was 1 µmol lipid/10^6 cells, as previously reported [115].

In order to discern between liposome binding on EC surfaces and actual internalization by ECs, cells were exposed to cytochalasin D and dithionite (Sigma Aldrich, St. Louis, MO) as described previously [116]. Double labeled liposomes (rhodamine dextran-loaded and NBD-DOPE-labeled) were used in these experiments. Surface binding was isolated by blocking cellular internalization with cytochalasin D. During EC activation, cytochalasin D was added to EGM-2 (final concentration of 0.2 µg/ml) containing IL-1α and incubated with cells 30 min prior to liposome incubations. At the end of the 6 h activation period, all wells were rinsed with 1X phosphate buffered

saline (PBS) (Life Technologies/Thermo Fisher Scientific, Grand Island, NY) and replaced with fresh EGM-2. Internalization was measured separately from binding by utilizing the dithionite assay, which uses dithionite to quench NBD-DOPE's fluorescence signal. 75 µl of dithionite solution (1 M Tris, pH 10) was added for 3 min to each well at the end of each liposome incubation period. All wells were rinsed with 1X PBS to eliminate excess dithionite.

Treated ECs were washed with PBS once again, harvested using a 0.25% trypsin solution, and collected in a polystyrene culture tube. Cells were further washed with ice cold PBS three times. Binding and uptake data were acquired using an LSRII flow cytometry analyzer (BD Immunocytometry Systems, San Jose, CA) and analyzed with WEASEL software developed by WEHI (Parkville, Australia). A total of 30,000 events per sample were analyzed to generate each histogram. The fold-over isotype value was calculated by dividing the mean fluorescence intensity for bare liposomes and liposomes conjugated with aVCAM1:aE-selectin by that of the IgG_1 isotype-conjugated liposomes. After careful analysis of the data, we concluded it would be best to present data in its raw format instead of a normalized version. Significant differences in liposome uptake were evaluated using a 2-way ANOVA statistical analysis. A p value less than 0.05 was considered statistically significant.

3.3 Results

3.3.1 Liposome Binding and Uptake as a Function of Time

We investigated the uptake and binding of liposomes to ECs as a function of liposome membrane fluidity and incubation time. Large unilamellar vesicles (LUVs) of

two different compositions: 95:5 DOPC:N-dod-PE and 95:5 DSPC:N-dod-PE were prepared via the extrusion method. The average diameters of unconjugated DOPC:N-dod-PE LUVs were 106 ± 5 nm, while the diameters of DSPC:N-dod-PE were 113 ± 5 nm. Diameter size was determined from dynamic light scattering. Antibody density characterization was determined, as previously described in Chapter 2, by using standardized microbeads that have calibrated binding sites on their surfaces and allow for the user to correlate fluorescence intensity to number of bound antibody molecules. Confocal microscopy and flow cytometry analysis of lipid coated microbeads verified successful conjugation of antibodies.

Liposome binding and uptake was measured by detecting the mean fluorescence intensity (MFI) values of rhodamine-labeled dextran encapsulated in liposomes. We evaluated the incubation of liposomes for 4 h and 1 h (**Figure 3.1** and **Figure 3.2**, respectively) with non-activated an activated endothelial cells. DOPC liposomes decorated with 1:1 and 0:1 aVCAM:aE-selectin had increased binding and uptake compared to their non-activated counterparts (**Figure 3.1 (A)**). This increase was statistically significant ($p < 0.001$). DSPC liposomes bearing a 0:1 aVCAM:aE-selectin ratio on their surfaces also had significantly higher binding and uptake by activated ECs than liposomes exposed to non-activated ECs (**Figure 3.1 (B)**). DSPC liposomes also displayed significantly greater binding and uptake by non-activated ECs than DOPC liposomes regardless of the antibody surface coating. Furthermore, in the absence of surface antibody, bare DSPC liposomes exposed to non-activated ECs also had higher MFI values than DSPC liposomes incubated with activated ECs. This difference was statistically significant ($p < 0.05$).

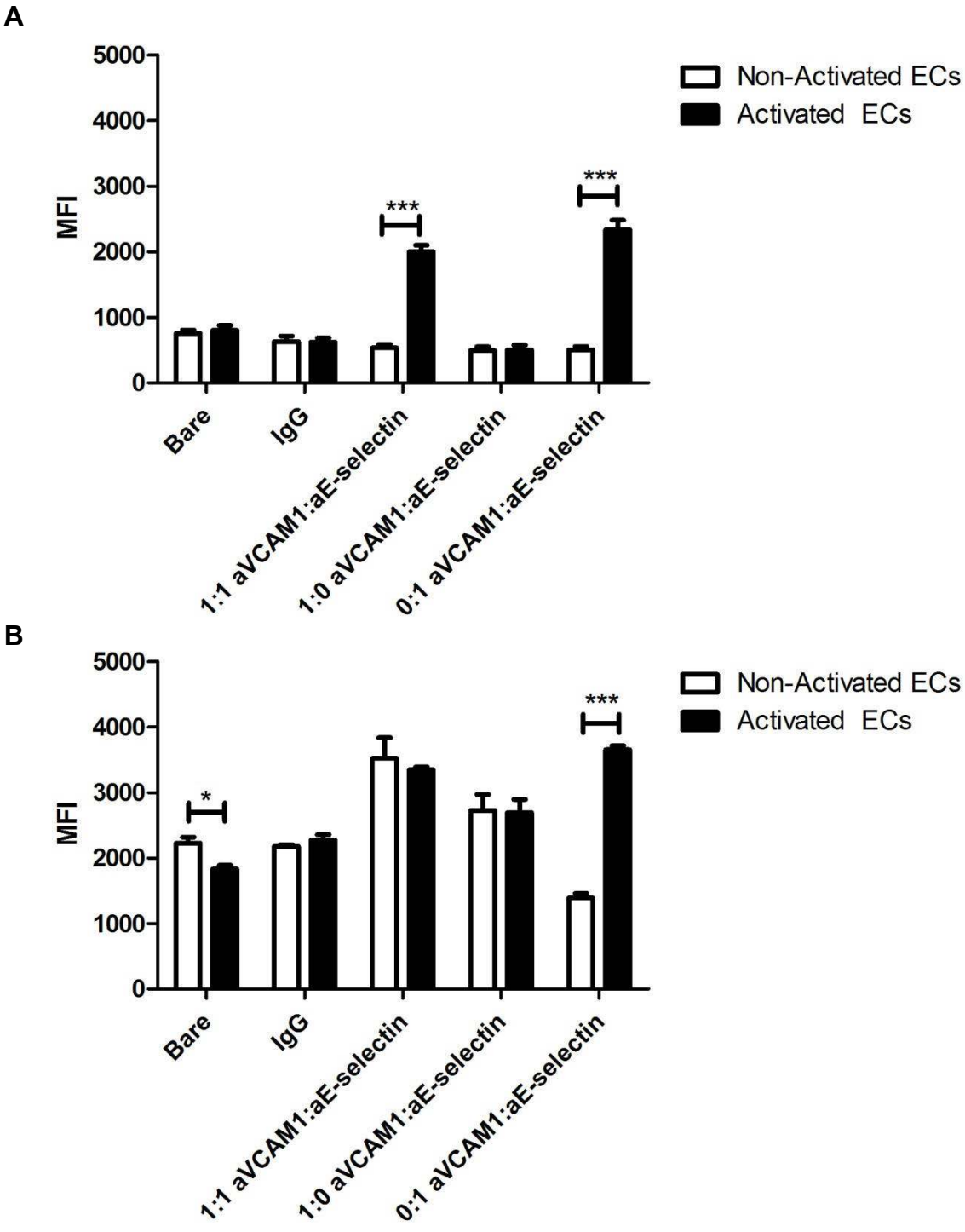

Figure 3.1: Flow cytometry evaluation of liposome binding and uptake by ECs after 4 h incubation. Non-activated and activated ECs (IL-1α, 6 h) were treated with either DOPC:N-dod-PE (95:5 mol:mol) (A) or DSPC:N-dod-PE (95:5 mol:mol) (B)

Figure 3.1 (Continued): liposomes encapsulating rhodamine-labeled dextran and conjugated with various ratios of aVCAM1:aE-selectin mAbs for 4 h. Results shown are raw mean fluorescence intensity (MFI) values. Error bars are reported as standard deviation, n = 3. Statistical significance was calculated using a two-way ANOVA test (*p < 0.05, **p < 0.01, and ***p < 0.001).

We assessed binding and uptake at a shorter incubation time of 1 h with non-activated and activated ECs again. Both DOPC (**Figure 3.2 (A)**) and DSPC (**Figure 3.2 (B)**) liposomes had significantly greater binding and uptake by activated ECs than by non-activated ECs when the liposomal surface displayed 1:1 and 0:1 aVCAM:aE-selectin. 1:1 aVCAM:aE-selectin DOPC liposomes had significantly higher binding and uptake than DSPC conjugated with the same antibody ratio. Our results also showed DSPC had significantly higher binding and uptake than DOPC regardless again of surface decoration when cells were not exposed to IL-1α. DSPC binding and uptake values, however, are lower than the values observed during the 4 h incubation with non-activated ECs.

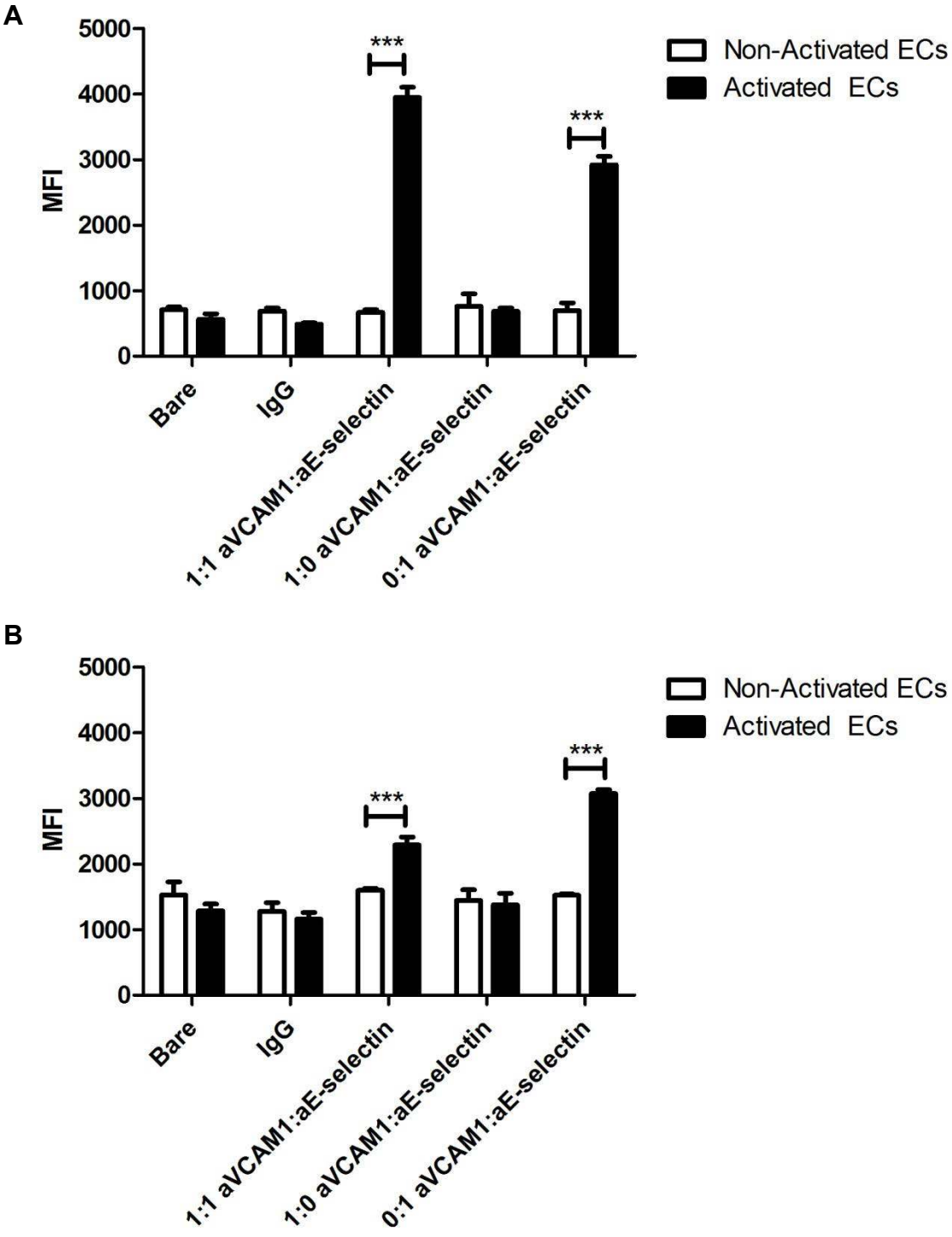

Figure 3.2: Flow cytometry evaluation of liposome binding and uptake by ECs after 1 h incubation. Non-activated and activated ECs (IL-1α, 6 h) were treated with either DOPC:N-dod-PE (95:5 mol:mol) (A) or DSPC:N-dod-PE (95:5 mol:mol) (B)

Figure 3.2 (Continued): liposomes encapsulating rhodamine-labeled dextran and conjugated with various ratios of aVCAM1:aE-selectin mAbs for 1 h. Results shown are raw mean fluorescence intensity (MFI) values. Error bars are reported as standard deviation, n = 3. Statistical significance was calculated using a two-way ANOVA test (*$p < 0.05$, **$p < 0.01$, and ***$p < 0.001$).

3.3.2 Liposome Binding and Uptake as a Function of Antibody Surface Density

We further investigated liposome binding and uptake as a function of antibody surface density. Antibody concentrations in percent format refer to the percent of the total antibody concentration calculated to saturate the surface of the liposomes. In other words, 100% of the antibody concentration refers to the total concentration of antibody required to bind all terminal carboxylic groups of N-dod-PE on the surface of the liposome. Based on our previous 1 h and 4 h binding and uptake results, we decided to conjugate only aE-selectin onto liposomes and incubate for 1 h for all subsequent experiments. Our results demonstrated DOPC's binding and uptake was significantly higher even at concentrations as low as 2.5%, which approximately correspond to 371 ± 85 antibody molecules/μm^2 on the liposome surface (**Figure 3.3 (A)**). On the other hand, DSPC only showed a significant difference only when its surface was completely coated with antibodies (100%) (**Figure 3.3 (B)**). However, DSPC liposomes had higher binding and uptake values regardless of the condition when cells were not activated ($p < 0.05$).

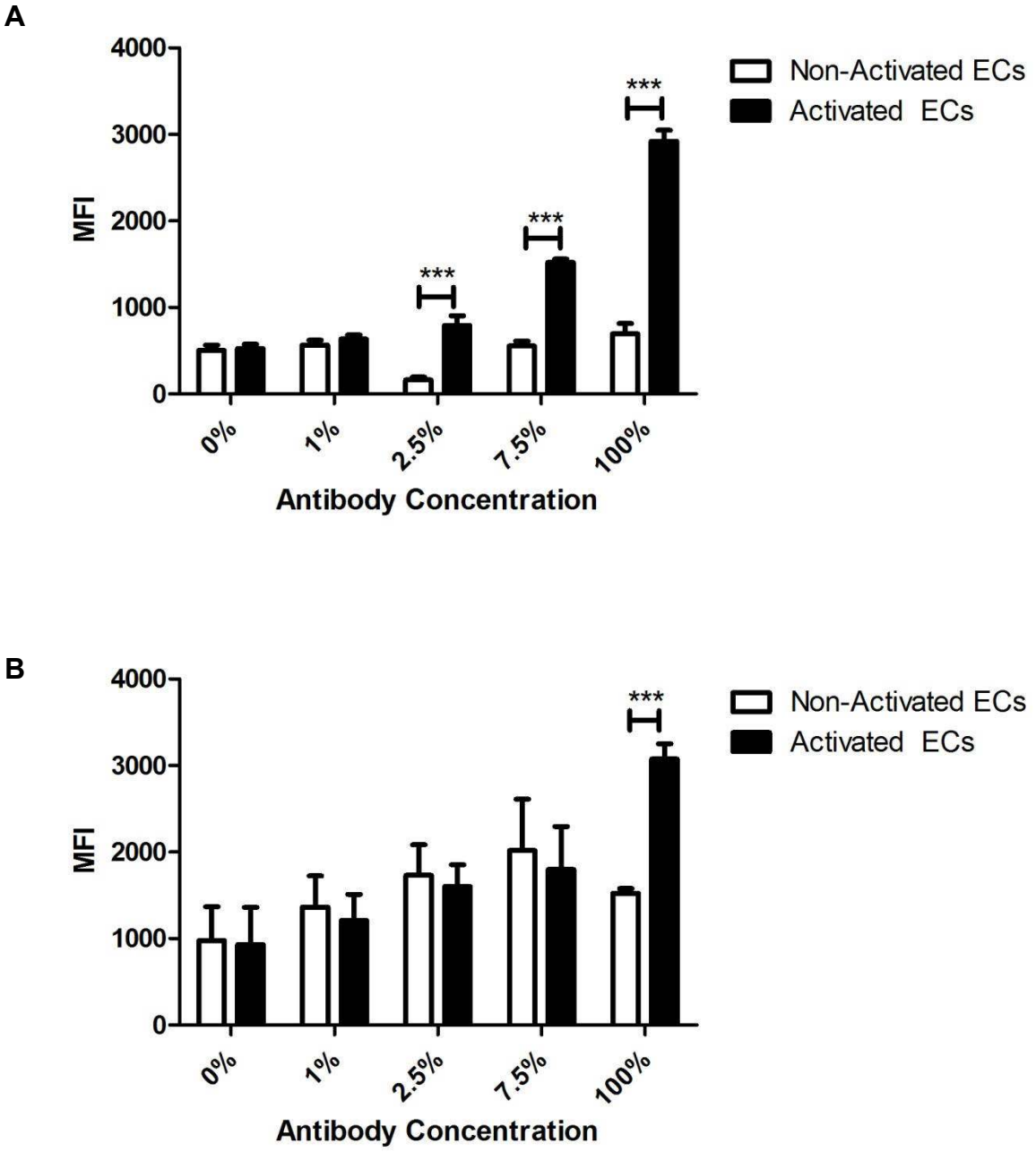

Figure 3.3: Liposome binding and uptake as a function of aE-selectin surface density. Mean fluorescence intensity (MFI) values were determined by flow cytometry. Non-activated and activated (IL-1α, 6 h) ECs were treated for 1 h with DOPC:N-dod-PE (95:5 mol:mol) liposomes (A) and DSPC:N-dod-PE (95:5 mol:mol) liposomes (B) encapsulating rhodamine-labeled dextran. The concentration of aE-selectin mAbs

Figure 3.3 (Continued): conjugated to the liposomal surface was also varied. Error bars are reported as standard deviation, n = 3. Statistical significance was calculated using a two-way ANOVA test (*$p < 0.05$, **$p < 0.01$, and ***$p < 0.001$).

In addition to conjugating increasingly higher E-selectin concentrations to the liposomal surface, we also conjugated IgG_1 concentrations corresponding to the same amounts used in the aE-selectin experiments, and we performed the experiments under the same conditions so as to provide a control for non-specific binding and uptake. No statistically significant differences were found in either DOPC (**Figure 3.4 (A)**) or DSPC (**Figure 3.4 (B)**) liposomes conjugated with the various concentrations of IgG_1. DSPC liposomes exhibited higher values than DOPC at all IgG_1 mAbs concentrations once again ($p < 0.05$). This time, nonetheless, the trend was apparent regardless of whether ECs were activated with IL-1α or not.

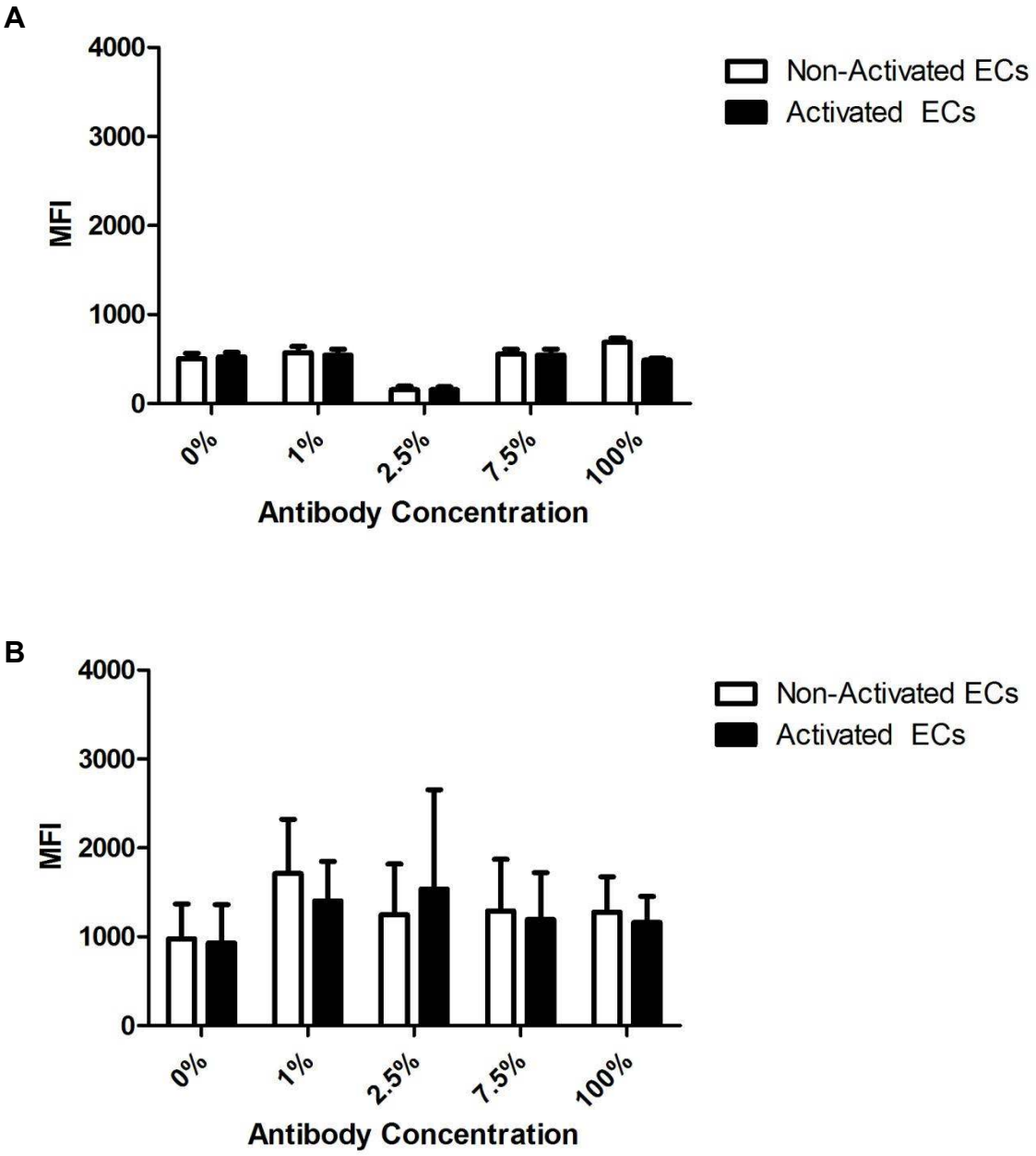

Figure 3.4: Liposome binding and uptake as a function of IgG_1 surface density. Mean fluorescence intensity (MFI) values were determined by flow cytometry. Non-activated and activated (IL-1α, 6 h) ECs were treated for 1 h with DOPC:N-dod-PE (95:5 mol:mol) liposomes (A) and DSPC:N-dod-PE (95:5 mol:mol) liposomes (B) encapsulating rhodamine-labeled dextran. The concentration of control IgG_1 mAbs

Figure 3.4 (Continued): conjugated to the liposomal surface was also varied. Error bars are reported as standard deviation, n = 3. Statistical significance was calculated using a two-way ANOVA test (*$p < 0.05$, **$p < 0.01$, and ***$p < 0.001$).

3.3.3 Differentiating Between Binding and Uptake

We investigated pure cellular surface binding vs. cellular internalization of liposomes, separately, by the application of two different assays. Liposomes were labeled with an NBD-conjugated lipid on their surface in addition to being loaded with rhodamine-labeled dextran. To dissociate from uptake and only quantify EC surface binding, ECs were treated with cytochalasin D, a cellular internalization inhibitor, and shorter incubation time points were tested (**Figure 3.5**). Both fluorescent probes, NBD (**Figure 3.5 (A)**) and rhodamine (**Figure 3.5 (B)**), were detected simultaneously by the flow cytometer. According to the membrane-bound NBD signal, DSPC liposomes reached their highest surface binding levels at 0.5 h then decreased. DOPC liposomes, on the other hand, increased gradually and did not reach maximum surface binding until 1 h. Rhodamine fluorescence indicated the exact same trend and correlated to the surface binding that was observed when tracking membrane-bound NBD. We performed cell surface binding control experiments with non-specific IgG_1 and bare liposomes (**Figure 3.6**). No significant differences were detected at any incubation time points.

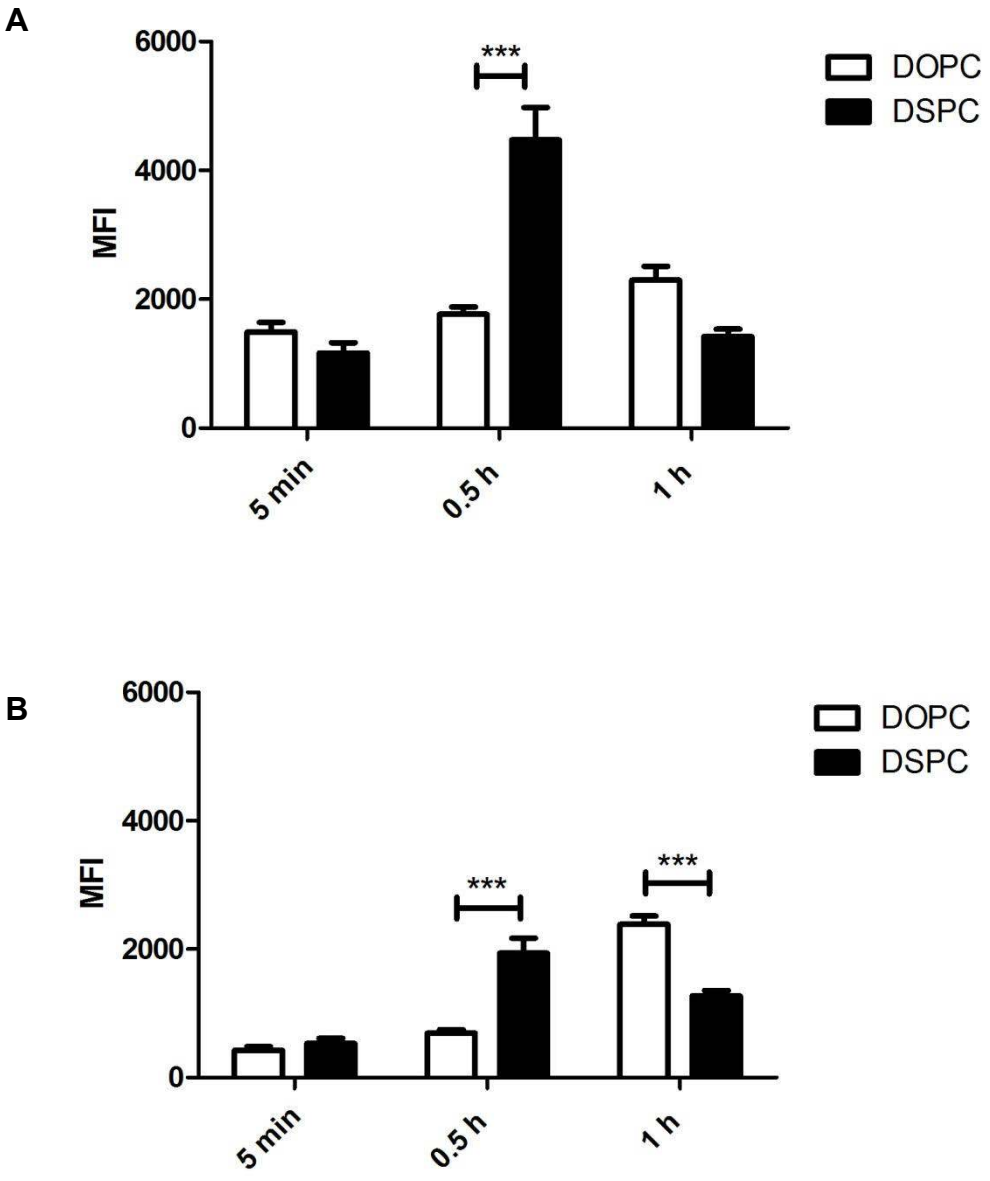

Figure 3.5: Flow cytometry evaluation of cellular surface binding. Activated ECs (IL-1α, 6 h) exposed to cytochalasin D (0.2 μg/ml, 30 min) were treated with NBD-DOPE membrane-labeled liposomes conjugated with aE-selectin and encapsulating rhodamine-labeled dextran. Results shown are raw mean fluorescence intensity (MFI) values of NBD (A) and rhodamine (B). Error bars are reported as standard deviation,

Figure 3.5 (Continued): n = 3. Statistical significance was calculated using a two-way ANOVA test (*p < 0.05, **p < 0.01, and ***p < 0.001).

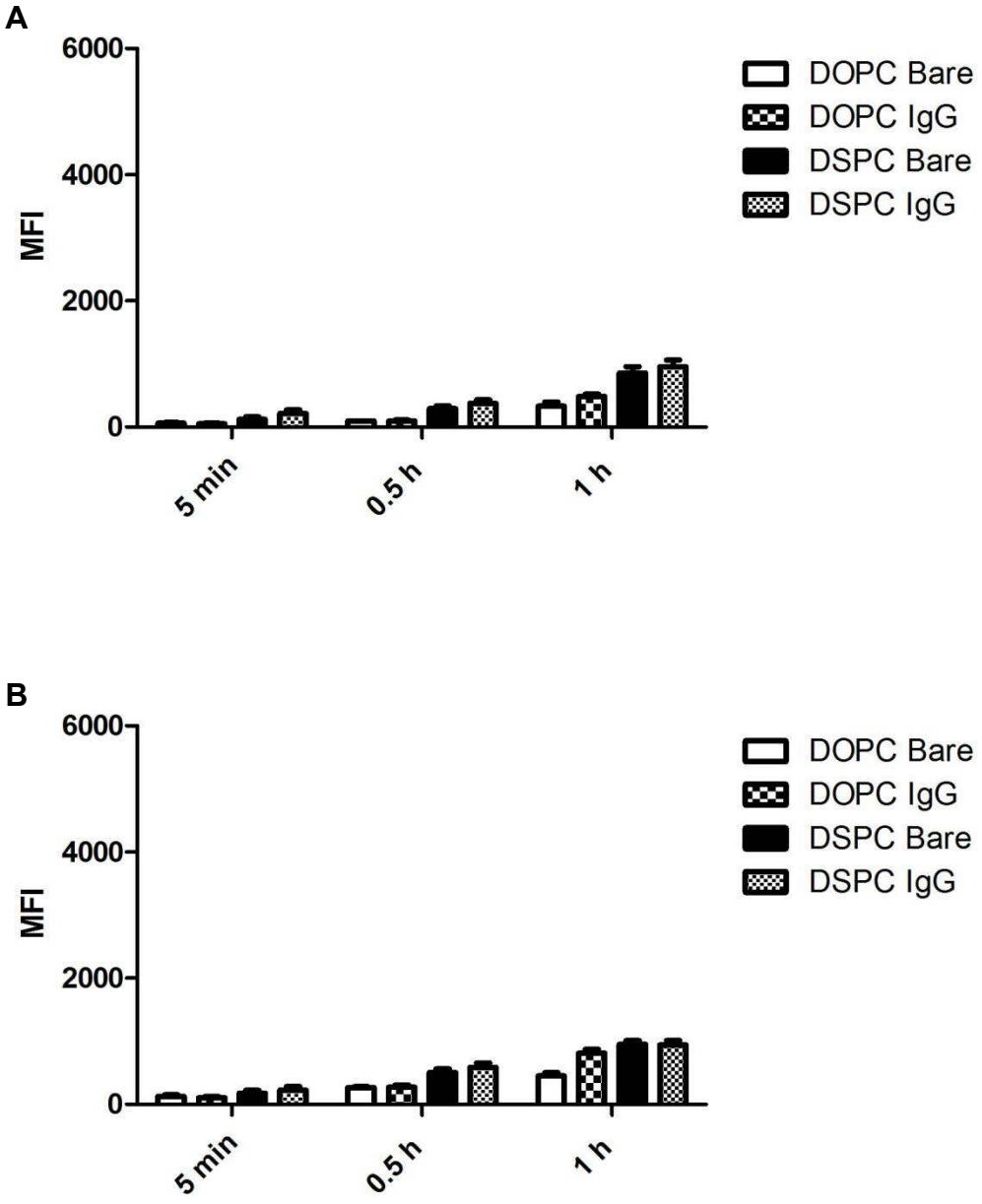

Figure 3.6: Cellular surface binding controls. Activated ECs (IL-1α, 6 h) exposed to cytochalasin D (0.2 μg/ml, 30 min) were treated with NBD-DOPE membrane-labeled liposomes conjugated with aE-selectin and encapsulating rhodamine-labeled dextran. Results shown are raw mean fluorescence intensity (MFI) values of NBD (A) and rhodamine (B). Error bars are reported as standard deviation, n = 3.

We examined cellular internalization via a dithionite assay, where dithionite was used to quench the NBD fluorescence signal. Dithionite is cell membrane impermeable, thus most of the NBD fluorescence detected originated from the cell interior as NBD was quenched on the exterior of the cell. Both DSPC and DOPC liposomes had increasing internalization as incubation time increased, and both saturated and unsaturated liposomes were internalized at a maximum level at 1 h time point (**Figure 3.7 (A)**). Rhodamine fluorescence detection (**Figure 3.7 (B)**) in this experiment did not reflect cellular internalization exclusively given that dithionite is supposed to only quench NBD. We performed cellular internalization control experiments with non-specific IgG_1 and bare liposomes (**Figure 3.8**). No significant differences were detected at any incubation time points, however, NBD fluorescence of DOPC and DSPC liposomes at 1 h was significantly higher than those observed with cell surface binding.

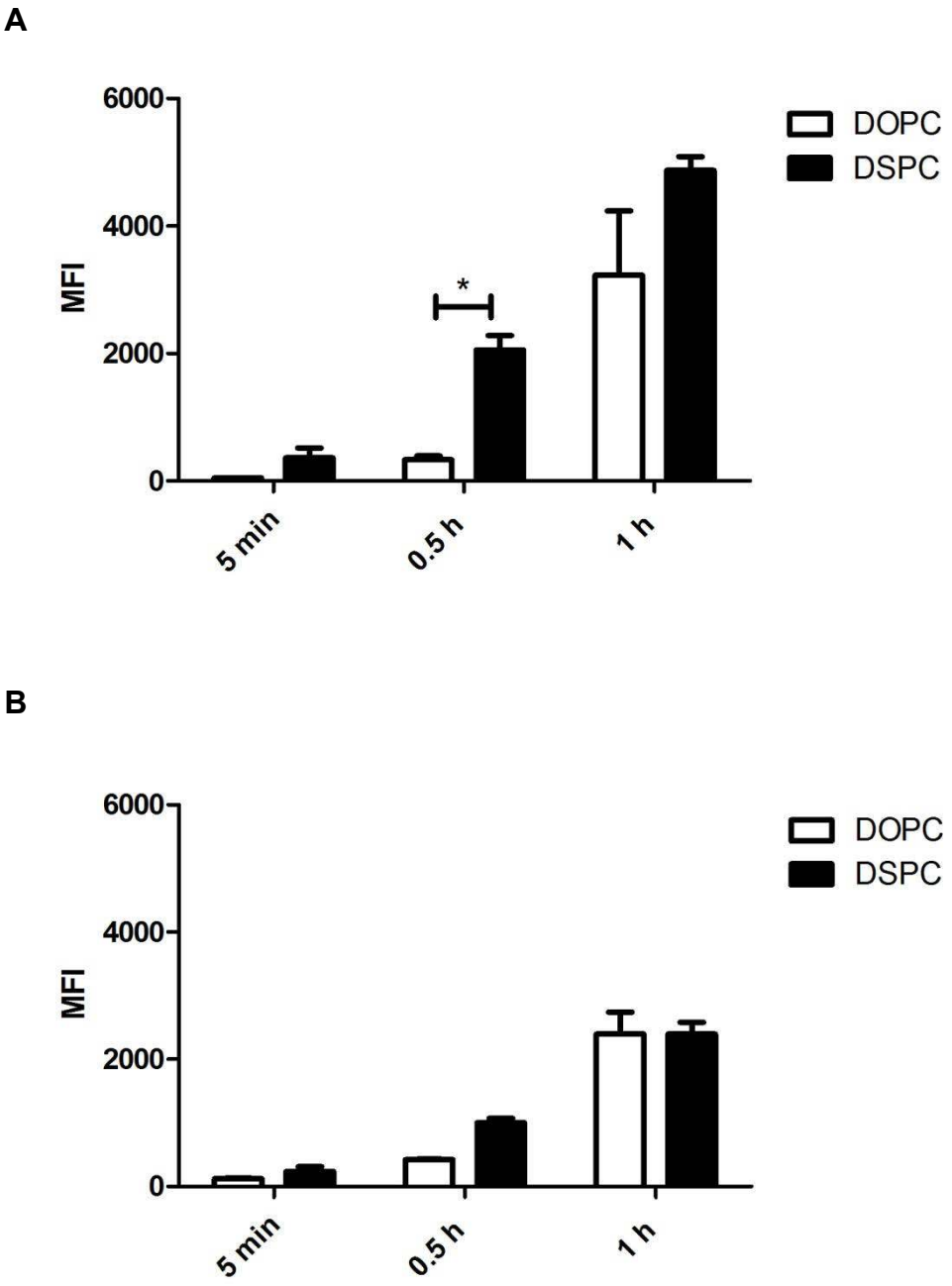

Figure 3.7: Flow cytometry evaluation of cellular internalization. Activated ECs (IL-1α, 6 h) exposed to dithionite (75 µl, 3 min) were treated with NBD-DOPE membrane-labeled liposomes conjugated with aE-selectin and encapsulating rhodamine-labeled dextran. Results shown are raw mean fluorescence intensity (MFI) values of NBD (A) and rhodamine (B). Error bars are reported as standard deviation, n = 3. Statistical

Figure 3.7 (Continued): significance was calculated using a two-way ANOVA test (*p < 0.05, **p < 0.01, and ***p < 0.001).

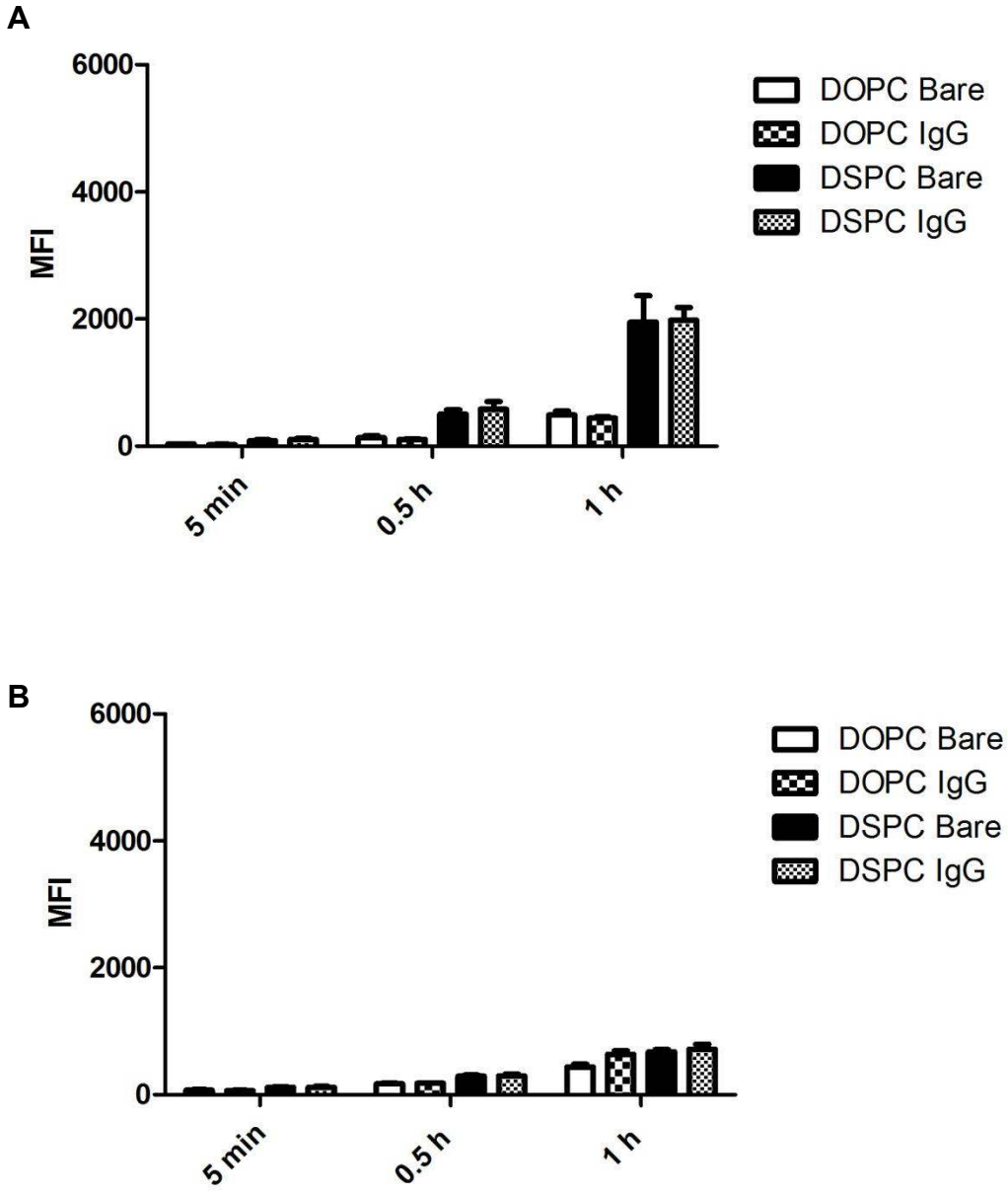

Figure 3.8: Cellular internalization controls. Activated ECs (IL-1α, 6 h) exposed to dithionite (75 µl, 3 min) were treated with NBD-DOPE membrane-labeled liposomes conjugated with aE-selectin and encapsulating rhodamine-labeled dextran. Results shown are raw mean fluorescence intensity (MFI) values of NBD (A) and rhodamine (B). Error bars are reported as standard deviation, n = 3.

3.4 Discussion

We have shown the effect of liposomal membrane fluidity on EC uptake and binding. Increased membrane fluidity of liposomes decorated with relatively low antibody concentrations may lead to considerably high uptake and binding in ECs stimulated by IL-1α. We prepared liposomes with fluid or gel phase lipids to test our antibody diffusivity hypothesis. We functionalized the surface of liposomes by conjugating antibodies against cell adhesion molecules that are upregulated on the surface of ECs in an inflammatory environment. We focused on targeting VCAM1 and E-selectin because these two molecules are temporally regulated by cytokines; this cytokine activation has been established to be reproducible [55,59]. In this aim, ECs were activated using IL-1α for 6 h. In our previous aim, we characterized and determined that exposing ECs to 5 ng/ml of IL-1α for 6 h yielded the highest amount of VCAM1 and E-selectin expression on EC surfaces.

Activated ECs incubated with DOPC liposomes conjugated with a 1:1 and 0:1 aVCAM1:aE-selectin for 4 h had increased mean fluorescence intensity (MFI) values. We had previously investigated DOPC liposomes with various aVCAM1:aE-selectin ratios and observed a complementary 1:1 aVCAM1:aE-selectin had the greatest binding and uptake [100]. In these studies, however, ECs were incubated with antibody labeled liposomes overnight. Shortening the liposome incubation time from approximately 12 h to 4 h did not produce the same uptake and binding results. Our results suggest that as incubation time is shortened from 12 h to 4h and further decreased to 1 h, E-selectin plays an increasingly important role in binding and uptake of liposomes, while VCAM1's role declines. The ratio of 0:1 aVCAM1:aE-selectin decorating both DOPC and DSPC

liposomes had significant uptake and binding by activated ECs (**Figures 3.1 and 3.2**). No significant differences were observed when liposomes were conjugated with a ratio of 1:0 aVCAM1:aE-selectin. Further characterization of the temporal E-selectin surface expression after activation with IL-1α is needed. Numerous studies have reported on the expression of E-selectin as a function of cytokine and cytokine activation [117], but the characterization of the temporal surface expression after activated ECs are no longer exposed to the cytokine has not been documented. However, it can be inferred that the surface expression of E-selectin rapidly decays after the 6 h activation period since a decrease is observed even when the cells are still exposed to the cytokine. This would potentially explain why binding and uptake increase with decreased incubation time. We and others have shown the time-dependent expression of E-selectin peaks after 4 – 6 h of cytokine activation and then declines to basal levels within 24 h to 48 h [56,100]. The results reported in this aim indicate the use of aE-selectin alone is sufficient to achieve rapid localization of liposomes, within 1h, to activated ECs. A possible clinical application where this scenario of rapid localization to injured tissue might be desirable is non-invasive molecular imaging of vulnerable atherosclerotic plaque [7].

DSPC liposomes had significant binding and uptake when conjugated with 0:1 aVCAM1:aE-selectin after both 1 h and 4 h incubations and when conjugated with 1:1 aVCAM1:aE-selectin after 1 h incubation. These results may indicate antibody diffusivity, as a result of membrane fluidity, has no effect on binding and uptake. However, the liposomal surfaces were completely saturated with antibodies. In order to more accurately probe the question of antibody diffusivity we had to test our hypothesis

at very low antibody surface densities that would allow for greater lateral mobility. It is also important to note from these studies that DSPC liposomes had significantly higher levels of non-specific binding and uptake than DOPC liposomes. This overall increase in binding and uptake by non-activated ECs is evident at both the 4 h and 1 h incubation times. Furthermore, non-specific IgG_1-bearing and bare DSPC liposomes had significantly greater binding and uptake by activated ECs. Although DSPC liposomes conjugated with high surface density of aE-selectin achieved high levels of binding and uptake, higher levels of binding to non-activated ECs present a problem for targeted drug delivery *in vivo*, are non-desirable, and suggest there is an additional *in vitro* binding and uptake mechanism other than the one initiated by E-selectin.

To further investigate our question regarding the effect of antibody diffusivity, we assessed binding and uptake as a function of antibody surface density and membrane fluidity. We hypothesized that if the lateral antibody mobility would play a role on binding, then even at very small liposomal surface concentrations, binding and uptake levels similar to those observed with fully antibody saturated liposomes would take place only with unsaturated liposomes. Using the antibody characterization technique of lipid coated glass microbeads presented in Chapter 2, we identified a specific regime in which a very limited number of antibody molecules would be bound on the liposomal surface. We concluded this regime to be ranging from 1% to 7.5% of the total antibody concentration used previously to saturate the liposomal surface. We determined these concentrations corresponded to a range of 7 ± 1 to 20 ± 3 aE-selectin molecules per DOPC liposome and between 5 ± 1 to 16 ± 6 aE-selectin molecules per DSPC liposomes. Notably, DOPC liposomes conjugated with 2.5% and 7.5% of aE-selectin

had significant binding and uptake by activated ECs while DSPC liposomes did not. Efficient targeting of DOPC liposomes at low antibody densities could be potentially explained by two factors: increased antibody accumulation due to increased diffusivity or better exposure of the antibody's binding sites due to a less crowded liposomal surface. At 100% aE-selectin concentration, when the liposomal surfaces were saturated, both DOPC and DSPC liposomes localized on or within stimulated ECs more than likely due to an increased rate of antibody-E-selectin bond formation. At low antibody densities, the non-specific binding and uptake of DSPC liposomes by non-activated ECs was high again. These results suggest again that DSPC liposomes may have a second binding and uptake mechanism in addition to targeted E-selectin binding and -mediated endocytosis.

We were interested in decoupling uptake and binding given that our previous experimental setup did not permit us to distinguish the fluorescence intensities of either one. Our surface binding studies demonstrated DOPC had the highest binding at 1 h while DSPC had its binding peak at 0.5 h. This rapid increase and decrease of DSPC binding remains unclear. Our cellular internalizations studies, in turn, showed both DSPC and DOPC had maximal internalization after 1 h. All non-specific binding control experiments showed no significant differences as expected.

Further studies are needed to continue investigating the role of antibody lateral mobility in liposome binding. Liposomes with a different formulation that allows for low non-specific binding yet also has high membrane rigidity would be ideal to address this question. The question of high levels of non-specific binding of saturated liposomes also requires further investigation. Despite the multiple questions that arose in this aim,

we were able to demonstrate that the coupling of aE-selectin to either saturated or unsaturated liposomes led to high levels of binding and uptake in ECs. DOPC liposomes with low antibody surface densities also had significant binding and uptake. This formulation could potentially continue to be explored for clinical drug delivery and targeting applications.

Chapter 4.

In vivo Evaluation of PEGylated Liposome Biodistribution

4.1 Introduction

Drug delivery systems that efficiently target inflamed vasculature can be beneficial for the detection and treatment of a wide range of diseases such as atherosclerosis. As previously mentioned, a range of nanoparticle drug delivery systems, including liposomes, has been studied for these applications [118]. Liposomes lacking any targeting moieties on their surfaces have been reported to efficiently deliver encapsulated dexamethasone to aortic plaques in an atherogenic mouse model [119]. Additionally, imaging agents targeting VCAM1 [10] and E-selectin [120] have been investigated for molecular imaging of unstable atherosclerotic plaque. Utilizing liposomes that target cell adhesion molecules and also carry imaging agents may lead to improved molecular imaging of unstable plaque. Such work was, unfortunately, out of the scope of our present project. In this study, we evaluated the *in vitro* uptake of DOPC PEGylated liposomes targeting E-selectin and assessed the biodistribution of these liposomes in mice. We hypothesized the presence of PEG would increase liposome circulation time in the bloodstream. We investigated how different surface densities and types of PEG functionalized lipids with varying polymer molecular weights had an effect on binding and uptake in ECs. *In vivo* administration of PEGylated liposomes was traced in live mice via an *in vivo* imaging system. Finally, liposome distribution was qualitatively examined by fluorescence imaging of tissue cryosections.

4.2 Materials and Methods

4.2.1 Liposome Preparation

Unilamellar liposomes were prepared by the extrusion method as previously described [13]. Two different types of functionalized polyethylene glycol (PEG) lipids were used for the *in vitro* and *in vivo* experiments in this aim: 1,2-distearoyl-*sn*-glycero-3-phosphoethanolamine-N-[amino(polyethylene glycol)-2000] (DSPE-PEG), 1,2-di-(9Z-octadecenoyl)-*sn*-glycero-3-phosphoethanolamine-N-[carboxy(polyethylene glycol)-5000], (DOPE-PEG) (Avanti Polar Lipids, Alabaster, AL). Mixtures of 99:1 DOPC:DSPE-PEG, along with 94:5:1 and 90:5:5 DOPC:N-dod-PE:DOPE-PEG in chloroform were dried under a nitrogen stream. The lipids were then dissolved in a mixture of DMSO:EtOH (7:3 v/v). Lipid mixtures (1 ml) were injected in 6 ml 10 mM TES (Sigma Aldrich, St. Louis, MO) buffer (pH 7.4) with or without rhodamine-conjugated dextran (1 mg/mL) while being agitated at 1000 rpm with a stir bar to yield 8.33 mM lipid. The multilamellar vesicles were subjected to 10 freeze-thaw cycles (utilizing liquid nitrogen) prior to extrusion. Large unilamellar vesicles were prepared by utilizing a LIPEX^{TM} extruder (Northern Lipids, Burnaby, BC, Canada). Vesicles were extruded 10 times through two 100 nm polycarbonate membranes (Whatman Nucleopore 25 mm track-etched membranes, GE Healthcare Biosciences, Piscataway, NJ). Dextran-encapsulated liposomes were dialyzed against 10 mM TES buffer using a Slide-A-Lyzer dialysis cassette (MWCO 20 kDa, Pierce Biotechnology, Inc., Rockford, IL) overnight at room temperature (RT). Liposome size was measured by dynamic light scattering on a ZetaPALS analyzer (Brookhaven Instruments, Corp., Holtsville, NY) in 10 mM TES buffer (pH 7.4). The exact same procedure was repeated when preparing liposomes

tagged with 1,1'-dioctadecyl-3,3,3',3'-tetramethylindodicarbocyanine perchlorate (DiD) (Life Technologies/Thermo Fisher Scientific, Grand Island, NY) for the *in vivo* experiments. The same lipid formulations were used except 0.1 mol % DiD was added to the mixtures prior to drying with nitrogen gas. DiD was kept sterile; all aliquots used for liposome preparation were prepared under sterile conditions.

The concentration of lipid in solution was determined by a phosphate assay as previously described [13]. Briefly, a diluted liposome sample was ashed with 0.2 ml sulfuric acid (10% v/v) at 200°C for 1 h, followed by addition of 50 µl hydrogen peroxide (30% v/v) and further heating at 200°C for 40 min. After the sample was cooled down to room temperature, 480 ml deionized water and 0.5 ml of color reagent (0.5% w/v ammonium molybdate, 2% w/v ascorbic acid) were added to each sample followed by heating at 45°C for 20 min. The samples were read at 820 nm using a Spectramax Plus 384 spectrophotometer (Molecular Devices, Sunnyvale, CA). A calibration curve was prepared with known phosphate quantities.

4.2.2 Liposome-Antibody Conjugation

Antibodies were conjugated to liposomes via the N-dod-PE anchor. EDC (3 mg) and NHS (4 mg) (Sigma Aldrich, St. Louis, MO) were added to 8.33 mM lipid (liposomes) in 10 mM TES buffer (pH 7.4) and incubated for 6 h at room temperature. Excess EDC and NHS were removed using Slide-a-Lyzer dialysis cassettes (20 kDa MWCO). IgG_1 isotype monoclonal antibody (mAb) (100 mol%, non-specific binding control) or aE-selectin mAbs were added to EDC-modified liposomes at a molar ratio of 1:1000 antibody:phospholipids and incubated overnight at room temperature. All mAbs

were purchased from R&D Systems (Minneapolis, MN). Free antibodies were separated using Float-a-Lyzer dialysis tubes (300 kDa, Spectrum Labs, Rancho Dominguez, CA) dialyzed against 10 mM TES buffer at pH 7.4.

4.2.3 Cell Culture

Human umbilical vein endothelial cells (ECs) were grown in endothelial growth medium-2 (EGM-2) with supplements as described by the distributor (Lonza, Allendale, NJ). Cells were maintained at 37°C in a humidified incubator with 5% CO_2 and used for experiments always at passage 4. Growth medium was changed the day after cell seeding and every other day thereafter.

4.2.4 Liposome Uptake by ECs

Liposome binding and uptake was first assessed by incubating ECs with liposomes encapsulating rhodamine-dextran. Liposome binding and uptake by ECs was analyzed using flow cytometry as previously described [21, 22]. ECs were seeded in 6-well plates (3×10^5 cells/well) and allowed to adhere overnight. After activation with IL-1α (5 ng/ml) for 6 h, ECs were incubated for 1 h at 37°C with PEGylated dextran-loaded: (1) nonspecific (IgG_1) liposomes; (2) bare liposomes (no antibodies conjugated on liposome surface); and (3) liposomes conjugated with aE-selectin mAbs. The dose or liposome concentration used with ECs was 1 μmol lipid/10^6 cells.

Treated ECs were washed with PBS, harvested using a 0.25% trypsin solution, and collected in a polystyrene culture tube. Cells were further washed with ice cold PBS three times. Binding and uptake data were acquired using an LSRII flow cytometry analyzer (BD Immunocytometry Systems, San Jose, CA) and analyzed with WEASEL

software developed by WEHI (Parkville, Australia). A total of 30,000 events per sample were analyzed to generate each histogram. Again we chose to present data in its raw format instead of a normalized version. Significant differences in liposome uptake were evaluated using a 2-way ANOVA statistical analysis. A p value less than 0.05 was considered statistically significant.

4.2.5 *In Vivo* Studies

All animal work was approved by Harvard University's Institutional Animal Care and Use Committee (IACUC). C57BL/6J female mice were obtained from the Jackson Laboratory (Bar Harbor, ME) and were between 7-8 weeks of age at the time of experiments. Four mice were given tail vein injections of 0.1 ml DiD-labeled liposomes. The detailed conditions are as follows: mouse #1 - bare liposomes containing 5% DOPE-PEG, mouse #2 – liposomes conjugated with aE-selectin mAbs, mice #3 and #4 – liposomes containing 5% DOPE-PEG and conjugated with aE-selectin mAbs. One of the mice, mouse #4, was injected with PEGylated liposomes conjugated with aE-selectin was also injected intravenously with 0.3 μg of IL-1α dissolved in 0.2 ml sterile 1X PBS. The cytokine injection was given 30 min prior to injecting liposomes. All four mice were imaged using the *in vivo* imaging Xenogen IVIS Spectrum (Caliper Life Sciences/Perkin Elmer, Hopkinton, MA) system to track the accumulation of fluorescent liposomes. The images were normalized by subtracting background signal prior to initializing the *in vivo* imaging procedure. Radiance measurements had units of photons/sec/cm^2/sr, which refers to the number of photons per second that are leaving a square centimeter of tissue and radiating into a solid angle of one steradian (sr). The fluorescence signals were quantified by an efficiency measurement where the emission

image is normalized (divided) by a stored reference image of the excitation light intensity and has arbitrary units (A.U.). This efficiency measurement was calculated by Living Image Software (Caliper Life Sciences/Perkin Elmer, Hopkinton, MA). Images were taken at 1 min, 1 h, 2h, 11h, and 12 h after intravenous liposome injections. Mice injected with bare, PEGylated and non-PEGylated, aE-selectin-conjugated liposomes were euthanized 1 h after liposome injection. Mice injected with PEGylated, aE-selectin-conjugated liposomes were imaged 1 h post-injection and euthanized 12 h post-injection.

4.2.6 Tissue Harvest

The following organs were immediately excised after euthanasia: liver, spleen, kidneys, heart, abdominal aorta, and lungs. The organs were imaged immediately after excision using the Xenogen IVIS Spectrum system. Once imaged, the organs were placed in a 30% sucrose solution within minutes and stored at 4 °C for a maximum of one day until the tissue samples were processed for morphologic analysis. Tissue samples were embedded in Tissue-Tek® O.C.T. Compound (VWR, Radnor, PA) and frozen at -80 °C. Frozen samples were cryosectioned at a 6 μm thickness using a Leica cryostat (Leica Biosystems, Buffalo Grove, IL) and tissue sections were placed on SuperFrost Plus glass slides (VWR, Radnor, PA). All samples were stored at -80 °C.

4.2.7 Fluorescence Imaging of Tissue Samples

Tissue sections were imaged using a Zeiss Axio Observer Z1 inverted fluorescence microscope (Carl Zeiss, Thornwood, NY) equipped with a Hammamatsu Orca-Flash camera using the DAPI and Cy5 filter cubes as well brightfield and phase

contrast modes. Images were taken using the 10X, 20X, and 40X objectives. Tissue sections were mounted with VECTASHIELD® mounting medium with DAPI (Vector Laboratories, Burlingame, CA) and sealed prior to imaging.

4.3 Results

4.3.1 In Vitro Evaluation of PEGylated Liposomes

It is now widely known the addition of a small fraction of PEG to liposome formulations dramatically increases the distribution half-life [121,122]. This has been demonstrated in pre-clinical studies [123,124] and in clinical studies [125]. Thus, we hypothesized incorporation of the polymer molecule would achieve similar blood circulation times in our *in vivo* studies. We investigated the binding and uptake of liposomes having the same basic formulation of unsaturated DOPC tested in the previous two aims, but this time we incorporated various amounts of DSPE-PEG and DOPE-PEG in their formulation.

First, we assessed the binding and uptake of liposomes that included 1 mol % of DSPE-PEG with a molecular weight of 2000 Da. Each lipid molecule was functionalized with one terminal amine group, as shown on **Figure 4.1 (A)**, which served as a conjugation anchor for antibodies in substitution for N-dod-PE's terminal carboxyl group used previously. Liposomes conjugated with aE-selectin showed again a significant different in binding and uptake by activated ECs compared to controls (**Figure 4.1 (B)**).

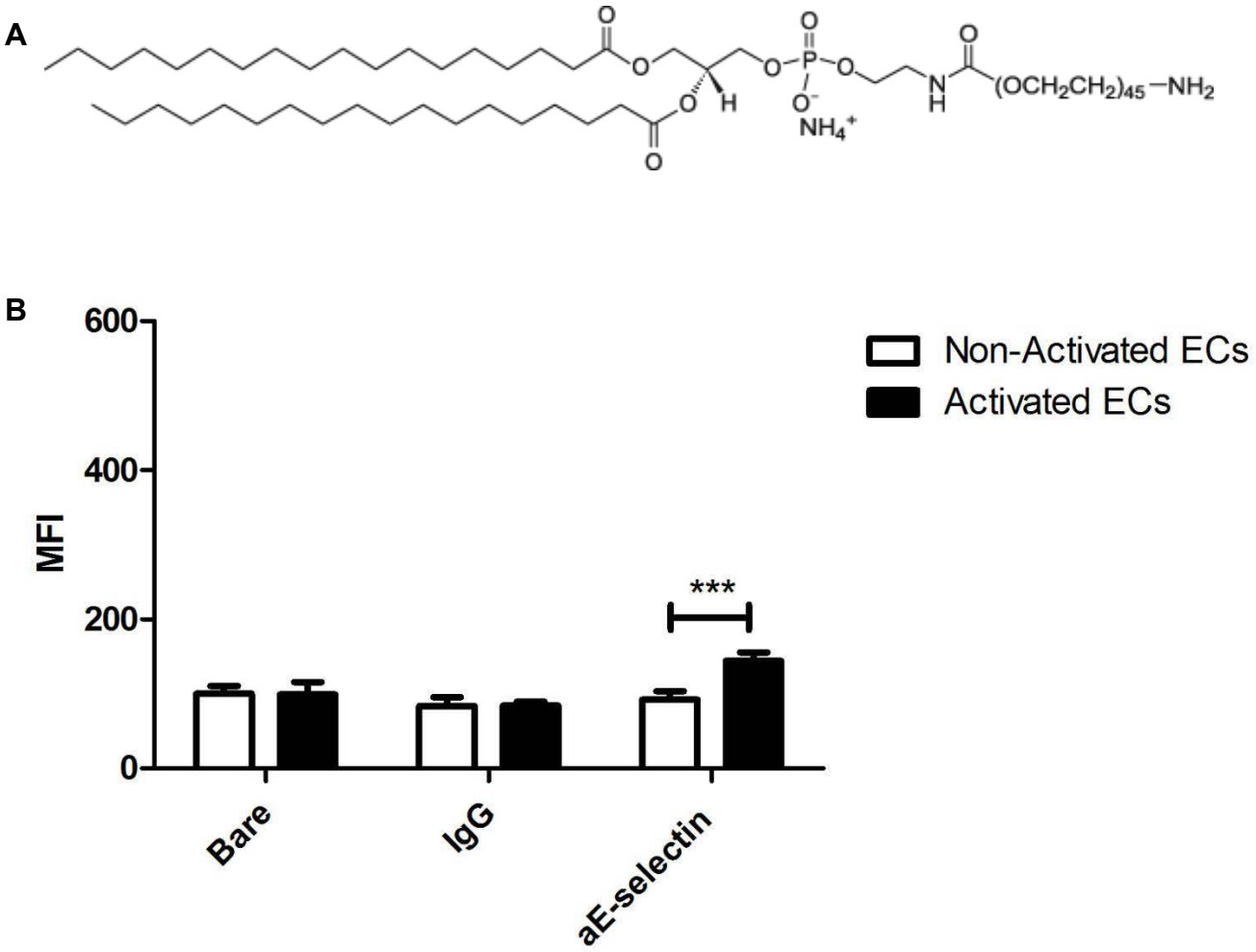

Figure 4.1: Flow cytometry evaluation of amine functionalized-PEGylated liposome binding and uptake by ECs after 1 h incubation. DSPE-PEG had a molecular weight of 2000 Da and was functionalized with a terminal amine group (A). Non-activated and activated ECs (IL-1α, 6 h) were treated with DOPC:DSPE-PEG (99:1 mol:mol) liposomes encapsulating rhodamine-labeled dextran and without antibody surface conjugation (bare) or conjugated with either IgG_1 or aE-selectin mAbs for 1 h (B). Results shown are raw mean fluorescence intensity (MFI) values. Error bars are reported as standard deviation, n = 3. Statistical significance was calculated using a two-way ANOVA test (*$p < 0.05$, **$p < 0.01$, and ***$p < 0.001$).

We simultaneously tested two other lipid formulations with unsaturated DOPE-PEG (**Figure 4.1 (A)**), which had a molecular weight of 5000 Da. 1 and 5 mol % of DOPE-PEG were incorporated into the formulation along with 5 mol % of N-dod-PE, which served as the antibody conjugation anchor. Both formulations had increased binding and uptake by activated ECs when aE-selectin mAbs were conjugated on the surface (**Figure 4.1 (B)** and **(C)**). However, DOPC liposomes containing 1 mol % DOPE-PEG had high non-specific binding and uptake by both bare and IgG_1 conjugated liposomes regardless of whether or not ECs were exposed to the cytokine. DOPC liposomes containing 5 mol % DOPE-PEG, on the other hand, had lower non-specific binding, but achieved similar results when conjugated with aE-selectin mAbs. Differences in binding and uptake for this condition were statistically significant.

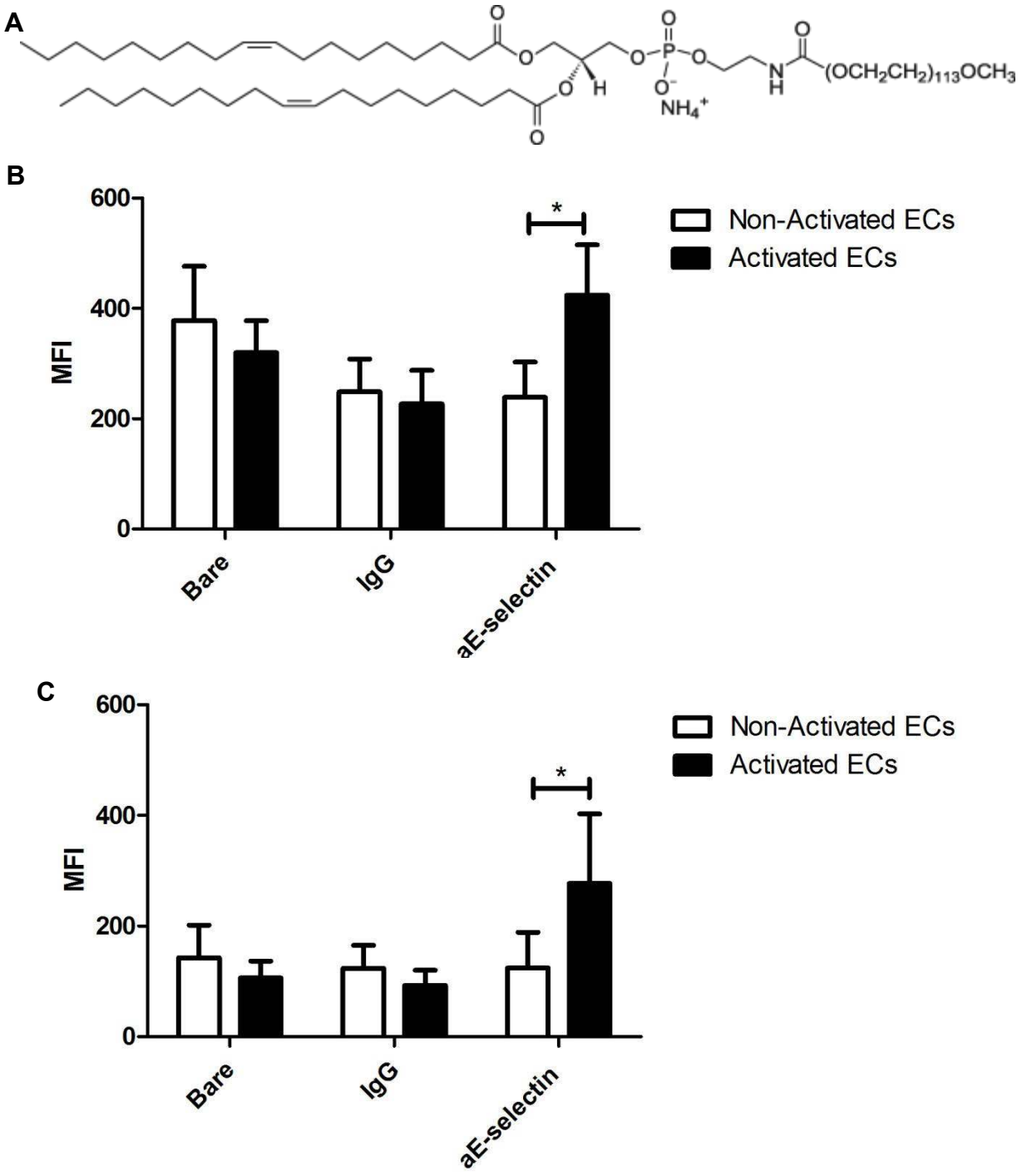

Figure 4.2: Flow cytometry evaluation of PEGylated liposome binding and uptake by ECs after 1 h incubation. DOPE-PEG (A) had a molecular weight of 5000 Da. Non-activated and activated ECs (IL-1α, 6 h) were treated with DOPC:N-dod-PE:DOPE-

Figure 4.2 (Continued): PEG (94:5:1 mol:mol:mol) (B) and DOPC:N-dod-PE:DOPE-PEG (90:5:5 mol:mol:mol) (C) liposomes encapsulating rhodamine-labeled dextran and without antibody surface conjugation (bare) or conjugated with either IgG_1 or aE-selectin mAbs for 1 h. Results shown are raw mean fluorescence intensity (MFI) values. Error bars are reported as standard deviation, n = 3. Statistical significance was calculated using a two-way ANOVA test (*p < 0.05, **p < 0.01, and ***p < 0.001).

4.3.2 In Vivo Evaluation of Biodistribution of DOPC PEGylated Liposomes

Based on the previously mentioned *in vitro* results, we decided to use DOPC:N-dod-PE:DOPE-PEG (90:5:5 mol:mol:mol) liposomes conjugated with aE-selectin for our small *in vivo* pilot study. An additional 0.5 mol % of DiD was added to the formulation in order to adequately label liposomes to be detected by the *in vivo* imaging system (IVIS). DiD is a lipophilic dialkylcarbocyanine dye which has been reported to have improved fluorescence yield and life-times when used in small rodents for in vivo imaging [126,127]. A total of four mice were used in this study. **Figures 4.3 and 4.4** demonstrate the rapid accumulation of liposomes (within 1 h) in the liver and spleen. Qualitatively speaking, the accumulation of PEGylated, bare liposomes seemed to be more evident in the spleen than in the liver; while accumulation of PEGylated, aE-selectin conjugated liposomes seemed to be high in both of these organs.

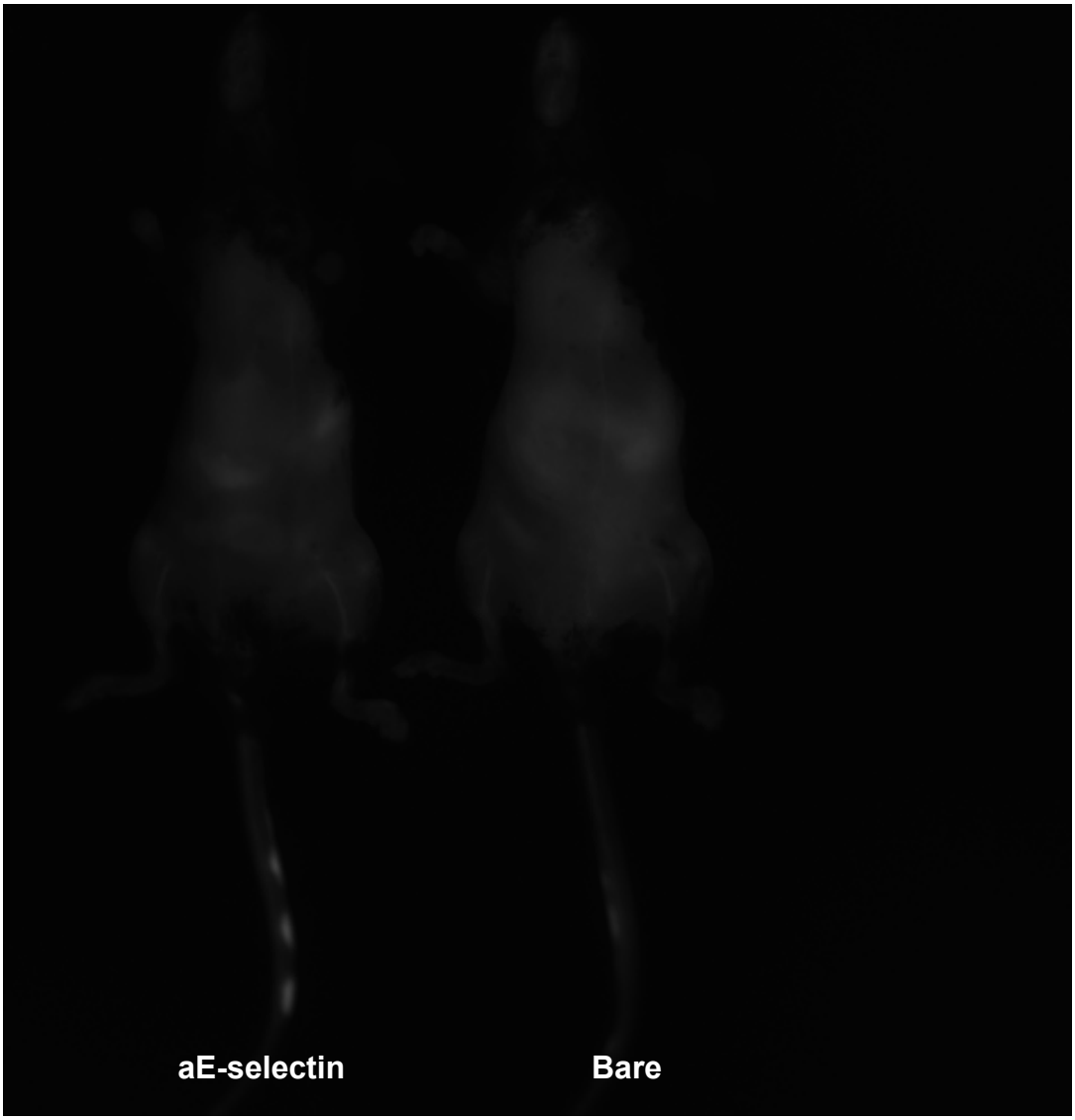

Figure 4.3: ***In vivo*** **fluorescence imaging of mice injected with DiD labeled liposomes at 1 min post-injection.** Mice received a tail vein injection of liposomes containing 5% PEG and 0.5% DiD with aE-selectin conjugated on the surface (left) and without any antibody conjugated (right). Image was captured after 1 min post-injection with a Xenogen IVIS Spectrum system to track the accumulation of fluorescent labeled liposomes.

Figure 4.4: ***In vivo*** **fluorescence imaging of mice injected with DiD labeled liposomes at 61 min post-injection.** Mice received a tail vein injection of liposomes containing 5% PEG and 0.5% DiD with aE-selectin conjugated on the surface (left) and without any antibody conjugated (right). Image was captured after 61 min post-injection with a Xenogen IVIS Spectrum system to track the accumulation of fluorescent labeled liposomes. Arrows indicate increased accumulation of liposomes in the liver and spleen.

After 1 h, the mouse which had been injected a dose of PEGylated, bare liposomes was euthanized and its organs excised and imaged via Xenogen IVIS Spectrum system as can be seen in **Figure 4.5**. The fluorescence signal was quantified by the radiant efficiency measurement. The liver and spleens emitted the highest amount of fluorescent signals compared to all other organs. The radiant efficiency of these organs was approximately 4.0 x 10^9 A.U.

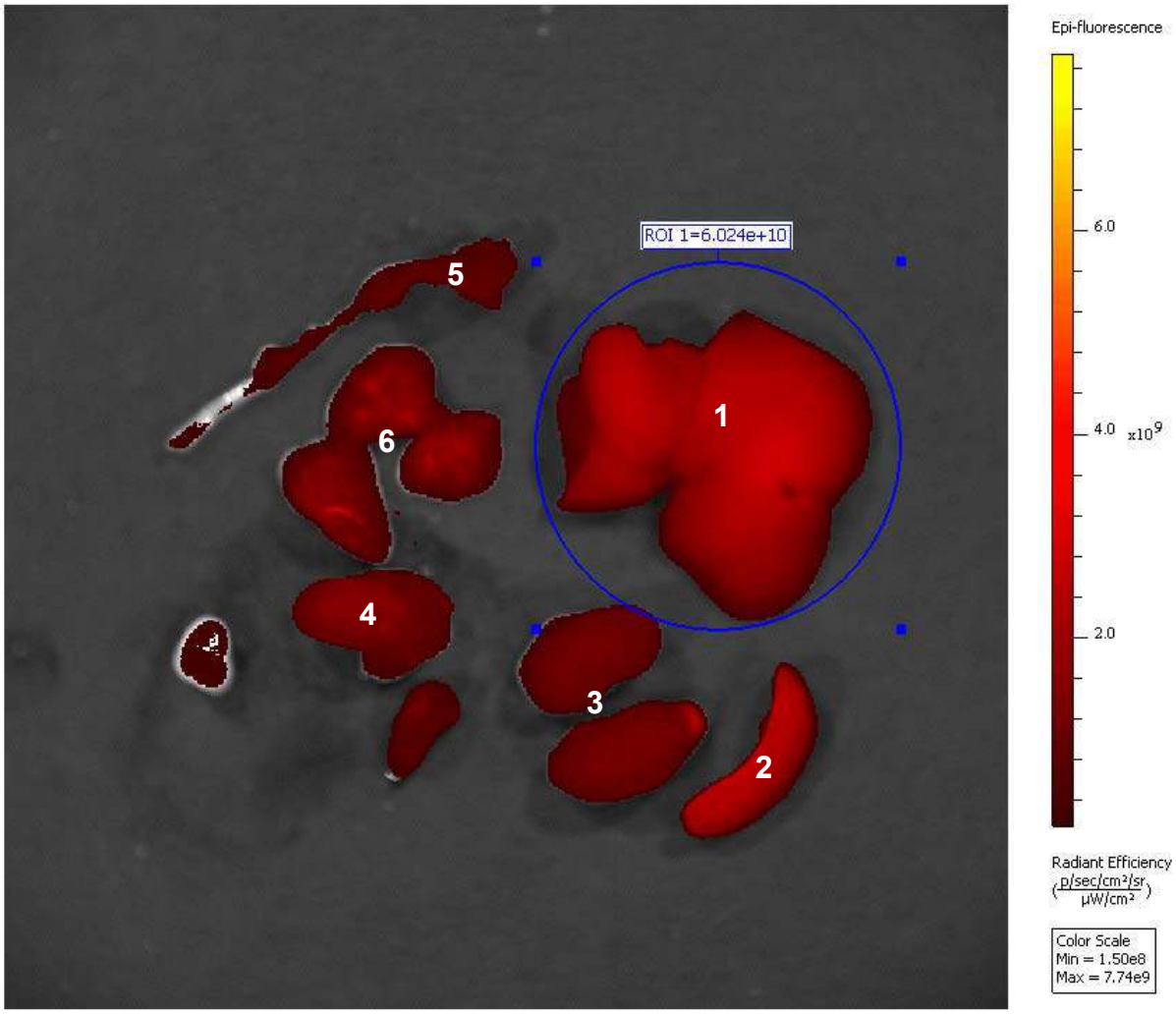

Figure 4.5: ***In vivo*** **fluorescence imaging of excised mouse organs; bare liposome condition.** Mouse received a tail vein injection of bare liposomes containing

Figure 4.5 (Continued): 5% PEG and 0.5% DiD and was sacrificed after 1 h. Liver (1), spleen (2), kidneys (3), heart (4), aorta (5), and lungs (6) were excised at this time. Image was captured immediately after organ excision with a Xenogen IVIS Spectrum system to track the accumulation of fluorescent labeled liposomes.

The mouse exposed to PEGylated, aE-selectin conjugated liposomes was kept alive for a total of 12 h. A third mouse, placed on the center as shown in **Figures 4.6** and **4.7**, was injected with 0.3 μg of IL-1α and then injected intravenously with PEGylated, aE-selectin conjugated liposomes. Immediately after, a fourth mouse, placed on the right as shown in **Figures 4.6** and **4.7,** was injected intravenously with only non-PEGylated, aE-selectin conjugated liposomes. After 1 min, no significant changes in fluorescent signal were apparent in the mouse exposed to the cytokine. At this same time point, the mouse injected with non-PEGylated, aE-selectin conjugated liposomes on the right appeared to have rapid liposome localization to possibly the lungs, liver, and spleen, as the entire upper section of the body had a high fluorescent signal. This same trend continued after 1 h (**Figure 4.7**) and there appeared to be no significant changes in the organ accumulation patterns of either three conditions.

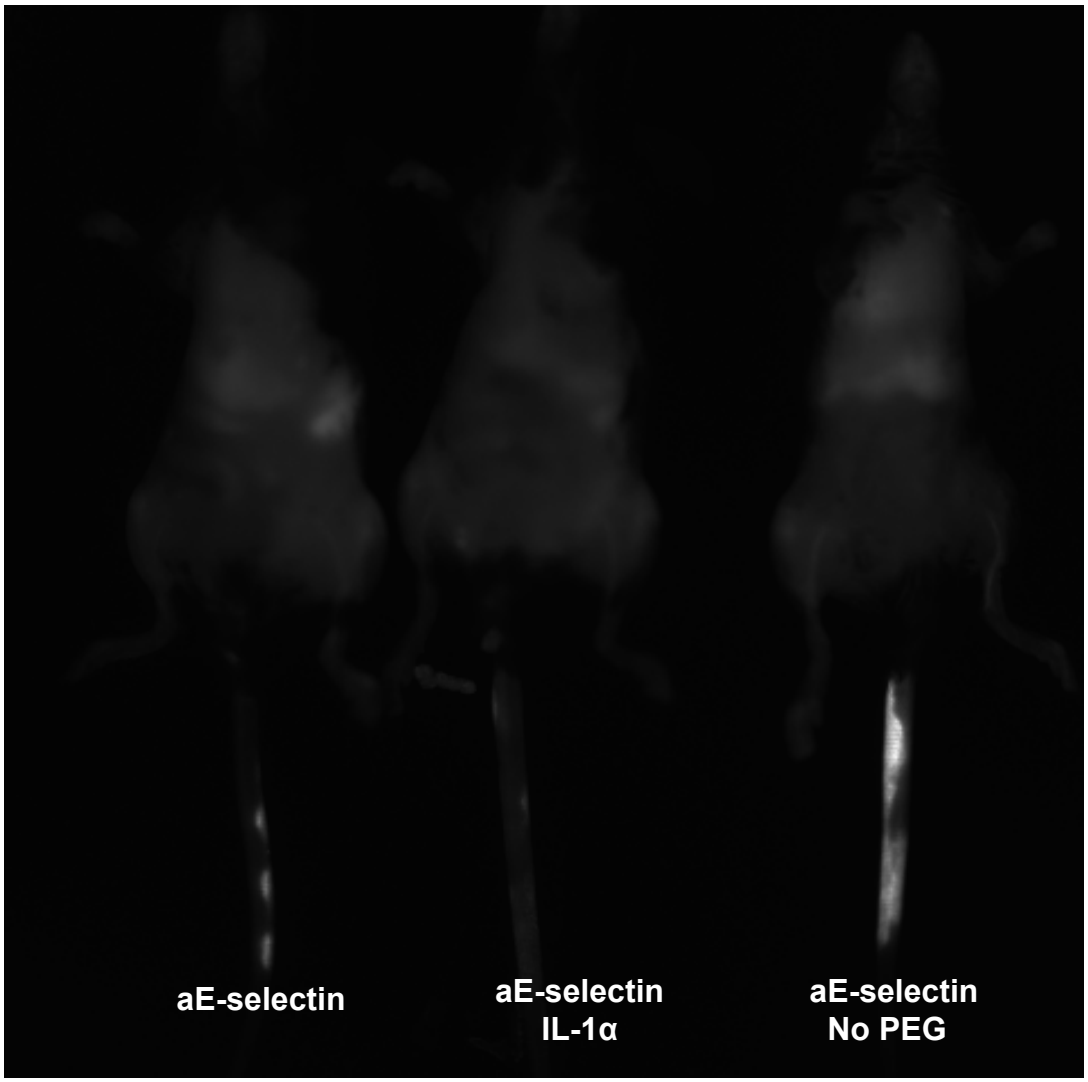

Figure 4.6: ***In vivo*** **fluorescence imaging of mice injected with DiD labeled liposomes at 61 and 1 min post-injection.** Mice received a tail vein injection of DiD labeled PEGylated liposomes with aE-selectin conjugated on the surface (center) and non-PEGylated liposomes (right). Only mouse on the center received 0.3 μg IL-1α intravenously prior to liposome injection. Mouse on the left was kept alive and is the same mouse from **Figures 4.3 and 4.4**. Image was captured after 61 min post-injection

Figure 4.6 (Continued): for mouse on the left and after 1 min post-injection for mice on the center and right with a Xenogen IVIS Spectrum system to track the accumulation of fluorescent labeled liposomes.

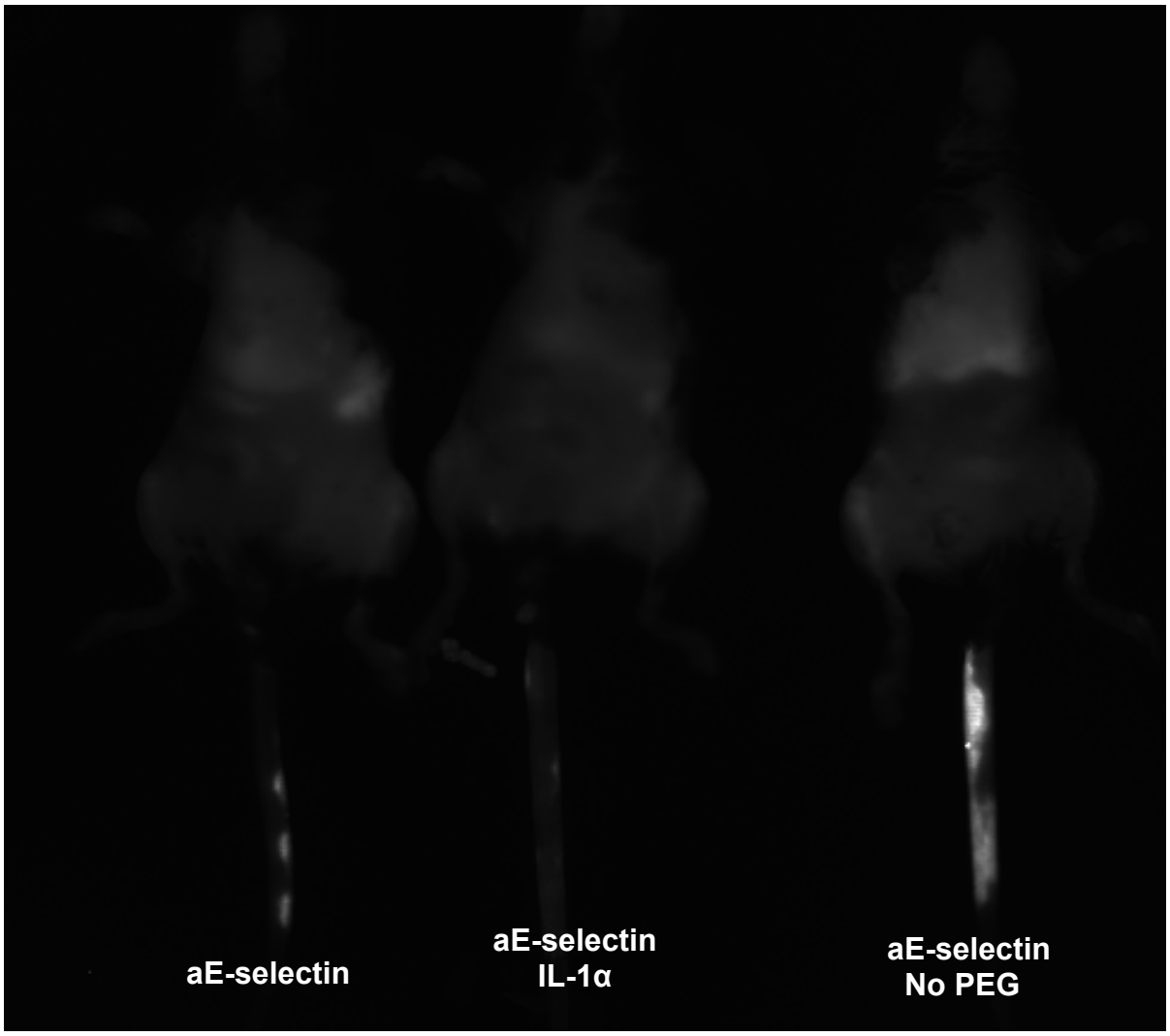

Figure 4.7: *In vivo* fluorescence imaging of mice injected with DiD labeled liposomes at 121 and 61 min post-injection. Mice received a tail vein injection of DiD labeled PEGylated liposomes with aE-selectin conjugated on the surface (center) and non-PEGylated liposomes (right). Only mouse on the center received 0.3 μg IL-1α

Figure 4.7 (Continued): intravenously prior to liposome injection. Mouse on the left was kept alive and is the same mouse from **Figures 4.3 and 4.4**. Image was captured after 121 min post-injection for mouse on the left and after 61 min post-injection for mice on the center and right with a Xenogen IVIS Spectrum system to track the accumulation of fluorescent labeled liposomes.

The mouse exposed to non-PEGylated, aE-selectin conjugated liposomes was euthanized 1 h after the liposome intravenous injection was administered to it. Its organs were excised and imaged as shown in **Figure 4.8**. High fluorescent signal was detected in the liver and spleen. Radiant efficiency values were approximated between 6×10^9 A.U. and 8×10^9 A.U.; the liver displayed the highest levels of fluorescence.

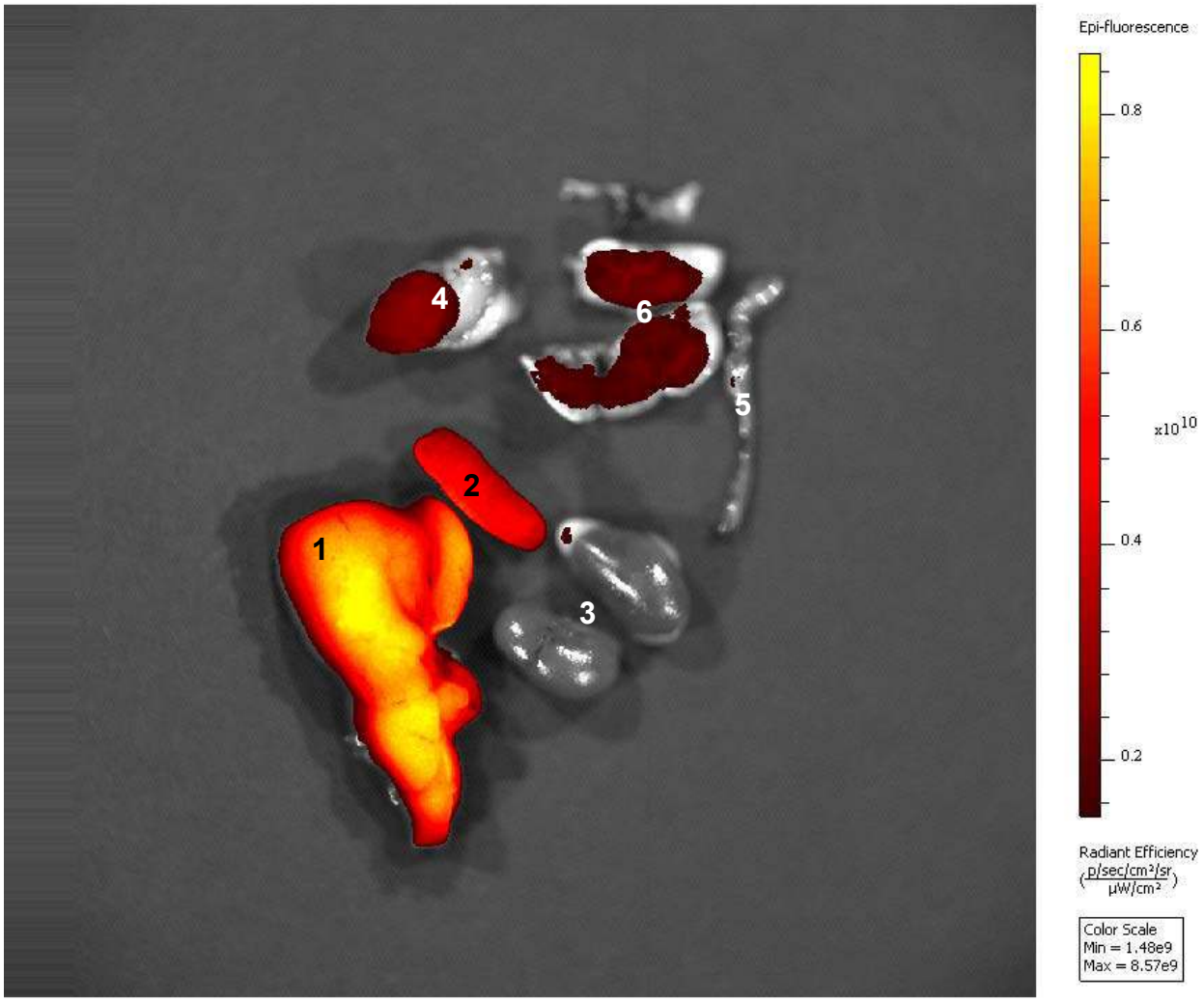

Figure 4.8: ***In vivo*** **fluorescence imaging of excised mouse organs; non-PEGylated, aE-selectin decorated liposome condition.** Mouse received a tail vein injection of non-PEGylated liposomes containing 0.5% DiD and aE-selectin on the surface. Liver (1), spleen (2), kidneys (3), heart (4), aorta (5), and lungs (6) were excised immediately after sacrificing the mouse at 1 h post-injection time. Image was captured promptly after organ excision with a Xenogen IVIS Spectrum system to track the accumulation of fluorescent labeled liposomes.

Both mice injected with PEGylated liposomes conjugated with aE-selectin were monitored for a total of 12 h. The image represented below (**Figure 4.9)** was taken at 11 h post-liposome injection time and 11.5 h after the cytokine injection for the mouse on the right. Although the large and small intestines have emitted some fluorescence signal, the highest liposome accumulation appeared to be in the spleen for both animals. At this time, 12 h had passed since the mouse on the left, which was not exposed to IL-1α, received the liposome injection and thus, it was euthanized. The last mouse (**Figure 4.9** (right)) was euthanized 1 h thereafter.

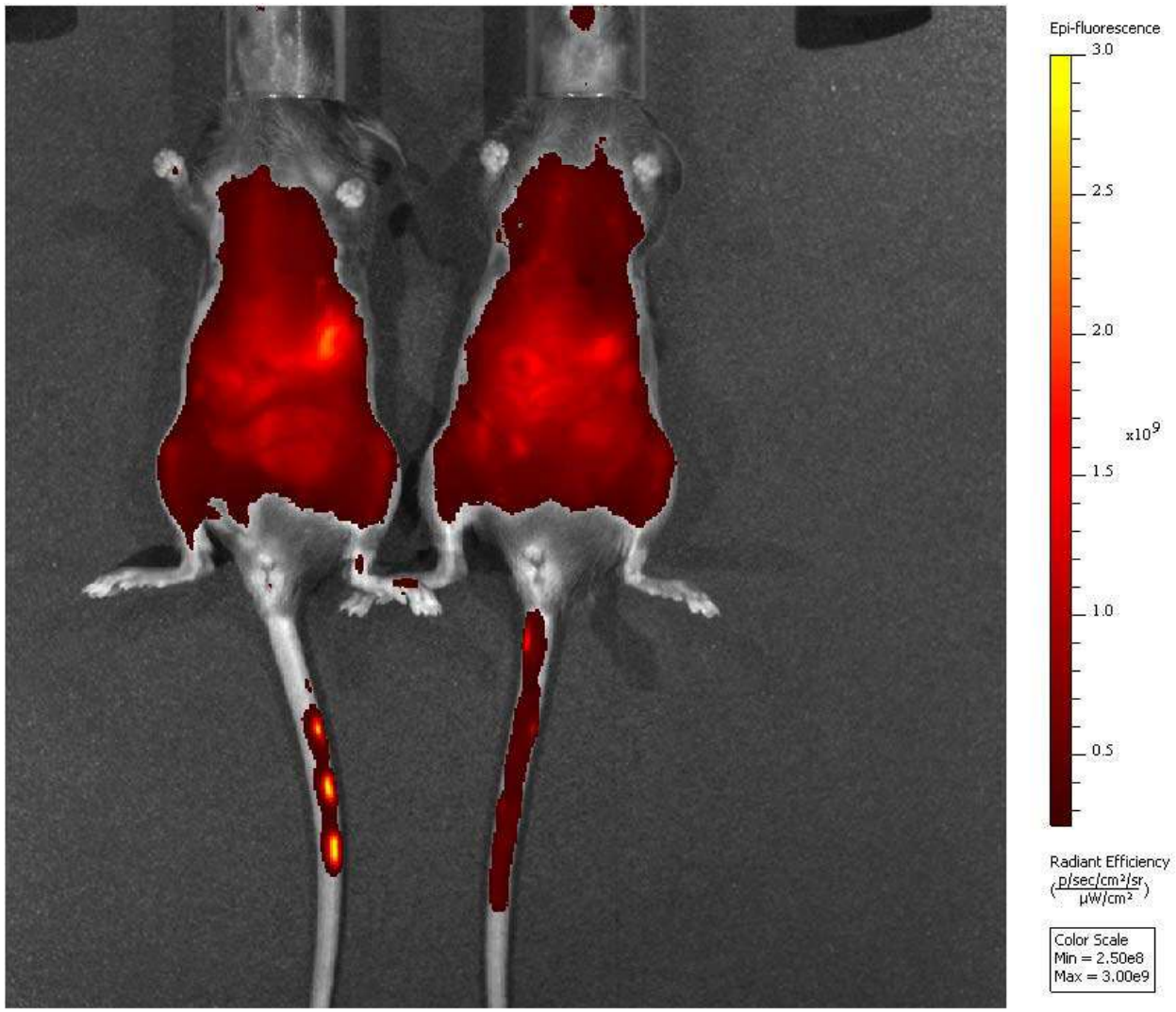

Figure 4.9: ***In vivo*** **fluorescence imaging of mice injected with DiD labeled**

Figure 4.9 (Continued): **liposomes at 12 h and 11 h post-injection.** Mice received a tail vein injection of DiD labeled PEGylated liposomes with aE-selectin conjugated on the surface. Only mouse on the right received 0.3 μg IL-1α intravenously prior to liposome injection. Image was captured after 12 h and 11 h post-injection for mice on the left and right, respectively, with a Xenogen IVIS Spectrum system to track the accumulation of fluorescent labeled liposomes.

Organs of both animals were excised immediately after euthanasia and imaged using the IVIS system again. Images are shown in **Figures 4.10** and **4.11**. The mouse not exposed to cytokine IL-1α **(Figure 4.10)** shows a remarkable liposome accumulation in the spleen with an approximate radiant efficiency value of 3×10^9 A.U. The liver and heart also display a high level of liposome accumulation, with radiant efficiency values of approximately 1.5×10^9 to 2×10^9 A.U. Liposome accumulation of mouse exposed to IL-1α was fairly similar **(Figure 4.11)**; the liver and spleen emitting the highest fluorescence intensity, which also oscillated from 1.5×10^9 to 2×10^9 A.U. The heart had a lower radiant efficiency consisting of approximately 1.0×10^9 A.U.

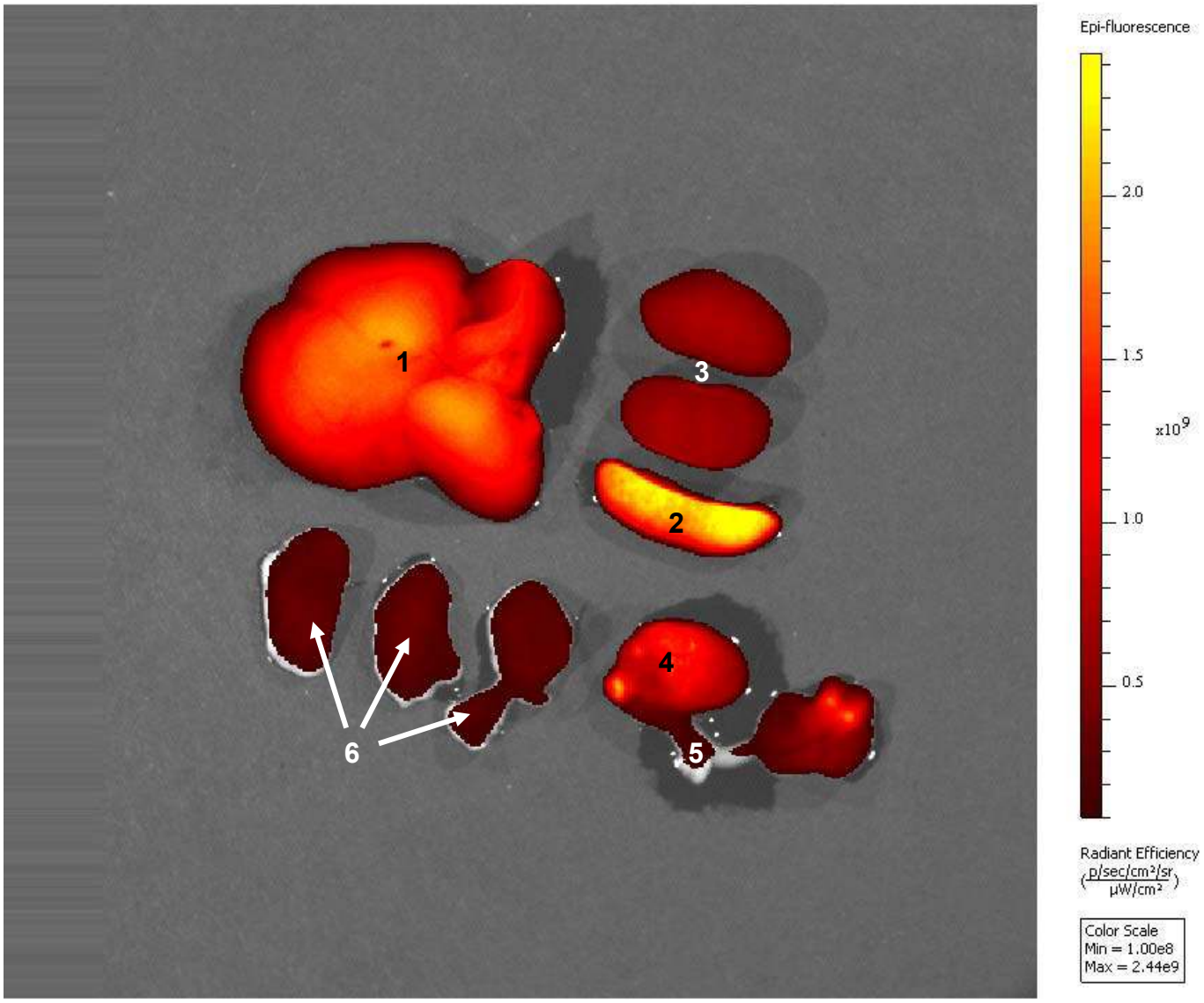

Figure 4.10: ***In vivo*** **fluorescence imaging of excised mouse organs; PEGylated, aE-selectin decorated liposome condition.** Mouse received a tail vein injection of PEGylated liposomes containing 0.5% DiD and aE-selectin on the surface. Liver (1), spleen (2), kidneys (3), heart (4), aorta (5), and lungs (6) were excised immediately after sacrificing the mouse at 12 h post-injection time. Image was captured promptly after organ excision with a Xenogen IVIS Spectrum system to track the accumulation of fluorescent labeled liposomes.

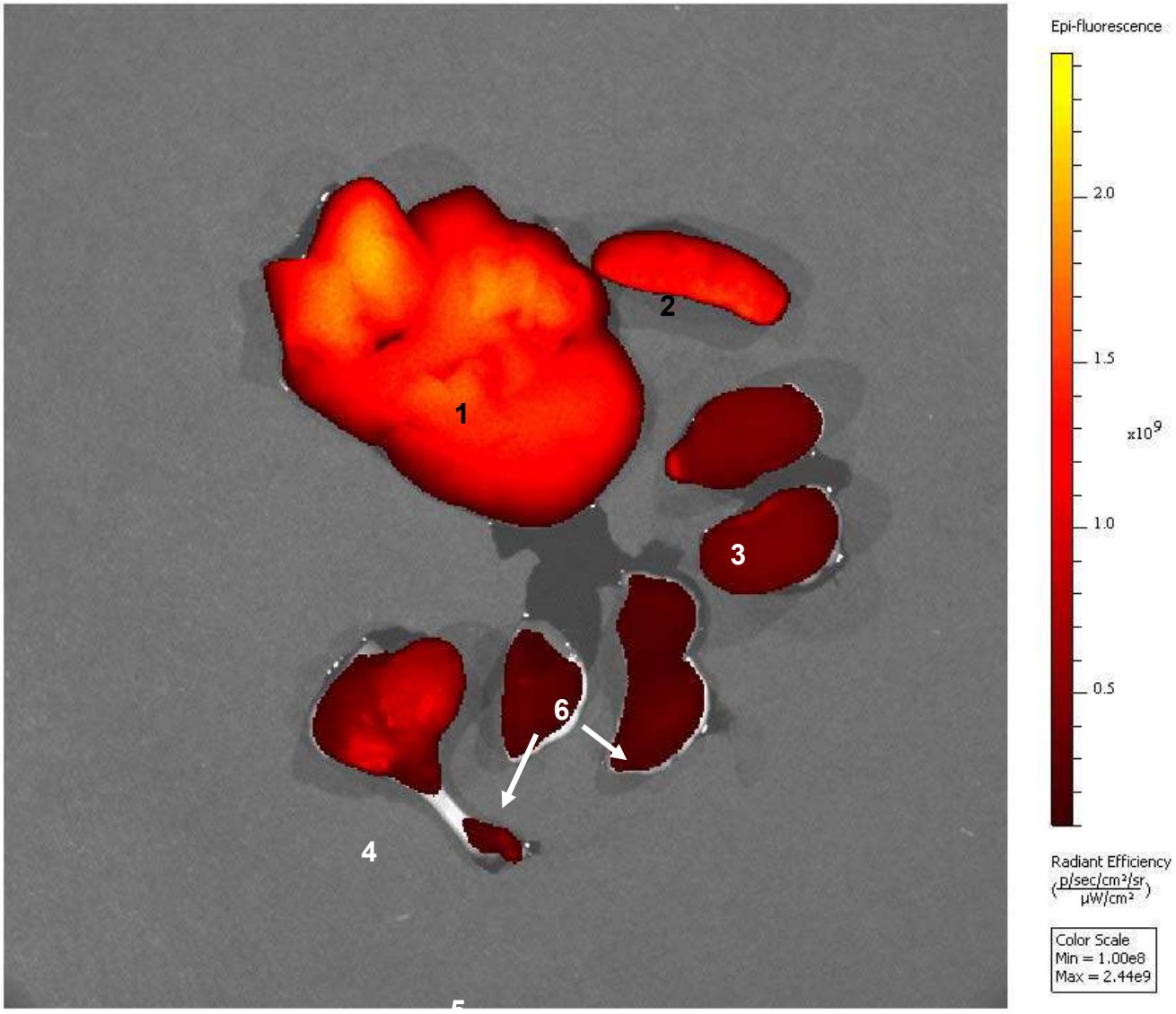

Figure 4.11: ***In vivo*** **fluorescence imaging of excised mouse organs; IL-1α and PEGylated, aE-selectin decorated liposome condition.** Mouse received 0.3 µg IL-1α intravenously and then received a second tail vein injection of PEGylated liposomes containing 0.5% DiD and aE-selectin on the surface. Liver (1), spleen (2), kidneys (3), heart (4), aorta (5), and lungs (6) were excised immediately after sacrificing the mouse at 12 h post-injection time. Image was captured promptly after organ excision with a Xenogen IVIS Spectrum system to track the accumulation of fluorescent labeled liposomes.

4.3.3 Fluorescence Imaging of Liver and Aorta Tissue Sections

Organs were preserved, processed, and cryosectioned into 6 μm thick sections. Liver tissue sections were stained with DAPI, mounted, and imaged under a fluorescence microscope. Images confirmed mice euthanized 1 h post-injection of bare, PEGylated liposomes (**Figure 4.12 (A)**) and of non-PEGylated, aE-selectin conjugated liposomes (**Figure 4.12 (B)**) both had a high accumulation in the liver. However, the distribution of the liposomes seemed to be different among different types of cells comprising the liver tissue. Fluorescence of non-PEGylated liposomes was very punctate while bare, PEGylated liposomes' fluorescence signal was uniformly distributed with round, small puncta of intense fluorescence.

Liver tissue sections of animals exposed to PEGylated liposomes conjugated with aE-selectin showed similar fluorescence overall (**Figure 4.13**). Tissue sections from the animal exposed to IL-1α also displayed very round puncta of intense fluorescence. On the other hand, these morphologic characteristics were not found in the cytokine-free condition, instead the general fluorescence pattern was similar to that of the non-PEGylated liposomes shown in **Figure 4.12 (B)**.

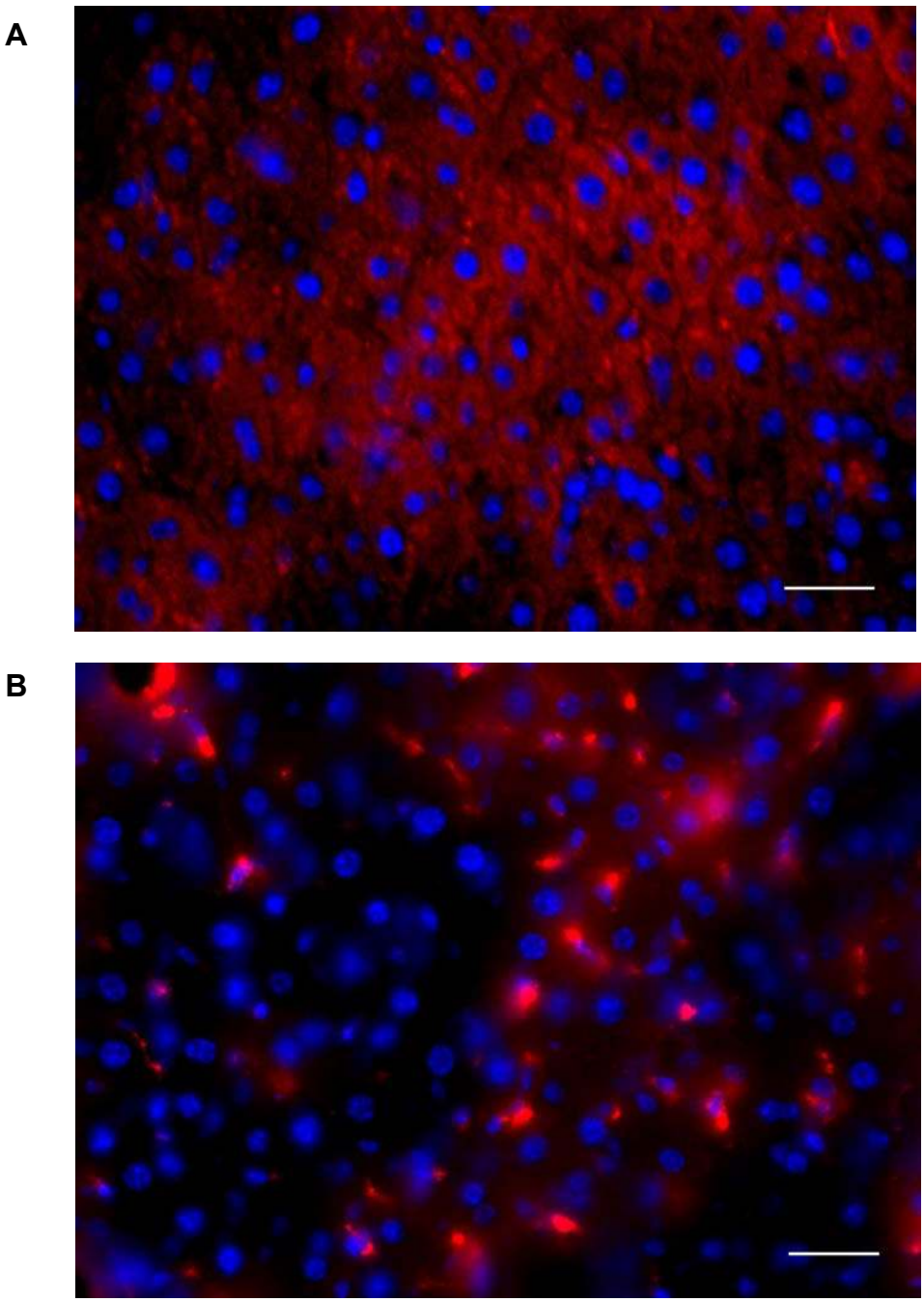

Figure 4.12: Fluorescence microscopy images of mouse liver tissue (bare vs. non-PEGylated liposomes). Mice received a tail vein injection of bare liposomes containing 5% PEG (A) and non-PEGylated liposomes decorated with aE-selectin (B). Merged images are showing 6 µm thick cryostat sections of liver tissue with DAPI stained cell nuclei (in blue) and liposomes containing DiD (in red). Scale bar, 20 µm.

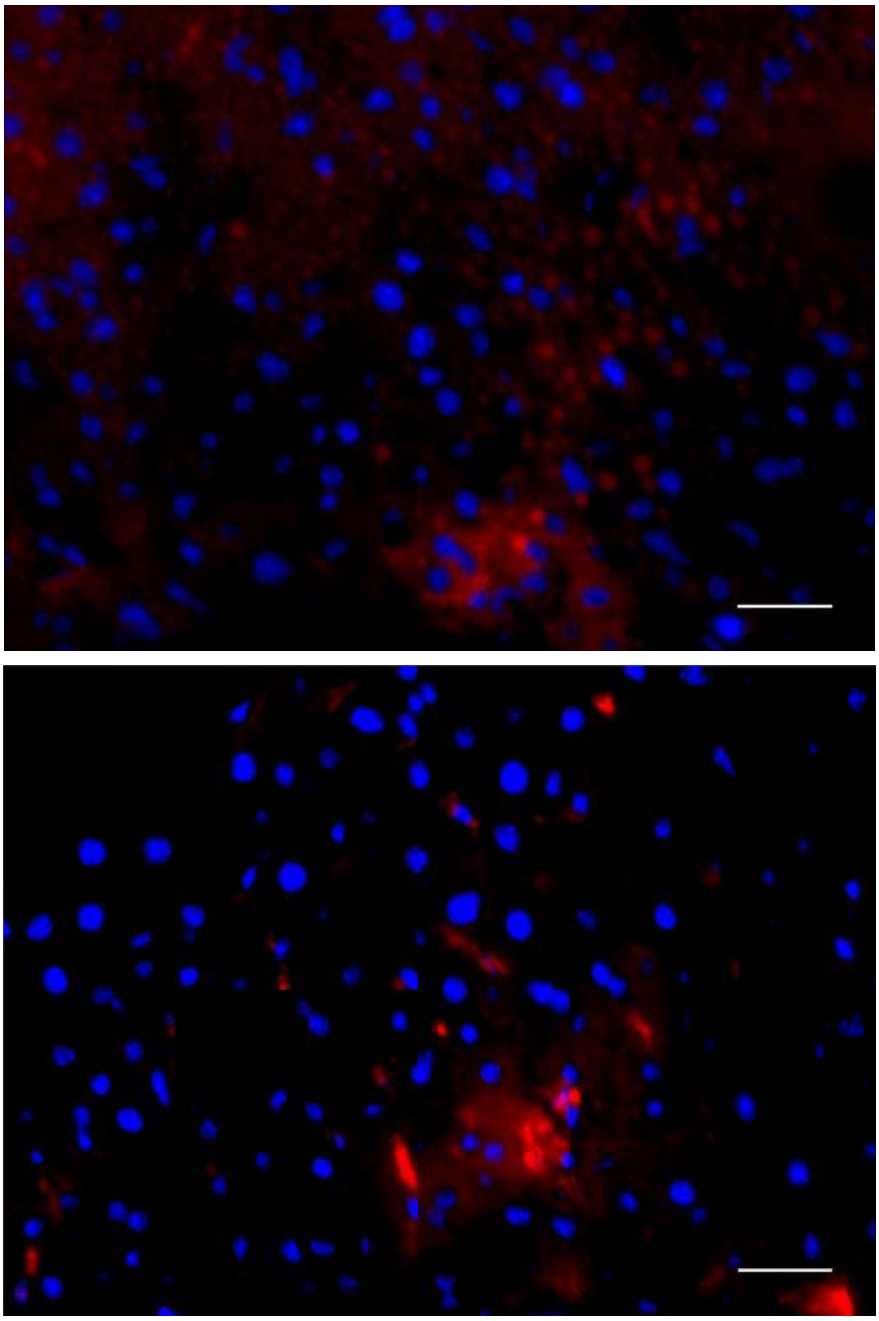

Figure 4.13: Fluorescence microscopy images of mouse liver tissue. Mice received a tail vein injection of PEGylated liposomes functionalized with aE-selectin. A tail vein injection of 0.3 μg IL-1α was given to mouse (A) but not to mouse (B). Merged images are showing 6 μm thick cryostat sections of liver tissue with DAPI stained cell nuclei (in blue) and liposomes containing DiD (in red). Scale bar, 20 μm.

Cross-sections of mouse aortas were cryosectioned and imaged. Two primary, different morphological characteristics of the outline of the tunica intima, media, and adventitia were observed. Sections of aortas from bare and aE-selectin conjugated, PEGylated liposome animal conditions had distinct folds (**Figures 4.14 and 4.16**) while the other two conditions displayed a normal oblong outline of the cross-sectioned blood vessel (**Figures 4.15 and 4.17**). Low amounts of liposomes localized in all four tissue sections. Bare, PEGylated liposomes displayed the most punctate fluorescence near the vicinity of the endothelium, most likely in the tunica media and adventitia (**Figure 4.14**). E-selectin conjugated liposomes appeared to have accumulated directly on the endothelial lining of the blood vessel and in tissue distal from the endothelium (**Figures 4.15 and 4.17**). High fluorescence signal was detected in the blood vessel lumen of the animal exposed to IL-1α (**Figures 4.16**).

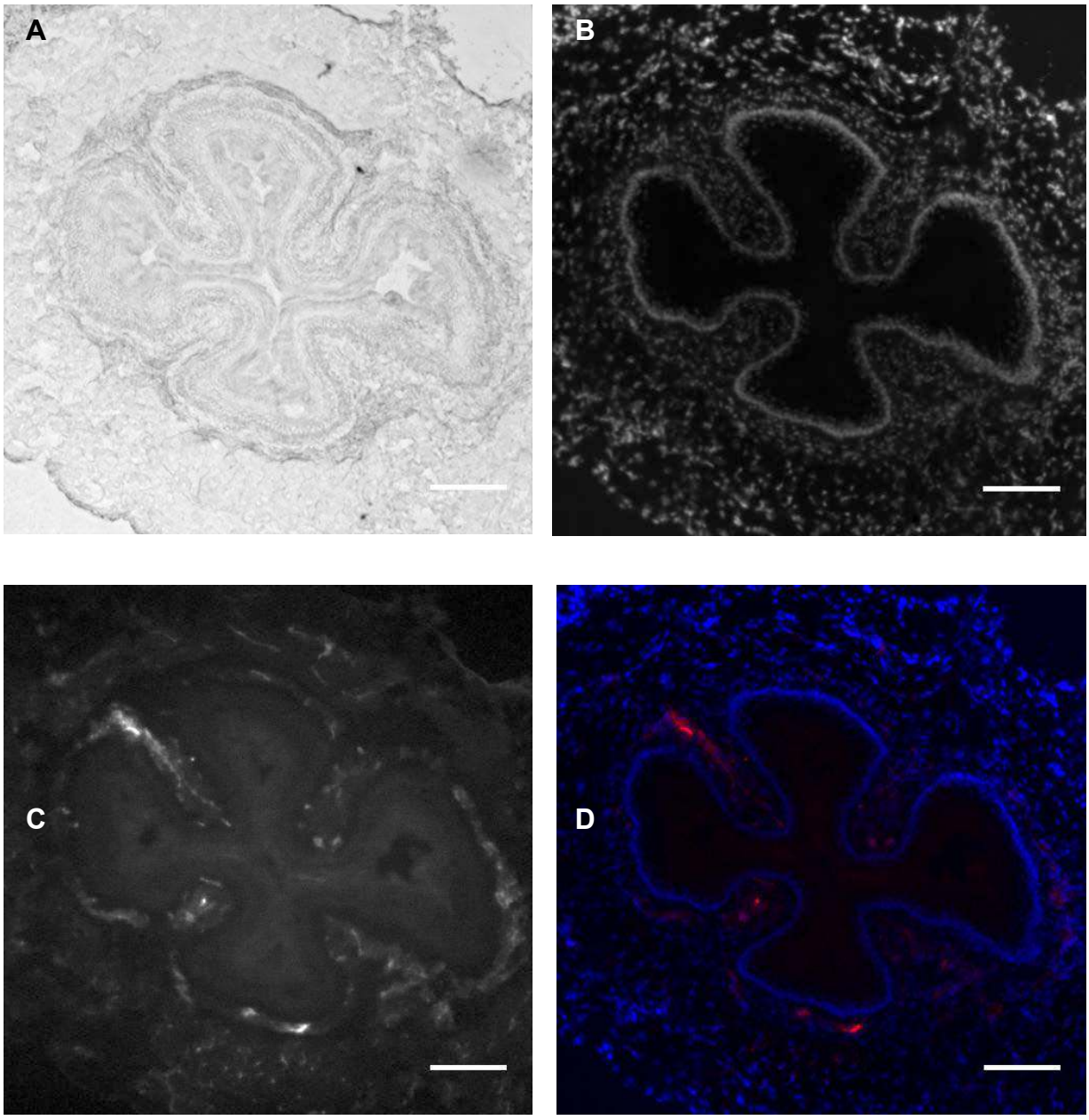

Figure 4.14: Microscopy images of mouse aortic tissue (bare liposomes). Mice received a tail vein injection of bare liposomes containing 5% PEG and decorated with aE-selectin. Images are showing 6 μm thick cryostat cross sectioned aortas under brightfield (A), DAPI fluorescence (B), DiD fluorescence (C), and the merged image with

Figure 4.14 (Continued): DAPI stained cell nuclei (in blue) and liposomes containing DiD (in red) (D). Scale bar, 40 μm.

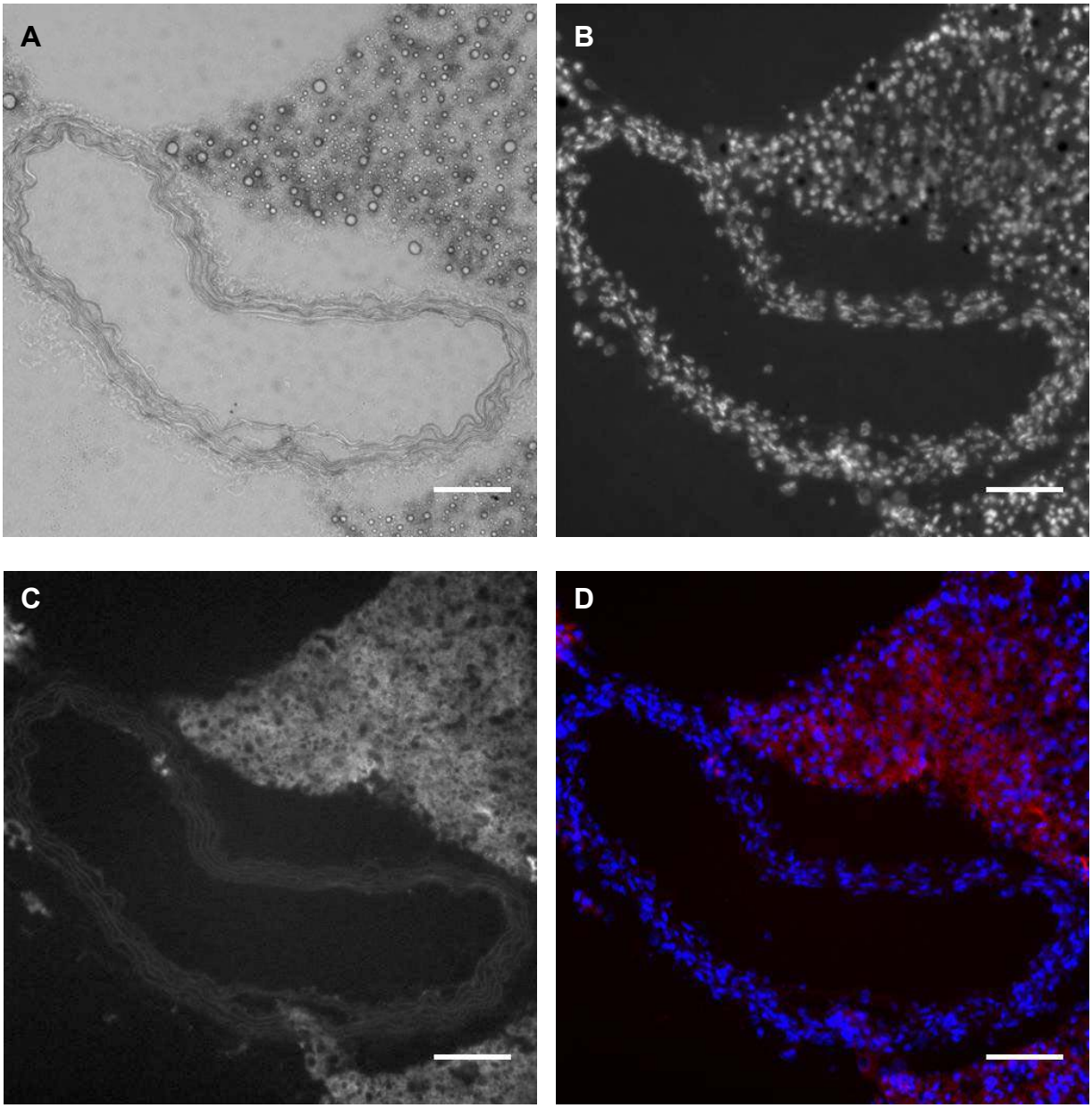

Figure 4.15: Microscopy images of mouse aortic tissue (non-PEGylated liposomes). Mice received a tail vein injection of liposomes decorated with aE-selectin. Images are showing 6 μm thick cryostat cross sectioned aortas under brightfield (A),

Figure 4.15 (Continued): DAPI fluorescence (B), DiD fluorescence (C), and the merged image with DAPI stained cell nuclei (in blue) and liposomes containing DiD (in red) (D). Scale bar, 40 μm.

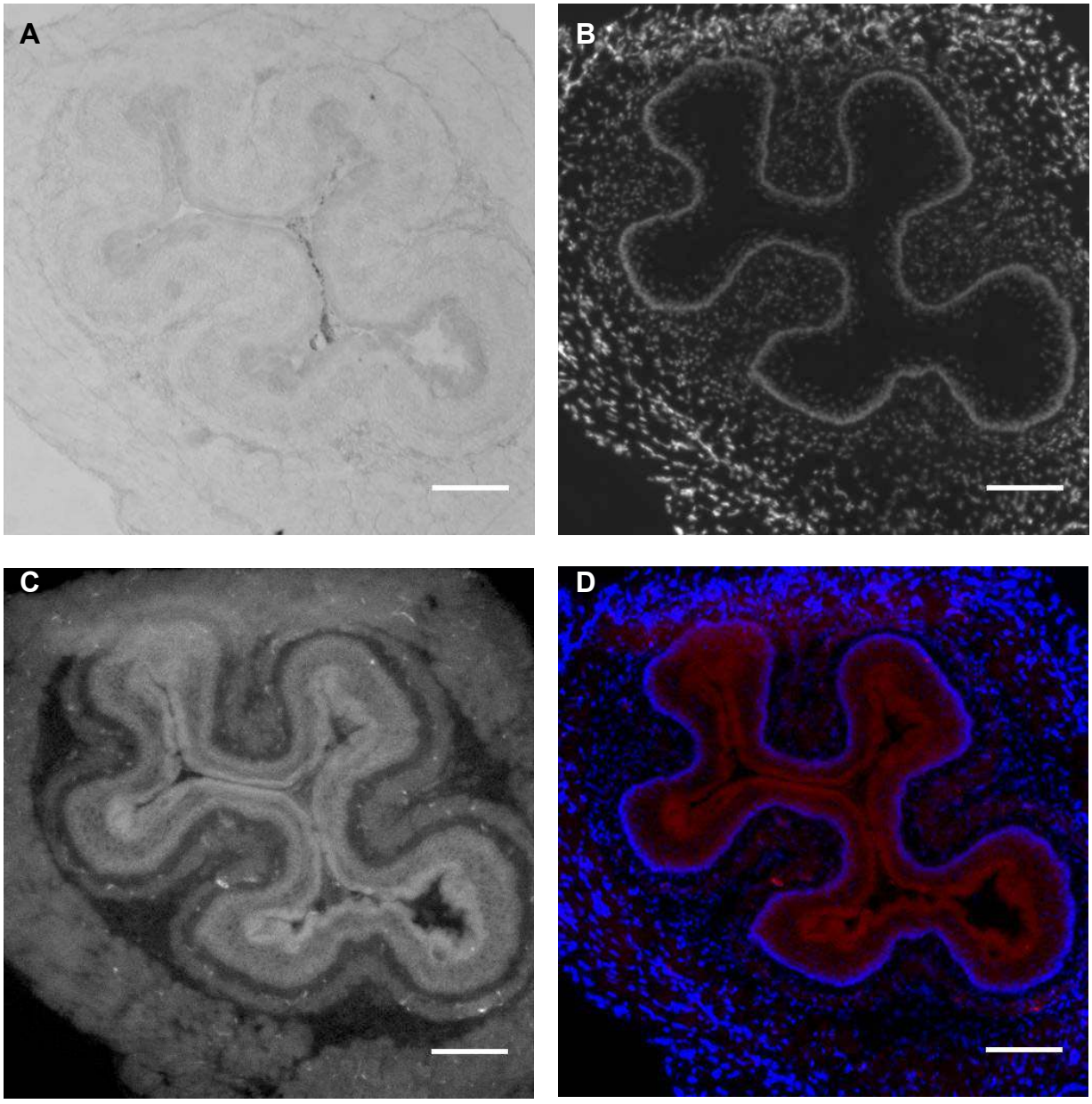

Figure 4.16: Microscopy images of mouse aortic tissue (IL-1α, aE-selectin-conjugated PEGylated liposomes). Mice received a tail vein injection of 0.3 μg IL-1α

Figure 4.16 (Continued): and a second injection of liposomes containing 5% PEG and decorated with aE-selectin. Images are showing 6 μm thick cryostat cross sectioned aortas under brightfield (A), DAPI fluorescence (B), DiD fluorescence (C), and the merged image with DAPI stained cell nuclei (in blue) and liposomes containing DiD (in red) (D). Scale bar, 40 μm.

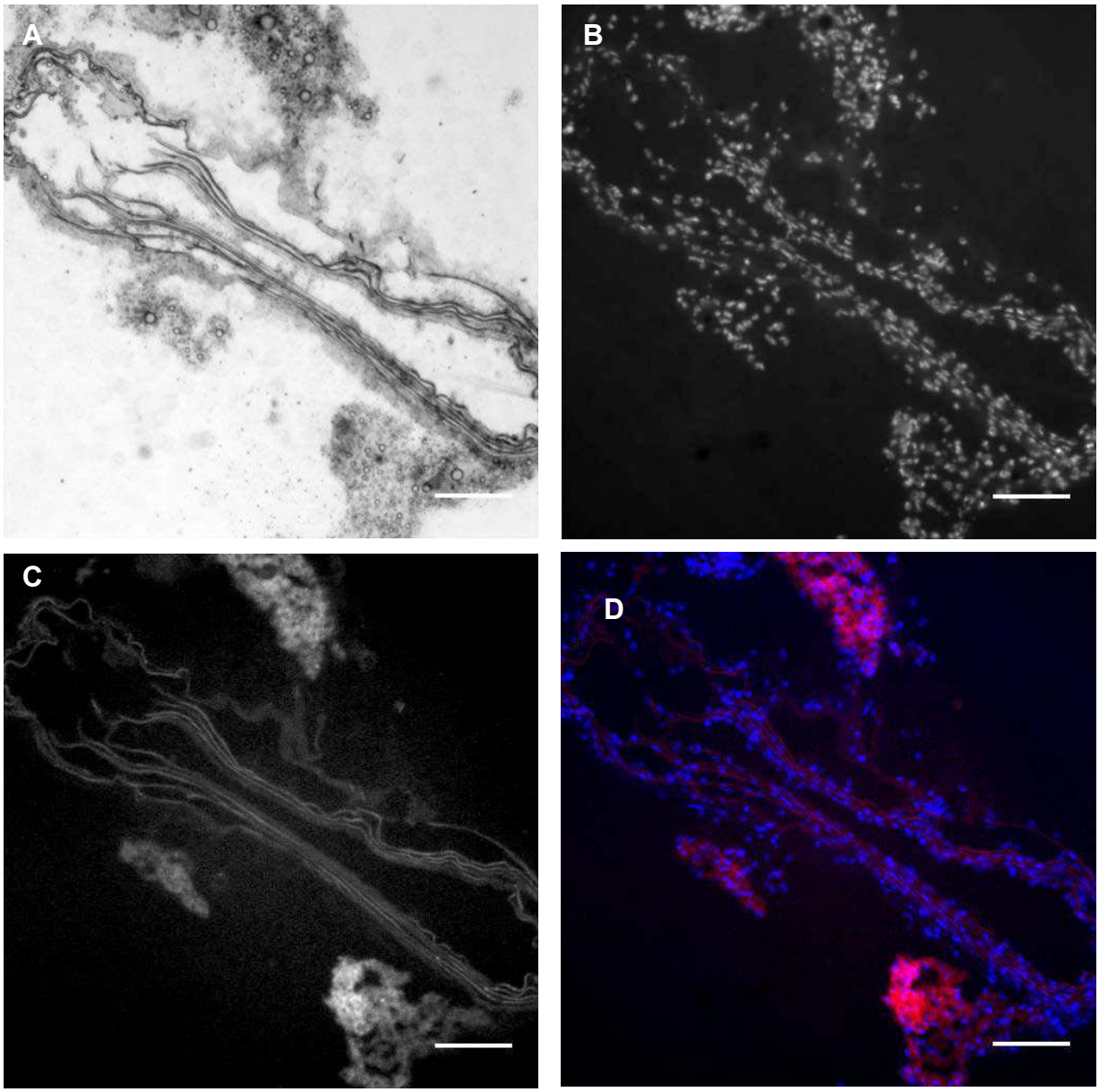

Figure 4.17: Microscopy images of mouse aortic tissue (aE-selectin-conjugated PEGylated liposomes). Mice received a tail vein injection of liposomes containing 5% PEG and decorated with aE-selectin. Images are showing 6 μm thick cryostat cross sectioned aortas under brightfield (A), DAPI fluorescence (B), DiD fluorescence (C), and the merged image with DAPI stained cell nuclei (in blue) and liposomes containing DiD (in red) (D). Scale bar, 40 μm.

4.4 Discussion

The initial goal of this aim was to assess the targeting efficiency of aE-selectin conjugated liposomes to atherosclerotic lesions in an ApoE-/- knockout mouse model. Due to time constraints, we were only able to conduct a small pilot *in vivo* study to assess liposome distribution in internal organ. Liposomes directly targeting inflamed vasculature may have potential useful applications in the imaging and treatment of inflammatory vascular diseases such as atherosclerosis. Previous studies have examined the targeting of aE-selectin conjugated liposomes to inflamed endothelium in different mouse models such as delayed type hypersensitivity (DTH) or skin inflammation [128], allergic or irritant contact dermatitis [129], glomerulonephritis [130], and rheumatoid arthritis [131]. In our studies, we examined the effect of PEG and cytokine IL-1α on the biodistribution of liposomes.

The use of PEG in liposome formulations to enhance blood plasma half-life is well documented [121–123,132]. We chose to compare the EC binding and uptake of rhodamine dextran loaded-liposomes bearing two different types of PEG molecules, amine functionalized DSPE-PEG(2000 Da) and DOPE-PEG(5000 Da), at three different concentrations. All three formulations had significant increase in uptake when conjugated with aE-selectin. Liposomes including 5 mol % of DOPE-PEG(5000 Da) had the lowest non-specific binding and was chosen to be tested *in vivo*. It should be noted, however, that all three formulations had significantly decreased MFI values *in vitro* compared to DOPC non-PEGylated liposomes studies discussed in the previous aim. Increasing the density of PEG moieties on nanoparticle surfaces has been shown to decrease uptake by non-parenchymal rat liver cells [133]. Further *in vitro* binding and

uptake characterization of our liposome system incorporating PEG is needed in order to optimize PEG type, concentration, and molecular weight to be used in our system.

We evaluated the biodistribution of DiD labeled liposomes with different surface modifications via the *in vivo* imaging Xenogen IVIS Spectrum system. **Table 4.1** summarizes the fluorescence radiant efficiencies of the organs with the highest accumulation of liposomes: liver, spleen, and heart.

Table 4.1: Summary of IVIS Fluorescence Quantification in Excised Organs

Condition	**Fluorescence Radiant Efficiency (A.U.)**		
	Liver	**Spleen**	**Heart**
Bare, 5% PEG	4×10^9	4×10^9	2×10^9
aE-selectin	8×10^9	6×10^9	2×10^9
IL-1α, aE-selectin, 5% PEG	1.5×10^9	1.5×10^9	1×10^9
aE-selectin, 5% PEG	2×10^9	3×10^9	1.5×10^9

Based on our results, we concluded PEG decreases the uptake of liposomes by the reticuloendothelial system (RES). Non-PEGylated liposomes had the highest accumulation in the liver and spleen. The overall low fluorescence values of organs excised from mice exposed to PEGylated, aE-selectin conjugated liposomes was possibly due to renal clearance by the mice since they were euthanized 12 h after the liposome injection was administered to them. The hearts and aortas had low fluorescence values across conditions. Injection of IL-1α did not seem to lead to vascular inflammation; however this was not assessed by immunocytochemistry or any

other means. Previously, intraplantar injections of TNF-α have been reported to induce local inflammation of mouse paw edema [131]. Intravenous injections of IL-1α have also been reported to induce production of IL-6 [134]. In addition, expression of E-selectin on mouse endothelial cells in the cremaster muscle venules was reported to have been induced via local injections of TNF-α. No studies have previously reported on the use of intravenous IL-1α in mice to induce vascular inflammation. Almost all studies addressing vascular inflammation targeting, in the context of atherosclerosis, have used the ApoE-/- knockout mouse model due to its capability to develop atherosclerotic lesions of all stages that closely resemble lesions found in humans [135]. Hence, more optimization of injection dose and timing along with complementary characterization of inflammation in the murine vasculature is required in order to confirm expression of cell adhesion molecules on EC surfaces as a result of intravenous delivery of IL-1α.

Liver and aorta tissue sections were examined by fluorescence microscopy. Based on literature reporting on liver tissue histology, cells displaying large, round nuclei have been identified to be hepatocytes, while those displaying dense, oblong nuclei are known to be either Kupffer cells or stellate cells if Ito [136]. Due the similarity in shape between our liposome fluorescence signal and immunocytochemistry images of Kupffer cells, we speculated the punctate regions we observed could potentially be liposomes that have been internalized by this type of cell [137]. Additionally, punctate regions of fluorescence coincide in location with smaller oblong nuclei, which further supports the idea that liposomes were internalized by these cells, which are the macrophages of the liver and part of the RES.

The fluorescence signal detected in aorta tissue sections was relatively low across conditions, which correlates with the results reported in **Table 4.1**. Variations in the morphology of aortic cross-sections could potentially be due to imperfections in the dissection of the four different vessels, which affected the placement of the vessels within the O.C.T. medium when processing the tissue. In addition, the vessels were more than likely not sectioned exactly at the same location, although we attempted to cryosection roughly the same depth. Intense fluorescence detected in the aortic lumen of the animal exposed to IL-1α. The lack of organ perfusion with saline to remove all blood in our studies prior to euthanasia may have led to auto-fluorescence of red blood cells detected in the vessel lumen.

In summary, we evaluated the biodistribution of liposomes including PEG and aE-selectin in their formulation. Non-PEGylated liposomes accumulated rapidly, within an hour, in the liver and spleen due to rapid clearance by the RES, more than likely. We determined the inclusion of PEG in our liposomal compositions enhanced blood circulation times by decreasing hepatic and splenic uptake. Further studies need to be done to optimize PEG concentration and an *in vitro* model of vascular inflammation via intravenous injection of IL-1α. Alternatively, an ApoE-/- knockout mouse model could be utilized to assess differences in DOPC and DSPC targeting to plaque lesions.

Chapter 5.

Future Directions and Dissertation Summary

In this section, we propose potential future experiments that may serve to address questions that stemmed from our work in the previous aims.

5.1 Further *In Vitro* Experiments

5.1.1 Optimization of New Liposome Formulation

To further probe the question of how antibody diffusivity affects binding and uptake of liposomes in ECs, we need to design a new liposomal formulation that can have low non-specific binding and uptake, in a level parallel to DOPC, but still retain a low membrane fluidity state. We propose two directions to optimize our formulation. The first is to replace DSPC with another saturated lipid that would be in a gel phase at temperatures close to 37 °C such as 1,2-diheptadecanoyl-*sn*-glycero-3-phosphocholine (T_m = 50 °C), 1,2-dinonadecanoyl-*sn*-glycero-3-phosphocholine (T_m = 62 °C), or 1,2-diarachidoyl-*sn*-glycero-3-phosphocholine (T_m = 66 °C). The second option is to keep DOPC as a main component of such new formulation but incrementally add cholesterol, which has been reported to rigidify membranes [138], and a saturated lipid as a third component. The cell membrane is not a pure fluid phase membrane; it is a mosaic with liquid ordered and disordered domains that has been shown to have constrained lateral diffusion [139]. A molar ratio of 35:35:30 unsaturated lipid:saturated lipid:cholesterol has been shown to induce lateral phase separation of lipids and lead to the formation of

domains in giant unilamellar vesicles (GUVs) [140,141], which attempts to mimic this constrained lateral diffusion found naturally in cell membranes. We have prepared GUVs with a ternary mixture composed of 1:1 DOPC:DSPC and 30% cholesterol and showed the formation of lipid domains (**Figure 5.1**). We have also prepared GUVs incorporating N-dod-PE and have shown the existence of domains at physiologically relevant temperature (37 °C) (**Figure 5.2**).

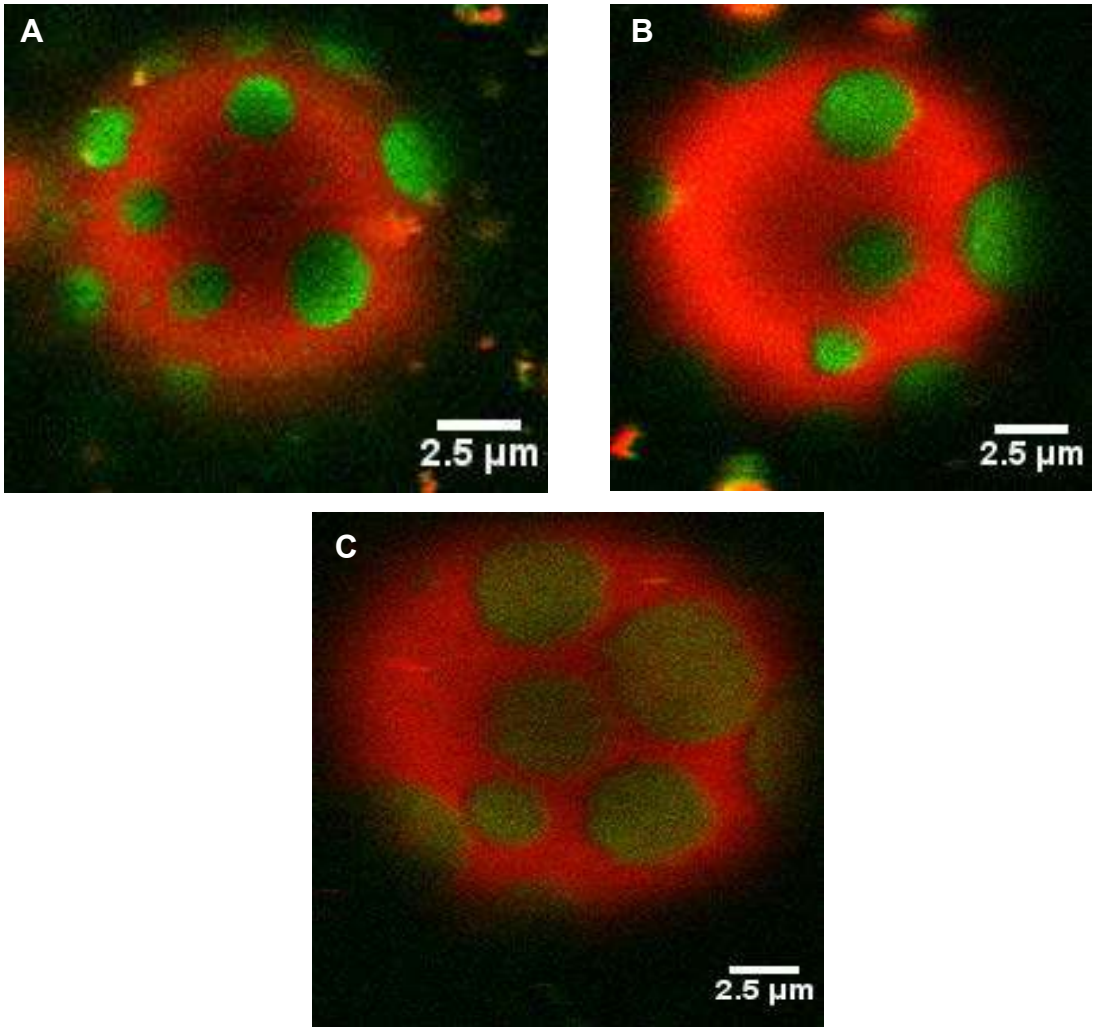

Figure 5.1: Giant unilamellar vesicles (GUVs) show lipid phase separation. GUVs were prepared via the hydration method using the following mixture of lipids: 1:1

Figure 5.1 (Continued): DOPC:DSPC and 30% cholesterol. The formulation also included 0.1% DiI and 0.1% Bodipy in order to fluorescently label liquid and gel phase domains, respectively. Confocal microscopy images (A) – (C) were taken at room temperature and show the formation of domains by different vesicles. Scale bar, 2.5 μm.

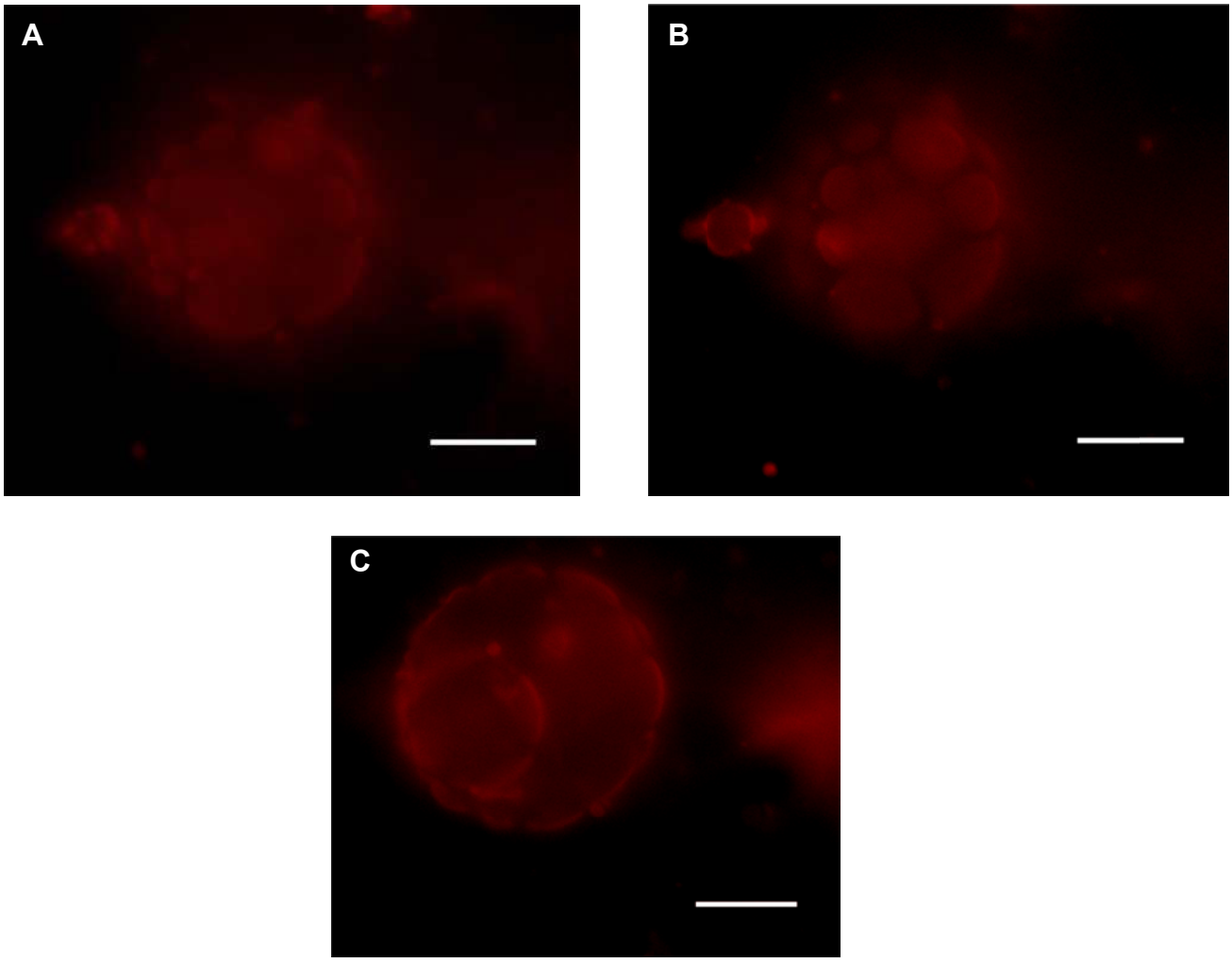

Figure 5.2: Giant unilamellar vesicles (GUVs) including N-dod-PE show lipid phase separation at 37 °C. GUVs were prepared via the hydration method using the following mixture of lipids: 1:1 DOPC:DSPC, 30% cholesterol, and 1% N-dod-DOPE.

Figure 5.2 (Continued): The formulation also included 0.1% DiI in order to fluorescently label the vesicles. Fluorescence microscopy images (A) – (C) were taken at 37 °C and show the vesicle on different imaging planes. Scale bar, 5 μm.

If we prepare liposomes that contain lipid domains, lateral diffusion of membrane components is likely to be less than that of pure DOPC liposomes. We can examine membrane fluidity in giant unilamellar vesicles (GUVs) using a Bodipy-cholesterol derivative as previously reported [142] to determine if these mixtures have decreased fluidity in comparison with 95:5 DOPC:N-dod-PE vesicles. If there are significant differences in membrane fluidity, we can investigate binding and uptake with 100 nm liposomes, as done previously in Chapters 2 and 3, and determine if liposomes composed of these new formulations show reduced non-specific binding.

5.1.2 Non-Specific Cell Binding of 95:5 DSPC:N-dod-PE Liposomes

The question of what gives rise to DSPC's high binding and uptake levels in non-activated ECs across conditions and in non-specific bare and IgG_1 conditions in activated ECs remains unanswered. Non-activated EC binding by DSPC liposomes was observed to be dependent on aE-selectin surface densities when antibody concentrations were low (**Figure 3.3**). Furthermore, binding and uptake was not dependent on the control IgG_1 surface densities; high levels are observed across antibody concentrations. These results suggest aE-selectin plays a role in driving the binding and uptake of DSPC liposomes in non-activated ECs. However, at 100% aE-selectin concentrations, non-activated ECs did not show increased binding and uptake

relative to bare liposomes in other experiments (**Figures 3.1 and 3.2**). These results could suggest a different mechanism, in addition to aE-selectin, such as differences in the physical properties between DOPC and DSPC that could influence binding and uptake in non-activated ECs.

Differences in liposomal membrane fluidity have been shown to have an effect on which opsonin molecules liposomes attract to their surface in the presence of serum [143]. Intracellular digestion of saturated liposomes occurs faster than of unsaturated liposomes and is also dependent on the lipid chain length [144]. Clearly, the physical properties of phospholipids have an effect on cells. We can further explore this area by determining if non-specific binding is an isolated event that only occurs with DSPC liposomes or if other saturated liposomes respond in the same manner. We can measure binding and uptake by flow cytometry, as we previously have, so that we are able to directly compare our results. We also propose to do a membrane fusion assay in order to determine if this non-specific binding is caused by spontaneous fusion of liposome and cell membranes. Membrane fusion experiments can be performed based on previous reports [145,146]. We can test the extent of membrane fusion, measured by lipid mixing, of liposomes incorporating saturated lipids at different concentrations with endothelial cells and target liposomes.

5.1.3 Potential Domain Formation in 95:5 DSPC:N-dod-PE Liposomes

Due to the main differences observed in EC binding and uptake between 95:5 DOPC:N-dod-PE and DSPC:N-dod-PE liposomes, the idea that segregation of N-dod-PE liposomes into lipid rafts occurred on 95:5 DSPC:N-dod-PE liposomes warrants

further investigation. Lipid rafts have been subject of increased attention; studies suggest lipid rafts bring proteins in close proximity to one another and activate cell signaling cascades [147]. Biological membranes are mostly composed of fluid, liquid disordered phase lipids, but also include gel phase lipids and cholesterol [148]. Lipid rafts or domains, both in cell and model membranes, are typically composed of saturated, liquid ordered lipids rich in cholesterol.

In model membranes, formation of domains composed of both liquid ordered and liquid disordered lipids have been observed. This suggests it is theoretically possible to observe fluid phase domains composed of N-dod-PE in our liposomes. Control over domain lipid composition in model membranes has been achieved by varying the ternary lipid mixture composition of saturated lipids, unsaturated lipids, and cholesterol, as mentioned previously [141]. It has become clear, based on the vast majority of lipid domain studies (both theoretical and experimental) done in giant unilamellar vesicles (GUVs) or lipid bilayers, that the presence of a sterol molecule such as cholesterol, is necessary to induce lipid domain formation [140,141,149,150]. Our lipid mixtures did not include cholesterol, which suggests the formation of liquid ordered domains would be unlikely. It is possible, however, that the coexistence of both liquid and gel phases could give rise to some aggregation of N-dod-PE molecules.

Feigenson et al. reported the coexistence of fluid and gel phases in GUVs composed of 80:20 saturated:unsaturated lipids observed by confocal fluorescence microscopy [151]. At this composition, fluid phase lipids did not form domains, but instead formed linear patterns. This type of formation, also termed viscous fingering, observed at high saturated lipid compositions, has also been reported by Veatch et al.

[141]. Furthermore, when Feigenson et al. increased the saturated lipid composition to 90%, no coexistence of fluid and gel phases was visually observed. It is possible viscous fingering still occurred but was unable to be detected with the current optical resolution. In this same study, the minimum size of domains was identified to be 300 nm by 300 nm in GUVs of approximately 20 μm in diameter. Based on these dimensions, the ratio of the surface area of one domain vs. the surface area of a GUV is calculated to be ~7%. Our calculations suggest conjugated antibodies occupied 10% of the total surface area of our liposomes (d = 100 nm). If we extrapolate this study's results and assume that: 1) N-dod-PE aggregation occurred in our liposomes and 2) the surface area coverage of a GUV by a domain is the same in our liposomes; then this would imply most of the antibodies and therefore N-dod-PE molecules would be segregated into one single patch or domain. This configuration may be possible, however the stability over time of this single domain formation is questionable, unless this configuration is energetically favorable.

It is important to take into account the timescales of domain formation in vesicles. The timescale of lipid molecule lateral exchange in membranes is in the order of (10^{-7} s) [151]. Current lipid domain detection methods such as fluorescence resonance energy transfer (FRET) cannot measure the characteristic lifetimes of nanoscopic domains due to the differences between the timescales of probe lifetimes (10^{-9} s) and lipid molecule exchange. In GUVs, macroscopic domains persist for at least 1 h at room temperature, but the timescale of nanoscopic domains is still unknown.

The formation of small aggregates of N-dod-PE molecules in our 95:5 DSPC:N-dod-PE liposomes is theoretically possible. However, the absence of cholesterol and

low unsaturated lipid content in our lipid mixtures, the formation of viscous fingering and not domains at high saturated lipid compositions, our liposome surface area constraints, and the rapid timescale of lipid molecule lateral exchange, suggest domain formation would be rather unlikely to occur. A possible experiment to investigate domain formation can be to form SLBs with fluorescently labeled N-dod-PE molecules via carbodiimide chemistry. Labeling can be done by forming a covalent bond between the terminal carboxyl group present in N-dod-PE and the primary amine group of lucifer yellow shown below in **Figure 5.3**.

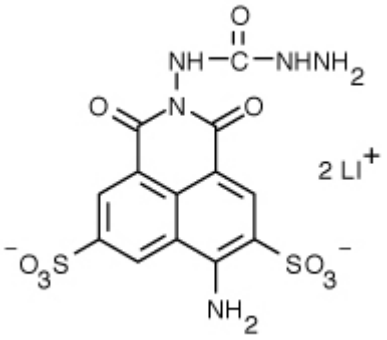

Figure 5.3: Chemical structure of fluorescent probe, lucifer yellow.

Bilayers can be examined by confocal microscopy to check for the presence of domains. In addition, A FRAP experiment including the following conditions can be conducted: 1) Rhodamine-DOPE labeled SLBs (100% DSPC), 2) lucifer yellow-labeled SLBs (95:5 DSPC:N-dod-PE), 3) 95:5 DSPC:N-dod-PE SLBs conjugated with FITC labeled aE-selectin. We can then compare the diffusivities obtained with our previous results (rhodamine-DOPE labeled 95:5 DSPC:N-dod-PE SLBs); if domain formation

occurs, we would expect to detect a significant decrease in membrane diffusivity as reported by Veatch et al. (~10^{-2} $\mu m^2/s$) [152] relative to 100% DSPC bilayers.

5.1.4 Low Binding and Uptake Levels of aVCAM1-Conjugated Liposomes

Liposomes, of both fluid and gel phase compositions, conjugated with 100% aVCAM1 showed binding and uptake levels comparable to that observed in non-activated ECs (**Figures 3.1** and **3.2**). Our previous report showed 2.8-fold increased binding of aVCAM1 conjugated liposomes by IL-1α activated ECs relative to IgG conjugated liposomes, however this was achieved at longer incubation times (12 h) [100]. It should be noted the same aVCAM1 monoclonal antibody, from the same vendor (R&D Systems) was utilized in these studies as well as in the studies presented in Chapter 3. We measured VCAM1 expression to be approximately 10^4 molecules/cell (after 6 h activation with IL-1α), which is at or below the threshold required to observe enhanced binding [153]. Therefore, the low levels of binding and uptake observed could be potentially due to the low amount of VCAM1 surface expression in combination with the shorter liposome incubation time of 1 h.

Our low binding levels could also be due to low aVCAM1 functionality, which we did not test extensively. We qualitatively assessed aVCAM1 functionality by immunocytochemistry of IL-1α activated ECs. After activation, ECs were incubated with mouse anti-human aVCAM1 antibody (R&D Systems, Minneapolis, MN) and then stained with FITC-conjugated goat anti-mouse antibody as shown in **Figure 2.4**. In order to quantitatively measure aVCAM1 functionality, we can perform a Western blot analysis of VCAM1 using EC lysates. The same aVCAM1 antibody used consistently

throughout all of our liposome binding and uptake studies (catalog # BBA6) is also optimized to work in Western blot analyses. aVCAM1 can be incubated with activated EC (IL-1α, 6 h) and non-activated EC lysate, in a serial dilution. Incubation with buffer can be used as a control. Binding can be quantified via chemiluminescence signal detection as reported previously [154]. A linear increase in signal with increased EC lysate concentration can quantitatively corroborate aVCAM1's binding efficiency.

Binding orientation of antibodies on nanoparticle surfaces is crucial for maximizing the functionality of the antibody and thus achieving optimal targeting. Our conjugation method involved the covalent attachment of antibodies to N-dod-PE's terminal carboxylic group via carbodiimide chemistry. Unfortunately, this conjugation method does not control the antibody orientation at all, which could lead to low conjugation efficiencies and poor targeting. To address the issue of the functionality of VCAM1 conjugated to liposomes, we can optimize antibody conjugation by further exploring other methods. Recently, Kumar et al. reported a directional method of conjugation of antibodies to gold nanoparticles [155]. They achieved directionality by conjugating the Fc or non-targeting region of the antibody to the nanoparticles via a hydrazide-PEG-dithiol linker. By using this linker, the Fab or targeting region of the antibody is exposed and directed away from the nanoparticle surface. We can potentially adopt this method to our liposomal system by incorporating gold-labeled lipids into our liposomal compositions. Dipalmitoyl phosphatidyl ethanolamine (DPPE) lipids conjugated with either 1.4 nm or 0.8 nm gold nanoparticles are commercially available (Nanoprobes, Yaphank, NY). We can substitute N-dod-PE with gold-DPPE at various concentrations less than 5% (mol) and evaluate antibody surface densities and

binding efficiencies. Additionally, the incorporation of gold-labeled lipids opens up a wide range of exciting imaging and diagnostic applications as well as therapeutic modalities such as temperature-controlled drug release.

5.2 Theoretical Models of Nanoparticle Binding and Endocytosis

One of the first mathematical models describing the mechanics of receptor-mediated endocytosis of nanoparticles was presented by Gao et al. in 2005. In their model, they investigated the effect of nanoparticle size on receptor-mediated endocytosis. The model assumes a spherical or cylindrical nanoparticle coated with immobile and evenly distributed ligands that is wrapped by a cell membrane containing mobile receptors. The premise of the model is that upon initial binding of the nanoparticle ligands to the cell membrane surface receptors, cell membrane receptors are induced (by local receptor depletion) to diffuse and accumulate at the binding site and further form additional bonds. An increase in the number of ligand-receptor bonds naturally gives rise to an increase in the binding energy. In order for wrapping to occur, the binding energy must be greater than the cell membrane's bending energy, κ, which is dependent upon the bending rigidity of the cell membrane, *B*, and is independent of nanoparticle size, as shown in the equation below.

$$\kappa = 8\pi B \tag{5.1}$$

The wrapping time and optimal nanoparticle size was calculated by keeping the following parameters constant: cell membrane bending rigidity (20 k_BT), estimated receptor-ligand adhesion energy (15 k_BT), diffusion of cell membrane receptors (10^4 nm^2/s), number of cell membrane receptors (50 – 500/μm^2), and number of ligands

(5000/μm^2). Gao et al. concluded that the optimal nanoparticle radius for maximal receptor-mediated endocytosis rate is in the order of 27 – 30 nm for spherical particles [111].

The effect of both nanoparticle size, shape, and ligand density on receptor-mediated endocytosis has been previously investigated [156,157]. Endocytosis of nanoparticles has been shown to be size and shape dependent. Furthermore, Yuan and Zhang showed that there exists an optimal range of nanoparticle size and ligand density at which the nanoparticle's endocytotic time is minimized. For example, for a nanoparticle with a radius of 30 nm, the optimal ligand density that gives rise to minimal wrapping time is calculated to be 1. In contrast, for a nanoparticle with a radius of 50 nm, similar to our liposome size, a ligand density of approximately 0.3 minimizes the endocytotic time. Our estimated maximum ligand density in both 95:5 DOPC:N-dod-PE and DSPC:N-dod-PE liposomes was approximately 0.1. These modeling results suggest that perhaps increasing our antibody densities from 0.1 to 0.3, by optimizing our antibody coupling method, can yield faster endocytotic uptake rates.

The bending rigidity of nanoparticles is often kept constant in mathematical models of endocytosis, yet it is a parameter that would obviously affect the process of nanoparticle wrapping by the cell membrane. The lack of consideration for this parameter should be addressed because this parameter varies greatly depending on the material used to synthesize nanoparticles. Polymer particles such as polybutadiene-polyethyleneoxide have a bending modulus in the order of 42 k_BT [158], however other materials such as stiffer polymers, ceramics, and metals are much more rigid [159,160]. The liposomes investigated herein possess rigidities that are variable,

and further depend on the liposomal compositions. For example, DOPC membranes have been shown to have a bending rigidity of 20 k_BT [161,162] while a bending modulus in the order of 44 k_BT has been measured in DSPC membranes [163].

Recently, theoretical models have focused on the effect particle rigidity has on endocytotic uptake. They have found that rigid particles are wrapped more easily by the cell membrane while softer particles are less prone to wrapping [164,165]. The adhesive interaction between a rigid particle and the cell membrane forces the membrane to deform upon binding. On the other hand, softer particles initially spread along the cell membrane and do not deform the membrane until much later in the wrapping process. This sudden rise in elastic energy at a later stage forces a larger adhesion energy to be present in order to achieve a balance and complete the endocytotic process. 95:5 DSPC:N-dod-PE liposomes functionalized with variety of ligand densities (including absence of ligands) had increased binding and uptake by cells displaying very low membrane receptor numbers, as well as at longer incubation times. Based on these results, we can speculate that the 2-fold increase in DSPC liposomes' bending modulus relative to DOPC may have played a role in the non-specific uptake observed. Our increased uptake of softer 95:5 DOPC:N-dod-PE liposomes by activated ECs can be explained under this model by assuming our softer vesicles had an increase in adhesion energy, enabled by 1:1 and 0:1 aVCAM1:aE-selectin ligand densities, that is potentially able to overcome the elastic energy at the later stages of wrapping.

Mathematical models of the kinetics of antigen-antibody binding have been elucidated in the context of cell-cell adhesion [166] and biosensor experiments such as

surface plasmon resonance [167]. These models suggest forward reaction rates are expected to be dependent on the order of diffusion of receptors and ligands; both forward and reverse rates are reduced when either ligands or receptors are bound to a surface. Nanoparticle size, shape, rigidity, cell membrane receptor diffusivity, and ligand densities have all been explored in theoretical models of receptor-mediated endocytosis. To our knowledge, no theoretical models have focused on the effect of surface ligand diffusivity on nanoparticle endocytosis, to date. Exploring the effects this parameter may have on nanoparticle uptake using theoretical models may be of great help in designing and optimizing liposomal parameters that may achieve enhanced endocytotic uptake rates.

5.3 Further *In Vivo* Experiments

An ideal next step after optimizing *in vitro* targeting efficiency to ECs would be to ultimately test this efficiency in a small rodent model of inflammation. If the application pursued is one for the development of therapeutic or diagnostic tool for atherosclerosis, then it would be best to perform studies in an apolipoprotein E-deficient (ApoE-/- knockout) mouse model. This model is well established in the field and is known to develop atherosclerotic lesions in mice in a course of 8 to 14 weeks [135,168].

We propose to continue to detect accumulation and targeting of liposomes to atherosclerotic plaque using the *in vivo* imaging system. The design of ApoE-/- mice experiments can follow previously reported studies [169,170]. We can have two groups of mice, one would be fed an atherogenic diet and the control group would receive

normal chow. At 12 weeks of age, mice can be administered a single dose of DiD labeled liposomes and we can image *in vivo* at t = 1 min, 1 h, 4 h, 12 h, and 24 h post-injection. Healthy and atherogenic mice can be further subdivided into 2 groups each, where one group would be euthanized after 1 h and the other after 24 h of liposome administration time. This would allow us to determine if liposome binding occurs during the first hour and if accumulation increases at the lesion site with time.

In order to assess the presence of cell adhesion molecules on the endothelium, quantify the extent of the atherosclerotic lesion, and further examine the distribution of liposomes, all organs should be dissected, fixed, and prepared for immunohistochemistry. Euthanasia can be performed by administering mice with 100 mg/kg of ketamine and 10 mg/kg of xylazine, as reported previously [169]. The mice should be perfused with PBS to eliminate traces of blood in the organs. Tissue preservation can be done by perfusing 4% paraformaldehyde administered transcardially. Tissues can be stained for CD31 or von Willebrand factor (vWf) to identify ECs as reported previously [171]. Oil Red O staining is a common histology method to quantify atherosclerosis development and can be used on aorta tissue sections [172]. Liposome accumulation in tissues can be measured by the IVIS Spectrum system immediately after dissection and by fluorescence microscopy on tissue sections. Biodistribution can be assessed by examining spleen and liver tissue sections under fluorescence microscopy as well.

5.4 Dissertation Summary

We first examined the temporal expression of cell adhesion molecules, VCAM1 and E-selectin, on ECs stimulated with IL-1α and TNF-α, guided by previous gene expression results from our lab. We determined an optimal concentration and exposure time to use in order to produce a high surface expression of VCAM1 and E-selectin on ECs *in vitro*. These results were used to investigate liposome targeting to inflamed ECs.

We characterized the membrane fluidity of liposomes and supported lipid bilayers composed mostly of fluid phase, DOPC, and gel phase, DSPC. We also quantified the antibody surface density of various ratios of antibodies conjugated to both DOPC and DSPC membranes. Based on these results, we tested our hypothesis of how antibody diffusivity affected binding and uptake on ECs. We decoupled liposome surface binding and internalization to further our understanding of liposomal fate once in contact with cells. Finally, we carried out a preliminary *in vivo* study where we looked at the biodistribution of liposomes conjugated with aE-selectin.

In general, this dissertation demonstrated that the presentation of only aE-selectin was necessary to achieve enhanced targeting of activated ECs at short incubation times. We determined that efficient targeting was also achieved at low antibody surface densities. We cannot clearly discern if antibody diffusivity alone played a role on EC binding and uptake because DSPC may have a secondary binding and uptake mechanism. However, we concluded that membrane fluidity influences EC binding and uptake, which should be further investigated. Our work can be further

continued to set the foundation for efficient targeted drug delivery liposomal carriers that may have diagnostic and/or therapeutic potential for a broad range of inflammatory diseases including atherosclerosis.

References

[1] Mackay, J, Mensah G. Atlas of Heart Disease and Stroke. World Heal. Geveva Press; 2004.

[2] Fonarow GC, Gawlinski A, Moughrabi S, Tillisch JH. Improved Treatment of Coronary Heart Hospitalization Atherosclerosis Management Program (CHAMP). Am J Cardiol 2001;9149:819–22.

[3] Abrams J. The Role of Nitrates in Coronary Heart Disease. Arch Intern Med 1995;155:357–64.

[4] Thompson PD, Buchner D, Pina IL, Balady GJ, Williams M a, Marcus BH, et al. Exercise and physical activity in the prevention and treatment of atherosclerotic cardiovascular disease: a statement from the Council on Clinical Cardiology (Subcommittee on Exercise, Rehabilitation, and Prevention) and the Council on Nutrition, Physical. Circulation 2003;107:3109–16.

[5] Michaels, AD, Chatterjee K. Angioplasty Versus Bypass Surgery for Coronary Artery Disease. Circulation 2002;106:187–90.

[6] Schuijf JD, Shaw LJ, Wijns W, Lamb HJ, Poldermans D, de Roos a, et al. Cardiac imaging in coronary artery disease: differing modalities. Heart 2005;91:1110–7.

[7] Camici PG, Rimoldi OE, Gaemperli O, Libby P. Non-invasive anatomic and functional imaging of vascular inflammation and unstable plaque. Eur Heart J 2012;33:1309–17.

[8] Zimmerman SK, Vacek JL. Imaging techniques in acute coronary syndromes: a review. ISRN Cardiol 2011;2011:359127.

[9] Jaffer F a, Libby P, Weissleder R. Molecular and cellular imaging of atherosclerosis: emerging applications. J Am Coll Cardiol 2006;47:1328–38.

[10] Nahrendorf M, Keliher E, Panizzi P, Zhang H, Hembrador S, Figueiredo J-L, et al. 18F-4V for PET-CT imaging of VCAM-1 expression in atherosclerosis. JACC Cardiovasc Imaging 2009;2:1213–22.

[11] Libby P. Inflammation and Atherosclerosis. Circulation 2002;105:1135–43.

[12] Pardi R, Inverardi L, Bender JR. Regulatory mechanisms in leukocyte adhesion: flexible receptors for sophisticated travelers. Immunol Today 1992;13:224–30.

[13] Galkina E, Ley K. Vascular adhesion molecules in atherosclerosis. Arterioscler Thromb Vasc Biol 2007;27:2292–301.

[14] Hansson GK, Libby P. The immune response in atherosclerosis: a double-edged sword. Nat Rev Immunol 2006;6:508–19.

[15] Bangham AD. Surrogate cells or Trojan hourses. The discovery of liposomes. BioEssays 1995;17:1081–8.

[16] Sipkins D a, Gijbels K, Tropper FD, Bednarski M, Li KC, Steinman L. ICAM-1 expression in autoimmune encephalitis visualized using magnetic resonance imaging. J Neuroimmunol 2000;104:1–9.

[17] Ulrich AS. Biophysical aspects of using liposomes as delivery vehicles. Biosci Rep 2002;22:129–50.

[18] Choudhury RP, Fisher E a. Molecular imaging in atherosclerosis, thrombosis, and vascular inflammation. Arterioscler Thromb Vasc Biol 2009;29:983–91.

[19] Pardridge WM. Drug and gene targeting to the brain with molecular Trojan horses. Nat Rev Drug Discov 2002;1:131–9.

[20] Pardridge WM. Blood-brain barrier drug targeting: the future of brain drug development. Mol Interv 2003;3:90–105, 51.

[21] Brasnjevic I, Steinbusch HW, Schmitz C, Martinez-Martinez P. Delivery of peptide and protein drugs over the blood-brain barrier. Prog Neurobiol 2009;87:212–51.

[22] Pardridge WM. Blood-brain barrier delivery of protein and non-viral gene therapeutics with molecular Trojan horses. J Control Release 2007;122:345–8.

[23] Shi N, Pardridge WM. Noninvasive gene targeting to the brain. Proc Natl Acad Sci U S A 2000;97:7567–72.

[24] Zhang, Y, Schlachetzki, F, Pardridge W. Global non-viral gene transfer to the primate brain following intravenous administration. Mol Ther 2003;7:11–8.

[25] Coloma MJ, Lee HJ, Kurihara a, Landaw EM, Boado RJ, Morrison SL, et al. Transport across the primate blood-brain barrier of a genetically engineered chimeric monoclonal antibody to the human insulin receptor. Pharm Res 2000;17:266–74.

[26] Zhang Y, Calon F, Zhu C, Boado RJ, Pardridge WM. Intravenous nonviral gene therapy causes normalization of striatal tyrosine hydroxylase and reversal of motor impairment in experimental parkinsonism. Hum Gene Ther 2003;14:1–12.

[27] Zhang Y, Zhang Y-F, Bryant J, Charles A, Boado RJ, Pardridge WM. Intravenous RNA interference gene therapy targeting the human epidermal growth factor

receptor prolongs survival in intracranial brain cancer. Clin Cancer Res 2004;10:3667–77.

[28] Gabizon AA. Liposome circulation time and tumor targeting: implications for cancer chemotherapy. Adv Drug Deliv Rev 1995;16:285–94.

[29] Carmeliet P, Jain RK. Angiogenesis in cancer and other diseases. Nature 2000;407:249–57.

[30] Yuan F, Leunig M, Huang SK, Berk DA, Papahadjopoulos D, Jam RK. Advances in Brief Microvascular Permeability and Interstitial Penetration of Sterically Stabilized (Stealth) Liposomes in a Human Tumor Xenograft ' 1994:3352–6.

[31] Campbell RB, Fukumura D, Brown EB, Mazzola LM, Izumi Y, Jain RK, et al. Advances in Brief Cationic Charge Determines the Distribution of Liposomes between the Vascular and Extravascular Compartments of Tumors 1 2002:6831–6.

[32] Campbell RB, Ying BO, Kuesters GM, Hemphill R. Fighting Cancer : From the Bench to Bedside Using Second Generation Cationic Liposomal Therapeutics 2009;98.

[33] Wu J, Lee A, Lu Y, Lee RJ. Vascular targeting of doxorubicin using cationic liposomes. Int J Pharm 2007;337:329–35.

[34] Lee CM, Tanaka T, Murai T. Novel Chondroitin Sulfate-binding Cationic Liposomes Loaded with Cisplatin Efficiently Suppress the Local Growth and Liver Metastasis of Tumor Cells in Vivo Novel Chondroitin Sulfate-binding Cationic Liposomes Loaded with Cisplatin Efficiently Suppress th. Cancer Res 2002;62:4282–8.

[35] Eichhorn ME, Ischenko I, Luedemann S, Strieth S, Papyan A, Werner A, et al. Vascular targeting by EndoTAG-1 enhances therapeutic efficacy of conventional chemotherapy in lung and pancreatic cancer. Int J Cancer 2010;126:1235–45.

[36] Gosk S, Moos T, Gottstein C, Bendas G. VCAM-1 directed immunoliposomes selectively target tumor vasculature in vivo. Biochim Biophys Acta 2008;1778:854–63.

[37] ElBayoumi T a, Torchilin VP. Tumor-targeted nanomedicines: enhanced antitumor efficacy in vivo of doxorubicin-loaded, long-circulating liposomes modified with cancer-specific monoclonal antibody. Clin Cancer Res 2009;15:1973–80.

[38] Chang D-K, Chiu C-Y, Kuo S-Y, Lin W-C, Lo A, Wang Y-P, et al. Antiangiogenic targeting liposomes increase therapeutic efficacy for solid tumors. J Biol Chem 2009;284:12905–16.

[39] Pastorino F, Brignole C, Di Paolo D, Nico B, Pezzolo A, Marimpietri D, et al. Targeting liposomal chemotherapy via both tumor cell-specific and tumor vasculature-specific ligands potentiates therapeutic efficacy. Cancer Res 2006;66:10073–82.

[40] Frézard F. Liposomes: from biophysics to the design of peptide vaccines. Braz J Med Biol Res 1999;32:181–9.

[41] Ishii N, Fukushima J, Kaneko T, Okada E, Tani K, Tanaka SI, et al. Cationic liposomes are a strong adjuvant for a DNA vaccine of human immunodeficiency virus type 1. AIDS Res Hum Retroviruses 1997;13:1421–8.

[42] Hartikka J, Bozoukova V, Yang CK, Ye M, Rusalov D, Shlapobersky M, et al. Vaxfectin, a cationic lipid-based adjuvant for protein-based influenza vaccines. Vaccine 2009;27:6399–403.

[43] Lindenstrøm T, Agger EM, Korsholm KS, Darrah P a, Aagaard C, Seder R a, et al. Tuberculosis subunit vaccination provides long-term protective immunity characterized by multifunctional CD4 memory T cells. J Immunol 2009;182:8047–55.

[44] Zidan AS, Spinks C, Fortunak J, Habib M, Khan M a. Near-infrared investigations of novel anti-HIV tenofovir liposomes. AAPS J 2010;12:202–14.

[45] Zolnik BS, González-Fernández A, Sadrieh N, Dobrovolskaia M a. Nanoparticles and the immune system. Endocrinology 2010;151:458–65.

[46] Vaccines L, Schwendener RA, Ludewig B, Cerny A, Engler O. Liposome-Based Vaccines. Liposomes, Methods Mol Biol 2010;605:163–75.

[47] Steers NJ, Peachman KK, McClain S, Alving CR, Rao M. Liposome-encapsulated HIV-1 Gag p24 containing lipid A induces effector CD4+ T-cells, memory CD8+ T-cells, and pro-inflammatory cytokines. Vaccine 2009;27:6939–49.

[48] Inoue J, Ideue R, Takahashi D, Kubota M, Kumazawa Y. Liposomal glycosphingolipids activate natural killer T cell-mediated immune responses through the endosomal pathway. J Control Release 2009;133:18–23.

[49] Combadière B, Mahé B. Particle-based vaccines for transcutaneous vaccination. Comp Immunol Microbiol Infect Dis 2008;31:293–315.

[50] Ishii M, Kojima N. Mucosal adjuvant activity of oligomannose-coated liposomes for nasal immunization. Glycoconj J 2010;27:115–23.

[51] Capini C, Jaturanpinyo M, Chang H-I, Mutalik S, McNally A, Street S, et al. Antigen-specific suppression of inflammatory arthritis using liposomes. J Immunol 2009;182:3556–65.

[52] Behr J, Zimmermann G, Baumgartner R, Leuchte H, Neurohr C, Brand P, et al. Lung Deposition of a Liposomal Cyclosporine A Inhalation Solution in Patients after Lung Transplantation 2009;22:121–9.

[53] Takeda K, Dow SW, Miyahara N, Kodama T, Koya T, Taube C, et al. Vaccine-induced CD8+ T cell-dependent suppression of airway hyperresponsiveness and inflammation. J Immunol 2009;183:181–90.

[54] Mantovani, A, Bussolino F DE. Cytokine regulation of endothelial cell function. Faseb 1992;6:2591–9.

[55] Bevilacqua MP, Pober JS, Wheeler ME, Cotran RS, Gimbrone M a. Interleukin 1 acts on cultured human vascular endothelium to increase the adhesion of polymorphonuclear leukocytes, monocytes, and related leukocyte cell lines. J Clin Invest 1985;76:2003–11.

[56] Bevilacqua MP. Endothelial-leukocyte adhesion molecules. Annu Rev Immunol 1993;11:767–804.

[57] Steeber A, Tedder F. The selectins : L-Selectin 1995;9:866–73.

[58] Gearing a J, Newman W. Circulating adhesion molecules in disease. Immunol Today 1993;14:506–12.

[59] Bevilacqua MP, Nelson RM, Mannori G, Cecconi O. Endothelial-leukocyte adhesion molecules in human disease. Annu Rev Med 1994;45:361–78.

[60] Cai H, Harrison DG. Endothelial dysfunction in cardiovascular diseases: the role of oxidant stress. Circ Res 2000;87:840–4.

[61] Lerman A, Zeiher AM. Endothelial function: cardiac events. Circulation 2005;111:363–8.

[62] Simone E, Ding B-S, Muzykantov V. Targeted delivery of therapeutics to endothelium. Cell Tissue Res 2009;335:283–300.

[63] Spragg DD, Alford DR, Greferath R, Larsen CE, Lee KD, Gurtner GC, et al. Immunotargeting of liposomes to activated vascular endothelial cells: a strategy for site-selective delivery in the cardiovascular system. Proc Natl Acad Sci U S A 1997;94:8795–800.

[64] Voinea M, Manduteanu I, Dragomir E, Capraru M, Simionescu M. Immunoliposomes directed toward VCAM-1 interact specifically with activated endothelial cells--a potential tool for specific drug delivery. Pharm Res 2005;22:1906–17.

[65] Gunawan RC, Auguste DT. The role of antibody synergy and membrane fluidity in the vascular targeting of immunoliposomes. Biomaterials 2010;31:900–7.

[66] Molecule- IA, Herbst SM, Klegerman ME, Kim H, Qi J, Shelat H, et al. articles Delivery of Stem Cells to Porcine Arterial Wall with Echogenic Liposomes Conjugated to Antibodies against 2009;7:3–11.

[67] Knop K, Hoogenboom R, Fischer D, Schubert US. Poly(ethylene glycol) in drug delivery: pros and cons as well as potential alternatives. Angew Chem Int Ed Engl 2010;49:6288–308.

[68] Parodi A, Quattrocchi N, van de Ven AL, Chiappini C, Evangelopoulos M, Martinez JO, et al. Synthetic nanoparticles functionalized with biomimetic leukocyte membranes possess cell-like functions. Nat Nanotechnol 2013;8:61–8.

[69] Pober, JS, Cotran R. Cytokines and Endothelial Cell Biology. Physiol Rev 1990;70:427–51.

[70] Arora a, Byrem TM, Nair MG, Strasburg GM. Modulation of liposomal membrane fluidity by flavonoids and isoflavonoids. Arch Biochem Biophys 2000;373:102–9.

[71] Papahadjopoulos, D, Jacobson, K, Nir, S, Isac T. Phase Transitions in Phospholipid Vesicles. Fluorescence Polarization and Permeability Measurements Concerning the Effect of Temperature and Cholesterol. Biochim Biophys Acta 1973;311:330–48.

[72] Borst JW, Visser N V, Kouptsova O, Visser a J. Oxidation of unsaturated phospholipids in membrane bilayer mixtures is accompanied by membrane fluidity changes. Biochim Biophys Acta 2000;1487:61–73.

[73] Lentz, BR, Barenholz, Y, Thompson T. Fluorescence Depolarization Studies of Phase Transitions and Fluidity in Phospholipid Bilayers. 2. Two-Component Phosphatidylcholine Liposomes. Biochemistry1 1976;15:4529–37.

[74] Itoh YH, Itoh T, Kaneko H. Modified Bartlett assay for microscale lipid phosphorus analysis. Anal Biochem 1986;154:200–4.

[75] Subramaniam AB, Lecuyer S, Ramamurthi KS, Losick R, Stone H a. Particle/Fluid interface replication as a means of producing topographically patterned polydimethylsiloxane surfaces for deposition of lipid bilayers. Adv Mater 2010;22:2142–7.

[76] Rafat M. Dual Antibody Functionalized Polyvinyl Alcohol and Alginate Hydrogels for Synergistic Endothelial Cell Adhesion. Harvard University, 2012.

[77] Eniola, OA, Hammer D. In vitro characterization of leukocyte mimetic for targeting therapeutics to the endothelium using two receptors. Biomaterials 2005;26:7136–44.

[78] Hansen CB, Kao GY, Moase EH, Zalipsky S, Allen TM. Attachment of antibodies to sterically stabilized liposomes: evaluation, comparison and optimization of coupling procedures. Biochim Biophys Acta 1995;1239:133–44.

[79] Schwartz a, Fernández Repollet E, Vogt R, Gratama JW. Standardizing flow cytometry: construction of a standardized fluorescence calibration plot using matching spectral calibrators. Cytometry 1996;26:22–31.

[80] Lentz BR. Use of fluorescent probes to monitor molecular order and motions within liposome bilayers. Chem Phys Lipids 1993;64:99–116.

[81] Williams EE. Membrane Lipids : What Membrane Physical Properties are Conserved during Physiochemically-Induced Membrane Restructuring ? 1 1998;290:280–90.

[82] Axelrod D, Koppel DE, Schlessinger J, Elson E, Webb WW. Mobility measurement by analysis of fluorescence photobleaching recovery kinetics. Biophys J 1976;16:1055–69.

[83] Kang M, Day C a, Kenworthy AK, DiBenedetto E. Simplified equation to extract diffusion coefficients from confocal FRAP data. Traffic 2012;13:1589–600.

[84] Ma Z, Janmey P a, Sharp K a, Finkel TH. Improved method of preparation of supported planar lipid bilayers as artificial membranes for antigen presentation. Microsc Res Tech 2011;74:1174–85.

[85] Lin W-C, Blanchette CD, Ratto T V, Longo ML. Lipid asymmetry in DLPC/DSPC-supported lipid bilayers: a combined AFM and fluorescence microscopy study. Biophys J 2006;90:228–37.

[86] Tamm LK. Lateral diffusion and fluorescence microscope studies on a monoclonal antibody specifically bound to supported phospholipid bilayers. Biochemistry 1988;27:1450–7.

[87] Ashley CE, Carnes EC, Phillips GK, Padilla D, Durfee PN, Brown P a, et al. The targeted delivery of multicomponent cargos to cancer cells by nanoporous particle-supported lipid bilayers. Nat Mater 2011;10:389–97.

[88] Davies MJ, Gordon JL, Gearing a J, Pigott R, Woolf N, Katz D, et al. The expression of the adhesion molecules ICAM-1, VCAM-1, PECAM, and E-selectin in human atherosclerosis. J Pathol 1993;171:223–9.

[89] Hubbard, AK, Rothlein R. Forum : Signal Transduction. Free Radic Biol Med 2000;28:1379–86.

[90] Chang, HM, Reitstetter, R, Gruener R. Lipid-Ion Channel Interactions: Increasing Phospholipid Headgroup Size but not Ordering Acyl Chains Alters Reconstituted Channel Behavior. J Membr Biol 1995;19:13–9.

[91] Lu Y, Harding SE, Michaelsen TE, Longman E, Davis KG, Ortega A, et al. Solution conformation of wild-type and mutant IgG3 and IgG4 immunoglobulins using crystallohydrodynamics: possible implications for complement activation. Biophys J 2007;93:3733–44.

[92] Muller W a. Leukocyte–endothelial-cell interactions in leukocyte transmigration and the inflammatory response. Trends Immunol 2003;24:326–33.

[93] Ley K, Laudanna C, Cybulsky MI, Nourshargh S. Getting to the site of inflammation: the leukocyte adhesion cascade updated. Nat Rev Immunol 2007;7:678–89.

[94] Koning G a, Schiffelers RM, Wauben MHM, Kok RJ, Mastrobattista E, Molema G, et al. Targeting of angiogenic endothelial cells at sites of inflammation by dexamethasone phosphate-containing RGD peptide liposomes inhibits experimental arthritis. Arthritis Rheum 2006;54:1198–208.

[95] Lebwohl M, Tyring SK, Hamilton TK, Toth D, Glazer S, Tawfik NH, et al. A novel targeted T-cell modulator, efalizumab, for plaque psoriasis. N Engl J Med 2003;349:2004–13.

[96] Kelly K a, Nahrendorf M, Yu AM, Reynolds F, Weissleder R. In vivo phage display selection yields atherosclerotic plaque targeted peptides for imaging. Mol Imaging Biol 2006;8:201–7.

[97] Muzykantov VR. Targeted Drug Delivery to Endothelial Adhesion Molecules. ISRN Vasc Med 2013;2013:1–27.

[98] Lee, R. J., Low PS. Delivery of Liposomes into Cultured KB Cells via Folate Receptor-mediated Endocytosis. J Biol Chem 1994;269:3198–204.

[99] Van Rooy I, Mastrobattista E, Storm G, Hennink WE, Schiffelers RM. Comparison of five different targeting ligands to enhance accumulation of liposomes into the brain. J Control Release 2011;150:30–6.

[100] Gunawan RC, Almeda D, Auguste DT. Complementary targeting of liposomes to IL-1α and TNF-α activated endothelial cells via the transient expression of VCAM1 and E-selectin. Biomaterials 2011;32:9848–53.

[101] Dicheva BM, ten Hagen TLM, Li L, Schipper D, Seynhaeve ALB, van Rhoon GC, et al. Cationic thermosensitive liposomes: a novel dual targeted heat-triggered drug delivery approach for endothelial and tumor cells. Nano Lett 2013;13:2324–31.

[102] Kowalski PS, Lintermans LL, Morselt HWM, Leus NGJ, Ruiters MHJ, Molema G, et al. Anti-VCAM-1 and anti-E-selectin SAINT-O-Somes for selective delivery of siRNA into inflammation-activated primary endothelial cells. Mol Pharm 2013;10:3033–44.

[103] Bandekar A, Zhu C, Gomez A, Menzenski MZ, Sempkowski M, Sofou S. Masking and triggered unmasking of targeting ligands on liposomal chemotherapy selectively suppress tumor growth in vivo. Mol Pharm 2013;10:152–60.

[104] Koren E, Apte A, Jani A, Torchilin VP. Multifunctional PEGylated 2C5-immunoliposomes containing pH-sensitive bonds and TAT peptide for enhanced tumor cell internalization and cytotoxicity. J Control Release 2012;160:264–73.

[105] Allen TM, Brandeis E, Hansen CB, Kao GY, Zalipsky S. A new strategy for attachment of antibodies to sterically stabilized liposomes resulting in efficient targeting to cancer cells. Biochim Biophys Acta 1995;1237:99–108.

[106] Laginha K, Mumbengegwi D, Allen T. Liposomes targeted via two different antibodies: assay, B-cell binding and cytotoxicity. Biochim Biophys Acta 2005;1711:25–32.

[107] Saul JM, Annapragada A V, Bellamkonda R V. A dual-ligand approach for enhancing targeting selectivity of therapeutic nanocarriers. J Control Release 2006;114:277–87.

[108] Scott RWJ, Wilson OM, Crooks RM. Synthesis, Characterization, and Applications of Dendrimer-Encapsulated Nanoparticles. J Phys Chem B 2005;109:692–704.

[109] Cullis P, Chonn a, Semple S. Interactions of liposomes and lipid-based carrier systems with blood proteins: Relation to clearance behaviour in vivo. Adv Drug Deliv Rev 1998;32:3–17.

[110] Decker C, Fahr A, Kuntsche J, May S. Selective partitioning of cholesterol and a model drug into liposomes of varying size. Chem Phys Lipids 2012;165:520–9.

[111] Gao H, Shi W, Freund LB. Mechanics of receptor-mediated endocytosis. Proc Natl Acad Sci U S A 2005;102:9469–74.

[112] Weikl TR, Asfaw M, Krobath H, Różycki B, Lipowsky R. Adhesion of membranes via receptor–ligand complexes: Domain formation, binding cooperativity, and active processes. Soft Matter 2009;5:3213.

[113] Marty C, Meylan C, Schott H, Ballmer-Hofer K, Schwendener R a. Enhanced heparan sulfate proteoglycan-mediated uptake of cell-penetrating peptide-modified liposomes. Cell Mol Life Sci 2004;61:1785–94.

[114] Curtsinger J, Deeths MJ, Pease P, Mescher MF. Artificial cell surface constructs for studying receptor-ligand contributions to lymphocyte activation. J Immunol Methods 1997;209:47–57.

[115] Gunawan RC, Auguste DT. The role of antibody synergy and membrane fluidity in the vascular targeting of immunoliposomes. Biomaterials 2010;31:900–7.

[116] Kessner S, Krause a, Rothe U, Bendas G. Investigation of the cellular uptake of E-Selectin-targeted immunoliposomes by activated human endothelial cells. Biochim Biophys Acta 2001;1514:177–90.

[117] Wyble CW, Desai TR, Clark ET, Hynes KL GB. Physiologic Concentrations of TNF-a and IL-1b Released from Reperfused Human Intestine Upregulate E-Selectin and ICAM-1. J Surg Res 1996;63:333–8.

[118] Psarros C, Lee R, Margaritis M, Antoniades C. Nanomedicine for the prevention, treatment and imaging of atherosclerosis. Nanomedicine 2012;8:S59–68.

[119] Chono S, Tauchi Y, Deguchi Y, Morimoto K. Efficient drug delivery to atherosclerotic lesions and the antiatherosclerotic effect by dexamethasone incorporated into liposomes in atherogenic mice. J Drug Target 2005;13:267–76.

[120] Kang HW, Josephson L, Petrovsky A, Weissleder R, Bogdanov A. Magnetic resonance imaging of inducible E-selectin expression in human endothelial cell culture. Bioconjug Chem 2002;13:122–7.

[121] Daemen T, Regts J, Meesters M, Ten Kate MT, Bakker-Woudenberg I a. J., Scherphof GL. Toxicity of doxorubicin entrapped within long-circulating liposomes. J Control Release 1997;44:1–9.

[122] Unezaki S, Maruyama K, Ishida O, Suginaka A. journal of pharmaceutics Enhanced tumor targeting and improved antitumor activity of doxorubicin by long-circulating liposomes containing amphipathic poly (ethylene glycol). Int J Pharm 1995;126:41–8.

[123] Gabizon, A, Shiota, R, Papahadjopoulos D. Pharmacokinetics and Tissue Distribution of Doxorubicin Encapsulated in Stable Liposomes with Long Circulation Times. J Natl Cancer Inst 1989;81:1484–14488.

[124] Gabizon AA, Barenholz, Y BM. 1993 Gabizon A - Prolongation of the Circulation Time of DOX Encapsulated in Liposomes containing PEG - studies in rodents and dogs.pdf. Pharmarceutical Res 1993;10:703 – 708.

[125] Gabizon a, Isacson R, Libson E, Kaufman B, Uziely B, Catane R, et al. Clinical studies of liposome-encapsulated doxorubicin. Acta Oncol 1994;33:779–86.

[126] Texier I, Goutayer M, Da Silva A, Guyon L, Djaker N, Josserand V, et al. Cyanine-loaded lipid nanoparticles for improved in vivo fluorescence imaging. J Biomed Opt 2013;14:054005.

[127] Frangioni J. In vivo near-infrared fluorescence imaging. Curr Opin Chem Biol 2003;7:626–34.

[128] Everts M, Koning G a, Kok RJ, Asgeirsdóttir S a, Vestweber D, Meijer DKF, et al. In vitro cellular handling and in vivo targeting of E-selectin-directed immunoconjugates and immunoliposomes used for drug delivery to inflamed endothelium. Pharm Res 2003;20:64–72.

[129] Henseleit U, Steinbrink K, Goebeler M, Roth J, Vestweber D, Sorg C, et al. E-selectin expression in experimental models of inflammation in mice. J Pathol 1996;180:317–25.

[130] Zwiers PJ, Morselt W, Moorlag HE, Bakker HI, Heeringa P, Kok JW, et al. Inhibition of proinflammatory genes in anti-GBM glomerulonephritis by targeted dexamethasone-loaded Ab Esel liposomes. Am J Physiol Ren Physiol 2008;294:554–61.

[131] Gompels LL, Madden L, Lim NH, Inglis JJ, McConnell E, Vincent TL, et al. In vivo fluorescence imaging of E-selectin: quantitative detection of endothelial activation in a mouse model of arthritis. Arthritis Rheum 2011;63:107–17.

[132] Gabizon A, Catane R, Uziely B, Kaufman B, Safra T, Cohen R, et al. Prolonged Circulation Time and Enhanced Accumulation in Malignant Exudates of Doxorubicin Encapsulated in Polyethylene-glycol Coated Liposomes Prolonged Circulation Time and Enhanced Accumulation in Malignant Exudates of Doxorubicin Encapsulated in Polyet. Cancer Res 1994;54:987–92.

[133] Dunn SE, Brindley A, Davis SS, Davies, MC IL. Polystyrene-Poly(Ethylene Glycol) (PS-PEG2000) Particles as Model Systems for Site Specific Drug Delivery. 2. The Effect of PEG Surface Density on the in Vitro Cell Interaction and in Vivo Biodistribution. Pharmarceutical Res 1994;11:1016–22.

[134] Neta, R, Vogel SN, Sipe, JD, Wong, GG, Nordan R. Comparison of In Vivo Effects of Human Recombinant IL 1 and Human Recombinant IL 6 in Mice. Lymphokine Res 1988;7:403–12.

[135] Nakashima Y, Plump a. S, Raines EW, Breslow JL, Ross R. ApoE-deficient mice develop lesions of all phases of atherosclerosis throughout the arterial tree. Arterioscler Thromb Vasc Biol 1994;14:133–40.

[136] Baratta JL, Ngo A, Lopez B, Kasabwalla N, Kenneth J, Robertson RT. NIH Public Access. Histochem Cell Bio 2009;131:713–26.

[137] Sadauskas E, Wallin H, Stoltenberg M, Vogel U, Doering P, Larsen A, et al. Kupffer cells are central in the removal of nanoparticles from the organism. Part Fibre Toxicol 2007;4:10.

[138] Shinitzky M, Inbar M. Difference in microviscosity induced by different cholesterol levels in the surface membrane lipid layer of normal lymphocytes and malignant lymphoma cells. J Mol Biol 1974;85:603–15.

[139] Marguet D, Lenne P-F, Rigneault H, He H-T. Dynamics in the plasma membrane: how to combine fluidity and order. EMBO J 2006;25:3446–57.

[140] Veatch S, Keller S. Organization in Lipid Membranes Containing Cholesterol. Phys Rev Lett 2002;89:268101.

[141] Veatch SL, Keller SL. Separation of liquid phases in giant vesicles of ternary mixtures of phospholipids and cholesterol. Biophys J 2003;85:3074–83.

[142] Ariola FS, Li Z, Cornejo C, Bittman R, Heikal A a. Membrane fluidity and lipid order in ternary giant unilamellar vesicles using a new bodipy-cholesterol derivative. Biophys J 2009;96:2696–708.

[143] Moghimi SM, Patel HM. Serum opsonins and phagocytosis of saturated and unsaturated phospholipid liposomes. Biochim Biophys Acta 1989;984:384–7.

[144] Patel, HM, Tuzel, NS, Stevenson R. Intracellular digestion of saturated and unsaturated phospholipid liposomes by mucosal cells . Possible mechanism of transport of liposomally entrapped macromolecules across the isolated vascularly perfused rabbit ileum. Biochim Biophys Acta 1985;839:40–9.

[145] Papahadjopoulos, D, Poste, G, Schaeffer, BE, Vail W. Membrane Fusion and Molecular Segregation in Phospholipid Vesicles. Biochim Biophys Acta 1974;352:10–28.

[146] Bailey a L, Cullis PR. Membrane fusion with cationic liposomes: effects of target membrane lipid composition. Biochemistry 1997;36:1628–34.

[147] Simons K, Toomre D. Lipid rafts and signal transduction. Nat Rev Mol Cell Biol 2000;1:31–9.

[148] Brown D a, London E. Functions of lipid rafts in biological membranes. Annu Rev Cell Dev Biol 1998;14:111–36.

[149] Risselada HJ, Marrink SJ. The molecular face of lipid rafts in model membranes. Proc Natl Acad Sci U S A 2008;105:17367–72.

[150] Crane JM, Tamm LK. Role of cholesterol in the formation and nature of lipid rafts in planar and spherical model membranes. Biophys J 2004;86:2965–79.

[151] Feigenson GW, Buboltz JT. Ternary phase diagram of dipalmitoyl-PC/dilauroyl-PC/cholesterol: nanoscopic domain formation driven by cholesterol. Biophys J 2001;80:2775–88.

[152] Cicuta P, Keller SL, Veatch SL. Diffusion of liquid domains in lipid bilayer membranes. J Phys Chem B 2007;111:3328–31.

[153] Park JW, Hong K, Kirpotin DB, Colbern G, Shalaby R, Baselga J, et al. Anti-HER2 Immunoliposomes: Enhanced Efficacy Attributable to Targeted Delivery. Clin Cancer Res 2002;8:1172–81.

[154] Kim I, Moon SO, Kim SH, Kim HJ, Koh YS, Koh GY. Vascular endothelial growth factor expression of intercellular adhesion molecule 1 (ICAM-1), vascular cell adhesion molecule 1 (VCAM-1), and E-selectin through nuclear factor-kappa B activation in endothelial cells. J Biol Chem 2001;276:7614–20.

[155] Kumar S, Aaron J, Sokolov K. Directional conjugation of antibodies to nanoparticles for synthesis of multiplexed optical contrast agents with both delivery and targeting moieties. Nat Protoc 2008;3:314–20.

[156] Huang C, Zhang Y, Yuan H, Gao H, Zhang S. Role of nanoparticle geometry in endocytosis: laying down to stand up. Nano Lett 2013;13:4546–50.

[157] Yuan H, Zhang S. Effects of particle size and ligand density on the kinetics of receptor-mediated endocytosis of nanoparticles. Appl Phys Lett 2010;96:1–3.

[158] Dimova R, Seifert U, Pouligny B. P HYSICAL J OURNAL E Hyperviscous diblock copolymer vesicles 2002;250:241–50.

[159] McManus AJ, Doremus RH, Siegel RW, Bizios R. Evaluation of cytocompatibility and bending modulus of nanoceramic/polymer composites. J Biomed Mater Res A 2005;72:98–106.

[160] Wang X, Li Y, Wei J, de Groot K. Development of biomimetic nano-hydroxyapatite/poly(hexamethylene adipamide) composites. Biomaterials 2002;23:4787–91.

[161] Rawicz W, Olbrich KC, McIntosh T, Needham D, Evans E. Effect of chain length and unsaturation on elasticity of lipid bilayers. Biophys J 2000;79:328–39.

[162] Pan J, Tristram-Nagle S, Kucerka N, Nagle JF. Temperature dependence of structure, bending rigidity, and bilayer interactions of dioleoylphosphatidylcholine bilayers. Biophys J 2008;94:117–24.

[163] Winterhalter M. On the molecular origin of the bending elastic moduli. Prog Colloid Polym Sci 1995;98:271–5.

[164] Vangasseri DP, Cui Z, Chen W, Hokey D a, Falo LD, Huang L. Immunostimulation of dendritic cells by cationic liposomes. Mol Membr Biol 2006;23:385–95.

[165] Yi X, Shi X, Gao H. Cellular Uptake of Elastic Nanoparticles. Phys Rev Lett 2011;107:1–12.

[166] Bell G. Models for the specific adhesion of cells to cells. Science (80-) 1978;200:618–27.

[167] Vijayendran R a, Ligler FS, Leckband DE. A computational reaction-diffusion model for the analysis of transport-limited kinetics. Anal Chem 1999;71:5405–12.

[168] Whitman SC. A Practical Approach to Using Mice in Atherosclerosis Research. Clin Biochem Rev 2004;25:81–93.

[169] Gandhi C, Khan MM, Lentz SR, Chauhan AK. ADAMTS13 reduces vascular inflammation and the development of early atherosclerosis in mice. Blood 2012;119:2385–91.

[170] Deguchi J, Aikawa M, Tung C-H, Aikawa E, Kim D-E, Ntziachristos V, et al. Inflammation in atherosclerosis: visualizing matrix metalloproteinase action in macrophages in vivo. Circulation 2006;114:55–62.

[171] Pusztaszeri MP, Seelentag W, Bosman FT. Immunohistochemical expression of endothelial markers CD31, CD34, von Willebrand factor, and Fli-1 in normal human tissues. J Histochem Cytochem 2006;54:385–95.

[172] Daugherty A, Whitman SC. Quantification of Atherosclerosis in Mice. Methods Mol Biol 2002;209:293–309.

Chapter 6.

Appendices

6.1 Appendix A: List of Publications

1. **Almeda D**, Auguste DT. Liposomes target cytokine-activated endothelial cells via optimized antibody density, ratio, and diffusivity. Submitted to Biomaterials.

2. Gunawan R, **Almeda D**, Auguste DT. Complementary targeting of liposome to IL-1α and TNF-α activated endothelial cells via the transient expression of VCAM1 and E-selectin, Biomaterials 2011; 32: 9848-9858.

6.2 Appendix B: Additional Statistical Analysis of Raw Flow Cytometry Data

Table 6.1: Additional Statistical Analysis of 1 h Binding and Uptake by Non-Activated ECs Study. Statistical significance was calculated using a two-way ANOVA test (ns = not significant, *p < 0.05, **p < 0.01, and ***p < 0.001).

	IgG vs. Bare	IgG vs. 1:1 aVCAM1:aE-selectin	IgG vs. 1:0 aVCAM1:aE-selectin	IgG vs. 0:1 aVCAM1:aE-selectin
DOPC	ns	ns	ns	ns
DSPC	*	**	ns	*

	Bare vs. 1:1 aVCAM1:aE-selectin	Bare vs. 1:0 aVCAM1:aE-selectin	Bare vs. 0:1 aVCAM1:aE-selectin
DOPC	ns	ns	ns
DSPC	ns	ns	ns

	1:1 aVCAM1:aE-selectin vs. 1:0 aVCAM1:aE-selectin	1:1 aVCAM1:aE-selectin vs. 0:1 aVCAM1:aE-selectin	1:0 aVCAM1:aE-selectin vs. 0:1 aVCAM1:aE-selectin
DOPC	ns	ns	ns
DSPC	ns	ns	ns

Table 6.2: Additional Statistical Analysis of 1 h Binding and Uptake by IL-1α-Activated ECs Study. Statistical significance was calculated using a two-way ANOVA test (ns = not significant, *p < 0.05, **p < 0.01, and ***p < 0.001).

	IgG vs. Bare	IgG vs. 1:1 aVCAM1:aE-selectin	IgG vs. 1:0 aVCAM1:aE-selectin	IgG vs. 0:1 aVCAM1:aE-selectin
DOPC	ns	***	ns	***
DSPC	ns	***	ns	***

	Bare vs. 1:1 aVCAM1:aE-selectin	Bare vs. 1:0 aVCAM1:aE-selectin	Bare vs. 0:1 aVCAM1:aE-selectin
DOPC	***	ns	***
DSPC	***	ns	***

	1:1 aVCAM1:aE-selectin vs. 1:0 aVCAM1:aE-selectin	1:1 aVCAM1:aE-selectin vs. 0:1 aVCAM1:aE-selectin	1:0 aVCAM1:aE-selectin vs. 0:1 aVCAM1:aE-selectin
DOPC	***	***	***
DSPC	***	***	***

Table 6.3: Additional statistical analysis of 4 h binding and uptake by non-activated ECs study. Statistical significance was calculated using a two-way ANOVA test (ns = not significant, *p < 0.05, **p < 0.01, and ***p < 0.001).

	IgG vs. Bare	**IgG vs. 1:1 aVCAM1:aE-selectin**	**IgG vs. 1:0 aVCAM1:aE-selectin**	**IgG vs. 0:1 aVCAM1:aE-selectin**
DOPC	ns	ns	ns	ns
DSPC	ns	***	***	***

	Bare vs. 1:1 aVCAM1:aE-selectin	**Bare vs. 1:0 aVCAM1:aE-selectin**	**Bare vs. 0:1 aVCAM1:aE-selectin**
DOPC	ns	ns	ns
DSPC	***	***	***

	1:1 aVCAM1:aE-selectin vs. 1:0 aVCAM1:aE-selectin	**1:1 aVCAM1:aE-selectin vs. 0:1 aVCAM1:aE-selectin**	**1:0 aVCAM1:aE-selectin vs. 0:1 aVCAM1:aE-selectin**
DOPC	Ns	ns	ns
DSPC	***	***	***

Table 6.4: Additional Statistical Analysis of 4 h Binding and Uptake by IL-1α-Activated ECs Study. Statistical significance was calculated using a two-way ANOVA test (ns = not significant, *p < 0.05, **p < 0.01, and ***p < 0.001).

	IgG vs. Bare	IgG vs. 1:1 aVCAM1:aE-selectin	IgG vs. 1:0 aVCAM1:aE-selectin	IgG vs. 0:1 aVCAM1:aE-selectin
DOPC	ns	***	**	***
DSPC	***	***	***	***

	Bare vs. 1:1 aVCAM1:aE-selectin	Bare vs. 1:0 aVCAM1:aE-selectin	Bare vs. 0:1 aVCAM1:aE-selectin
DOPC	***	ns	***
DSPC	***	***	***

	1:1 aVCAM1:aE-selectin vs. 1:0 aVCAM1:aE-selectin	1:1 aVCAM1:aE-selectin vs. 0:1 aVCAM1:aE-selectin	1:0 aVCAM1:aE-selectin vs. 0:1 aVCAM1:aE-selectin
DOPC	***	**	***
DSPC	***	**	***

Table 6.5: Additional Statistical Analysis of Surface Binding Studies. Statistical results of surface binding of IL-1α-activated ECs with mean fluorescence intensity values of NBD (A) and rhodamine (B). Statistical significance was calculated using a two-way ANOVA test (ns = not significant, *$p < 0.05$, **$p < 0.01$, and ***$p < 0.001$).

A

	5 min vs. 0.5 h	**5 min vs. 1 h**	**0.5 h vs. 1 h**
DOPC	ns	ns	Ns
DSPC	***	ns	***

B

	5 min vs. 0.5 h	**5 min vs. 1 h**	**0.5 h vs. 1 h**
DOPC	ns	***	***
DSPC	***	**	**

Table 6.6: Additional Statistical Analysis of Cellular Internalization Studies. Statistical results of cellular internalization of IL-1α-activated ECs with mean fluorescence intensity values of NBD (A) and rhodamine (B). Statistical significance was calculated using a two-way ANOVA test (ns = not significant, *p < 0.05, **p < 0.01, and ***p < 0.001).

A

	5 min vs. 0.5 h	**5 min vs. 1 h**	**0.5 h vs. 1 h**
DOPC	ns	***	**
DSPC	*	***	**

B

	5 min vs. 0.5 h	**5 min vs. 1 h**	**0.5 h vs. 1 h**
DOPC	ns	***	***
DSPC	*	***	***